ULTRASONIC STUDIES OF MOLECULAR AGGREGATION IN POLYMERIC MATERIALS(Dissertation_全文)

AUTHOR(S):

Nitta, Kohei

ULTRASONIC STUDIES OF MOLECULAR AGGREGATION IN POLYMERIC MATERIALS

KOH-HEI NITTA

1991

CONTENTS

GENERAL INTRODUCTION

In recent years, condensed matters in polymeric materials have been of great interest in respect of ordering, metastability, phase transition and so on. An exact understanding of molecular aggregation in condensed states can be essential for clarification of properties which are indispensable to many practical applications, but is not sufficient at present: for example, the nonlinear viscoelasticity of crystalline polymers[1] and the physical aging of glassy polymers.[2,3]

Polymeric materials are characterized by the high molecular weight, the broad molecular weight distribution, and the anisotropic molecular shape. These characteristics may induce a long relaxation time, a broad relaxation time distribution and an anisotropy of molecular interaction. As a result, different molecular aggregation states may appear in condensed states of polymeric materials. Thus, in order to clarify unsolved problems in physical properties of polymeric materials, it should be necessary to elucidate molecular aggregation states on the basis of molecular interaction.

The term "ultrasonic wave" is defined as a sound wave having frequencies above the audible range; that is, above about 20 kHz. The wavelength of ultrasonic waves is short, and therefore the directivity can be enhanced. This point enables us to deal with ultrasonic waves geometrically and it also enhances the accuracy in measurements of the sound velocity and the absorption coefficient.

Traditionally, the ultrasonic propagation has been used for the high frequency dynamic test.[4,5] Currently, ultrasonics plays many roles, ranging from physical and bioengineering applications to the study of fundamental properties of materials. It is greatly owing to the recent developments in electronics and

hardware. For example, ultrasonic measurements have become of major interest as non-destructive evaluation *(NDE)* tools for detecting failure-including flaws concealed below solids such as metals, plastics, ceramics, and composites.[6-13]

Use of the ultrasonic wave as a "*probe*" should be helpful to an understanding of the aggregation state on the basis of the molecular interaction. As a matter of fact, the ultrasonic wave propagating through materials travels by molecular interaction and is sensitive to small scale changes in the material structure.[14,15]

The purpose of this thesis is to characterize the molecular aggregation state by the ultrasonic measurement and to clarify unsolved problems in physical properties of polymeric materials from a structural point of view.

Part I (Chapters 1 and 2) is concerned with a review of ultrasonic studies. **Chapter 1** contains the historical and theoretical backgrounds of ultrasonic studies, which will serve as a basis for discussion in succeeding chapters. In **Chapter 2**, the experimental principle and method for determination of ultrasonic velocity and attenuation coefficient are described.

Part II (Chapters 3-6) contains applications of ultrasonic measurements to the nonlinear viscoelasticity of crystalline polymers. **Chapter 3** describes the method for measurement of ultrasonic properties under oscillatory deformation. One calls "*dynamic ultrasonics*". From the measurement, "*dynamic ultrasonic velocity*", "*dynamic attenuation coefficient*", and "*dynamic density*" can be determined. In **Chapter 4**, the dynamic ultrasonic properties are examined for undrawn polyethylene films and the nonlinearity in dynamic mechanical properties is discussed. In **Chapter 5**, the dynamic ultrasonic properties are examined for drawn polyethylene films, and the nonlinearity is compared with that for undrawn films. In **Chapter 6**, the ultrasonic properties are measured under a constant rate of deformation, and the nonlinearity in stress-strain relationship is examined.

Part III (Chapters 7-9) contains the examination of molecular aggregation in noncrystalline polymers by the ultrasonic measurement. In **Chapter 7**, changes in molecular aggregation accompanied with phase separation are examined for styrene-butadiene-styrene triblock copolymers. In this chapter, the concept of molecularly ordered aggregation formed under nonequilibrium condition is introduced. In **Chapter 8**, the effect of physical aging and/or heat-treatment on the molecular aggregation in poly(trimethylsilyl-1-propyne) films showing high gas permeability is examined. It was found that the change in the molecular aggregation affects their gas permeability. In **Chapter 9**, the phase transition between isotropic and liquid crystalline phases on Hydroxypropyl-cellulose solutions is examined using an ultrasonic measurement. Moreover, the liquid-crystalline-like molecular aggregation remaining on Hydroxypropyl-cellulose solids (or films) is also examined.

REFERENCES

1. I. M. Ward, "*Mechanical Properties of Solid Polymers*," John Wiley & Sons, New York (1971).
2. L. C. E. Struik, "*Physical Aging in Amorphous Polymers and Other Materials*," Elsevier, Amsterdam, (1978).
3. A. J. Kovacs, J. J. Aklonis, J. M. Hutchinson, and A. R. Ramos, *J. Polym. Sci., Polym. Phys. Ed.*, **17**, 1097 (1979).
4. A. M. North, and R. A. Pethrick, "*Developments in Polymer Characterization*," Appl. Sci. Pub., London, **2**, 183 (1980).
5. R. A. Pethrick, *ibid*, **4**, 177 (1983).
6. "*ME*" Feb. (1984). "*Listening for Defects in Materials*," pp.30 article by L. M. Sheppard.
7. "*High Technology*," Vol.2, No.6 Sep./Oct. (1982). "*Acoustic Microscope Probes Material*," pp.78 article by T. Adams.
8. G. A. Sofer and E. A. Hauser, *J. Polym. Sci.*, **8**, 6 (1952).
9. B. G. Martin, *Mater. Eval.*, **34**, 49 (1976).
10. J. Chottiner, Z. N. Sanjna, M. Kodani, K. W. Lengei, and G. B. Rosenblatt, *Polym. Compos.*, **3**, 59 (1982).
11. R. H. Harrold and Z. N. Sanjana, *Polym. Eng. Sci.*, **26**, 367, (1986).
12. L. Erwin and J. Dohner, *ibid.*, **24**, 1277 (1984).
13. A. M. Ibrahim, A. R. Wedgewood, and J. C. Seferis, *ibid.*, **26**, 593 (1986).
14. J. W. S. Rayleigh, "*The Theory of Sound*," Dover Pub., New York (1945).
15. R. Truell, C. Elbaum, and B. B. Chick, "*Ultrasonic Methods in Solid State Physics*," Academic Press, New York (1969).

PART I

CHAPTER 1

BACKGROUND OF ULTRASONIC STUDIES

1-1 Historical Background

Ultrasonics has been studied over past six decades. The first application of ultrasonics to the study of fundamental properties of materials was in 1925 when Pierce invented an ultrasonic interferometer and measured the ultrasonic velocity in gases accurately.[1] Extensive studies on the ultrasonic velocity and absorption were carried out in gases and liquids until the 1940's. The studies led to the conclusion that the velocity is related to the modulus or compressibility and that the absorption coefficient to the viscosity or internal friction. It was since early 1950's that ultrasonic studies were applied to solids, although a few ultrasonic studies carried out in fibrous and rubbery materials in the 1940's.[2-6] It was found that the absorption in solids arises from several physical causes such as the dislocation,[7] intergrain thermoelastic effect,[8] anharmonic coupling between phonons,[9] and interaction of sound wave with electrons,[10,11] rather than from the viscothermal (classical) absorption.[12,13] It was also found that the ultrasonic velocity in solids depend less on temperature and frequency in contrast to gases and liquids.

It was not until quite recently that ultrasonic techniques were applied to polymeric materials in solid.[14-21] Most of these studies have been concerned with the investigation of dynamic properties using high-frequency sound waves. However, Pethrick *et al.* have indicated that the ultrasonics has potential as a

method of investigating morphology in polymeric materials:[22-24] they indicated that the orientation and crystallinity could be estimated from the ultrasonic velocity, and that the size of voids generating during drawing could be evaluated from the ultrasonic attenuation.

1-2 Theoretical Background

The propagation of elastic waves (sonic waves) in solids and liquids was theoretically investigated by Stokes, Poisson, Rayleigh, and Kelvin during the last century. The investigation was aimed to theoretically derive the velocity and the attenuation.[25,26] The velocity was derived from the equation of motion, in which the velocity is determined by the dispersion equation, *i.e.* the relationship between the angular frequency and the wave number.[27] The term "attenuation" is used as energy loss when sound waves propagate through material. The attenuation is usually determined from the decrease in the amplitude of sound wave at a given distance. The amplitude A at a given distance x is expressed by the following equation.

$$A = A_0 \exp(-\alpha x) \tag{1-1}$$

where A_0 is the amplitude at $x=0$, and α the attenuation coefficient.

Now consider the wave propagation in the elastic medium where stress and strain are linearly related by an elastic constant, *i.e.* the Hooke's law is obeyed. Then, the equation of motion is obtained by equating the products of masses and accelerations to the elastic forces, and can be written as in the following equation:

$$\rho \frac{\delta^2}{\delta t^2} \Psi(x,t) = E \frac{\delta^2}{\delta x^2} \Psi(x,t) \tag{1-2}$$

where $\Psi(x,t)$ is the displacement of the medium, E the elastic coefficient, and ρ the density. The equation was derived by D'Alambert (1750), which is referred as the "*classical wave equation*". This equation gives a plane wave as a solution and

the plane wave can be expressed by means of complex variables as follows:

$$\Psi(x,t) = \Psi_0 \exp\ [i(\omega t - kx)] \tag{1-3}$$

where k is the wave vector, ω the angular frequency of the traveling wave, and $i=\sqrt{-1}$, indicating that the $\Psi(x,t)$ propagates in the x or k direction with velocity $v=d\omega/dk$. It should be noted that the solution of Eq.(1-2) has the form of $\Psi(x,t)=\phi(x)\psi(t)$, where $\phi(x)$ is a function of x only and $\psi(t)$ is a function of t only. This implies that the displacement $\Psi(x,t)$ is separable in space and time.

Substituting Eq.(1-3) in Eq.(1-2), lead to:

$$v = \sqrt{\frac{E}{\rho}} \tag{1-4}$$

When a longitudinal plane wave propagates in a bounded elastic body, the medium deforms in the propagation direction, obeying to the Hooke's law. Then, the elastic constant E becomes Young's modulus. In addition to longitudinal waves, pure share, namely transversal waves, can propagate in solids. In this case, the displacement of the medium is at right angle to the direction of propagation. The equation for transverse motions of the medium is identical to that for longitudinal motions at small amounts of deformation. In this case, however, Young's modulus E is replaced by shear modulus G. The velocity of longitudinal wave is greater than that of transverse wave (*i.e.* E is greater than G)

In an extended solid, other type of elastic wave can propagate along the surface; it is known as *Rayleigh waves*, and its disturbance decays exponentially with depth. The surface wave falls off more slowly with distance than other type of elastic waves, since it spreads only in two dimensions, but travels with lower velocity.

In the above, the author referred to progressive waves propagating through an ideal medium in which the density is constant and the elastic coefficient is uniform was discussed. For most real solids, in particular for polymeric solids, however, both density and modulus are not uniform. In such a case, the differential equation of motion becomes:

$$\rho(x)\frac{\delta^2}{\delta t^2}\Psi(x,t)=\frac{\delta}{\delta x}\left[E(x)\frac{\delta}{\delta x}\Psi(x,t)\right] \tag{1-5}$$

where both $E(x)$ and $\rho(x)$ are functions of x. The equation is named as *Sturm-Liouville equation*, and it cannot be solved in general. One useful approximate method for solving the equation is the perturbation method.[28,29] This method is applicable only when the fluctuation in the density and the modulus is small. For the sake of simplicity, let us consider only the case in which the modulus is constant, and in which the density is a function of x. Assuming that $\Psi(x,t)$ is proportional to a function of x times $e^{i\omega t}$ and using similar solution to the solution of Eq.(1-2), the following equation can be obtained:

$$E\frac{\delta^2}{\delta x^2}\phi(x)+\rho(x)\omega^2\phi(x)=0 \tag{1-6}$$

where $\phi(x)$ is the part of $\Psi(x,t)$ depending on x. The density $\rho(x)$ can be expanded by the perturbation parameter λ as follows;

$$\rho(x)=\rho_0+\lambda\rho_1(x)+\lambda^2\rho_2(x)+\cdots\cdots \tag{1-7}$$

where ρ_0 is a constant and λ is very small. When the density $\rho(x)$ equals to ρ_0 (*i.e.* it is constant), the equation Eq.(1-5) can be soluble and there exists the wave function $\phi_0(x)$ and frequency ω_0 satisfying the following equation:

$$E\frac{\delta^2}{\delta x^2}\phi_0(x)+\rho_0\omega_0^2\phi_0(x)=0 \tag{1-8}$$

This wave equation is well-known as *Helmholtz wave equation*. Since the wave function $\phi(x)$ and frequency ω is nearly equal to the $\phi_0(x)$ and ω_0, respectively, the both functions should be expanded as follows;

$$\phi(x)=\phi_0(x)+\lambda\phi_1(x)+\lambda^2\phi_2(x)+\cdots\cdots$$

$$\omega=\omega_0+\lambda\omega_1+\lambda^2\omega_2+\cdots\cdots \tag{1-9}$$

Substituting Eq's.(1-7) and (1-9) into Eq.(1-6) and using Eq.(1-8), one obtains

$$\omega^2\simeq\omega_0^2\left[1-\lambda\int_0^L\rho_1(x)\phi_0(x)^2dx\right] \tag{1-10}$$

Therefore, the wave velocity v in heterogeneous medium is given by

$$v\simeq v_0\left[1-\lambda\int_0^L\rho_1(x)\phi_0(x)^2dx\right]^{1/2} \tag{1-11}$$

where the $v_0=\sqrt{E/\rho_0}$ is the wave velocity in homogeneous medium.

If the density perturbation $\lambda\rho_1(x)$ is positive, the velocity for heterogeneous medium becomes lower than that for homogeneous one, as is indicated by Eq.(1-11).

Materials such as polymeric solids depart from Hooke's low and show a typical viscoelastic behavior. The motion equation is obtained by equating the products of masses and accelerations to elastic and viscous forces and is given by the following equation.[5,30]

$$\rho\frac{\delta^2}{\delta t^2}\Psi(x,t)=\left[E+\eta\frac{\delta}{\delta t}\right]\frac{\delta^2}{\delta x^2}\Psi(x,t) \tag{1-12}$$

where η is the viscosity. By substituting a solution in Eq.(1-3) with Eq.(1-12) and placing $\tau=\eta/E$, one obtains:

$$\omega^2=\frac{E}{\rho}(1+i\omega\tau)k^2 \tag{1-13}$$

where τ is known as the retardation time. This obviously gives for the sound velocity $d\omega/dk$ a complex value. When one keeps ω real and allows k to take complex values $k^*(=\kappa-i\alpha)$, where both κ and α are real and positive, the solution becomes:

$$\Psi(x,t)=\Psi_0\exp\left[i(\omega t-k^*x)\right] \tag{1-14}$$

$$=\Psi_0\exp(-\alpha x)\exp\left[i(\omega t-kx)\right] \tag{1-15}$$

The real part of Eq.(1-15) represents plane wave which propagates along the positive x with the velocity $v=\omega/\kappa$. The amplitude decreases exponentially with

increasing x. Therefore, the imaginary part of k^* gives the attenuation coefficient.

If one substitutes the k^* in Eq.(1-13), one obtains the relations as follows:

$$v = \sqrt{\frac{E}{\rho}} \cdot \frac{\sqrt{1+(\alpha/\kappa)^2}}{1-(\alpha/\kappa)^2} \tag{1-16}$$

and

$$\alpha = \frac{1}{2} \cdot \frac{\omega^2 \tau}{v} [1-(\alpha/\kappa)^2] \tag{1-17}$$

The equations indicate the frequency dependence of the velocity and attenuation coefficient. When α/κ is small compared with unity, as is usually the case in solids,[12] the velocity is given by $v_0 = \sqrt{E/\rho}$ and is the same as that for elastic solids; on the other hand, the attenuation coefficient becomes:

$$\alpha \simeq \frac{\tau}{2v_0}\omega^2 = \frac{2\pi^2 \rho \kappa v_0}{E^2} \cdot f^2 \tag{1-18}$$

As is evident, α is proportional to the square of the frequency $f = \omega/2\pi$. This type of the attenuation is generally referred as the "*classical absorption*", and Eq.(1-18) is called *Navier-Stokes expression.*[12,13]

A solution of the type Eq.(1-14) evidently corresponds to the experimental set-up where the amplitude of the plane progressive waves excited in the medium is measured at different distances from the acoustic source. On the other hand, the appropriate measurements of the dissipative effects, namely the time rate of decay of sound energy, can be evaluated by the expedient of taking k real and letting $\omega^* = \nu + i\beta$, the solution for the plane wave becomes:

$$\Psi(x,t) = \Psi_0 \exp[i(\omega^* t - kx)] \tag{1-19}$$

$$= \Psi_0 \exp(-\beta t) \exp[i(\nu t - kx)] \tag{1-20}$$

where the β is called the damping coefficient. Setting $\omega^* = \nu + i\beta$ in Eq.(1-13), the β can be written as follows;

$$\beta = \frac{1}{2} v_0^2 \tau k^2 \simeq \frac{1}{2} \tau \omega^2 \tag{1-21}$$

Therefore, the damping coefficient is related to the attenuation coefficient by the following equation:

$$\beta = \alpha v \tag{1-22}$$

The viscous effect is one important cause of ultrasonic attenuation but there are many other mechanisms responsible for it. The viscous effect in particular for solids is usually small and frequently overshadowed by other mechanisms. Typical mechanisms for attenuation are described below:

1) Heat Conduction. When the acoustic wave propagates through a solid body, compressed parts become hotter and expanded parts cooler. The sound wave makes the local temperature gradient through which heat will flow, and consequently it loses energy as heat. The attenuation due to the energy loss is described by[8,31]

$$\alpha_h = \frac{\pi}{v_0} \cdot \frac{C_p - C_v}{C_v} R \frac{f_0 f}{f_0 + f} \tag{1-23}$$

where f_0 denotes relaxation frequency, and is given by

$$f_0 = \frac{\Lambda}{\rho C_p d^2} \tag{1-24}$$

where C_p and C_v are heat capacities at constant pressure and at constant volume, respectively, Λ the thermal conductivity, and d the domain size. The parameter R in Eq.(1-23) represents the anisotropy due to the modulus differences between the domains, given by

$$R = \frac{\langle (E - \langle E \rangle_{av})^2 \rangle_{av}}{\langle E^2 \rangle_{av}} \tag{1-25}$$

where E is the longitudinal modulus. The suffix av denotes the statistical average. This type of the attenuation mechanism corresponds to the Zener loss peaks[8] in polycrystalline metals. In the case of polyethylene, for example, spherulites disperse within amorphous phase.[32,33] The size of the spherulites is from 5 to 50 μm, whereas the width of the crystalline lamellae or amorphous zones is from 5

to 50 nm depending on the crystallinity of the material. The characteristic frequency for the heat flow from one spherulite to another one is estimated using Eq.(1-24). In the case of 5 μm domains, the characteristic frequency becomes in order of 10 kHz. Thus, the losses due to inter-spherulite heat flow can be ruled out in usual ultrasonic frequency regions. In the case of heat flow between crystalline and amorphous zones, the characteristic frequency would be in order of GHz.

2) Scattering by voids and defects. Attenuation of the sound wave may occur as a consequence of scattering by heterogeneities or defects. The wavelength of the sound wave which is estimated from the velocity is usually much larger than the void and defect dimension. The Rayleigh condition is therefore satisfied. The ultrasonic attenuation caused by viscoelastic spheres suspended in a viscoelastic medium was predicted on the basis of the Rayleigh condition by Okano[34] as follows.

$$\alpha_s = \frac{8\pi^4 a^3}{v_0^4} f^4 \cdot \left[\frac{1}{3}\left(\frac{B_1 - B_0}{B_1}\right)^2 + \left(\frac{\rho_1 - \rho_0}{2\rho_1 + \rho_0}\right)^2\right] \phi \qquad (1\text{-}26)$$

where a denotes the radius of the sphere, B the bulk modulus, and ϕ the volume fraction of the sphere. Suffix 1 and 0 denote the sphere and medium, respectively. The attenuation due to such scattering can be estimated by letting the spheres correspond to air voids and the surrounding polymer constitute the medium. The previous studies of Pethrick *et al.*[23,24] suggested that the scattering is dominant cause of the attenuation for crystalline polymeric solids.

3) Phonon-phonon scattering. Attenuation can be also caused by anharmonic interaction of the applied sound waves (*i.e.* sound-phonons) with the thermal vibrations (*i.e.* thermal phonons). The phonon-phonon scattering may be predicted on the basis of the theory of Woodruff and Ehrenreich for long- and short-lived phonons.[9] The attenuation due to the phonon scattering is given by:

$$\alpha_p = \frac{4\pi^2 \gamma_G^2 f \Lambda T}{v_0^5} \qquad (1\text{-}27)$$

where γ_G denotes the Grüneisen parameter and T the absolute temperature. The life-time of the phonon in polymeric solids around room temperature is in order of 10^{-13} sec and so it is much shorter than the period of ultrasonic wave. Thus, for usual polymeric materials, the attenuation due to the phonon scattering will be considerably small.

REFERENCES

1. G. W. Pierce, Proc. *Am. Acad. Arts Sci.*, **60**, 271 (1925).
2. J. W. Ballou and S. Silverman, *J. Acoust. Soc. Am.*, **16**, 113 (1944): *Textile Res. J.*, **14**, 282 (1944).
3. A. W. Nolle, *J. Acoust. Soc. Am.*, **19**, 194 (1949).
4. J. W. Ballou and J. C. Smith, *J. Appl. Phys.*, **20**, 493 (1949).
5. K. W. Hillier, *Proc. Phys. Soc. (London)*, **B62**, 111, 701 (1949).
6. R. S. Witte, B. A. Mrowca, and E. Guth, *J. Appl. Phys.*, **22**, 481 (1949).
7. A. Granato and K. Lücke, *J. Appl. Phys.*, **27**, 583 (1956a).
8. C. Zener, *Proc. Phys. Soc.*, **52**, 152 (1940).
9. T. O. Woodruff and H. Ehrenreich, *Phys. Rev.*, **123**, 1553 (1961).
10. H. E. Bömmel, *Phys. Rev.*, **96**, 220 (1954).
11. L. Mackinnon, *Phys. Rev.*, **98**, 1181 (1955).
12. A. B. Bhatia, "*Ultrasonic Absorption*," Oxford Univ. Press, London (1967).
13. K. F. Herzfeld and T. A. Litovitz, "*Absorption and Dispersion of Ultrasonic Waves*," Academic Press, New York (1953).
14. D. W. Phillips and R. A. Pethrick, *J. Macromol. Sci. Rev. Macromol. Chem.*, **16**, 1 (1978).
15. P. K. Datta and R. A. Pethrick, *Polymer*, **19**, 145 (1978).
16. A. M. North, R. A. Pethrick, and D. W. Phillips, *Macromolecules*, **10**, 992 (1977).
17. S. B. Clough, N. S. Schneider, and A. O. King, *J. Macromol Sci.-Phys.*, **B2**, 641 (1968).
18. S. L. Cooper and A. V. Tobolsky, *J. Appl. Polym. Sci.*, **10**, 1837 (1966).
19. P. D. Davidse, H. I. Waterman, and J. B. Westerdijk, *J. Polym. Sci.*, **59**, 389 (1962).
20. M. Baccaredda and E. Butta, *J. Polym. Sci.*, **22**, 217 (1956).
21. J. Schuyer, *J. Polym. Sci.*, **36**, 475 (1959).
22. R. A. Pethrick, *Progr. Polym. Sci.*, **9**, 197 (1983).

23. K. Adachi, G. Harrison, J. Lamb, A. M. North, and R. A. Pethrick, *Polymer*, **22**, 1026 (1981).
24. K. Adachi, G. Harrison, J. Lamb, A. M. North, and R. A. Pethrick, *ibid.*, **22**, 1032 (1981).
25. W. P. Mason, "*Physical Acoustics and the Properties of Solids*," Van Nostrand, Princeton, New Jersey (1958).
26. H. Kolsky, "Stress Waves in Solids," Clarendon Press, Oxford (1953).
27. L. Brillouin, "*Wave Propagation and Group Velocity*," Academic Press, New York (1960).
28. J. C. Slater and N. H. Frank, "*Mechanics*," McGraw-Hill, New York (1947).
29. J. B. Marion, "*Classical Dynamics of Particles and Systems*," Academic Press, New York (1965).
30. K. Lücke, *J. Appl. Phys.*, **27**, 1433 (1956).
31. K. Eiermann, *Kolloid Z.*, **201**, 3 (1965).
32. P. H. Geil, "*Polymer Single Crystals*," Intersci. Pub., New York (1963).
33. B. Wonderlich, "*Macromolecular Physics*," Academic Press, New York (1973).
34. K. Okano, in *6th Int. Congr. Acoust. (Tokyo)*, H-6 (1968).

CHAPTER 2

MEASUREMENT TECHNIQUES

2-1 Pulse Method

The ultrasonic velocity and absorption coefficient are determined mostly by the following three methods: (a) the interferometric method which is used for gases and liquids[1-3]; (b) the optical method which is also used for gases and liquids[4-7]; (c) the pulse method for liquids and solids.[8-10] In the interferometric and optical methods, ultrasonic disturbance is continuously supplied to the medium, and a resultant standing wave is utilized for the determination of ultrasonic velocity and absorption coefficient. Thus, one can obtain the phase velocity and the damping coefficient. In the pulse method, on the other hand, a wave packet traveling through a given distance is utilized for the determination. Therefore, one can obtain the propagating velocity (group velocity[11-13]) and the attenuation coefficient. The pulse method was used entirely in the present study.

For the pulse method to be successful, the following two requirements must be satisfied. First, the distance between transducer and receiver must be longer than the wavelength of the ultrasonic pulse so that no standing waves are formed. Second, the distance should not be so large that the intensity of ultrasonic wave is in distinguishable at the receiver.

2-2 Transducer

Transducer is a device for converting an electric signal to a mechanical vibration or vice versa. Two same piezoelectric transducers supplied from NF Electric Instruments were used as transmitter and receiver in the present measurements. (The diameter of the transducers was 0.72 cm.)

The ultrasonic velocity of polymeric solids is commonly 10^4-10^5 cm/sec. The pulse method requires the frequency above 100 kHz in the case of a traveling distance from 2 to 4 cm. While the ultrasonic wave in the MHz region attenuates too much to obtain a distinguishable intensity at the distance for polymeric solids. Hence, the commercially available transducers with the frequency of 150kHz were chosen. Besides, Truell *et al.*[14] reported that in the frequency region from 100 kHz to 1 MHz, there are very important ultrasonic loss mechanism such as dislocation damping associated with plastic deformation, which relate directly to the mechanical properties of a solid.

2-3 Experimental Methods

Ultrasonic measurements were carried out as follows: Two transducers were put in direct with the sample (see Fig.2-1). An electrical impulse with duration time of 50 nsec was converted by means of one transducer into an impulsive mechanical vibration. After traveling through the sample, the ultrasonic wave was received by another transducer. The latter transducer converted the ultrasonic wave into electrical signal again. The electric signal after passing through a differential preamplifier and a discriminator was stored in a transient memory. The signal displayed visually on a recorder or an oscilloscope. Also, the signal was transmitted into a microcomputer and then the velocity and/or the attenuation coefficient were computed.

Fig.2-2 shows a schematic ultrasonic signal after traveling through a sample. The traveling time is indicated by Δt, as shown in the figure. From Δt

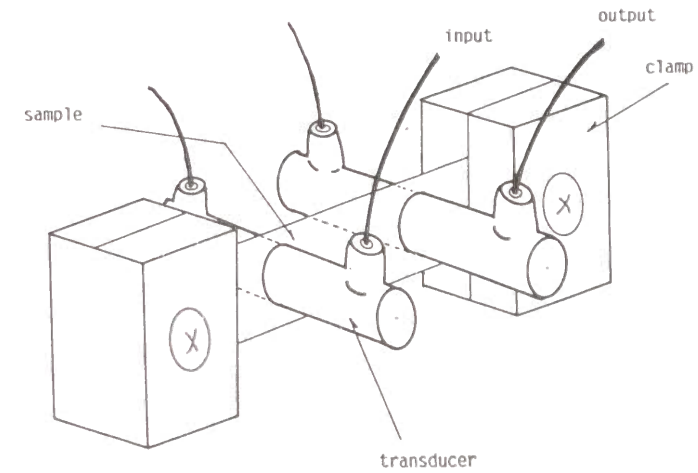

Fig.2-1 *Schema of the experimental setup for the generation of the ultrasonic wave.*

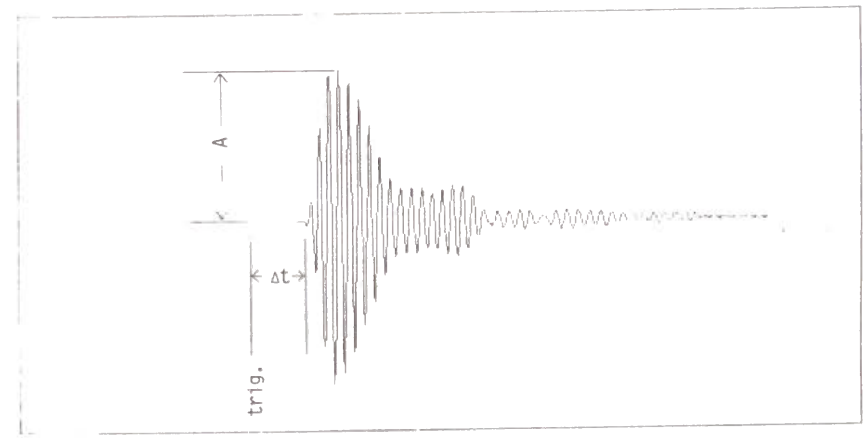

Fig.2-2 *Typical ultrasonic wave after passing through the sample specimen.* Δt *indicates a traveling time, and A an amplitude of the wave.*

and the distance between two transducers L, the ultrasonic velocity v can be determined using the following equation.

$$v = \frac{L}{\Delta t} \qquad (2\text{-}1)$$

Fig.2-3 shows a plot of traveling time against traveling distance of the ultrasonic wave at 40° C for a linear low density polyethylene (LLDPE) film. The plot shows a straight line, of which slope gives the ultrasonic velocity. The traveling time Δt was determined using the shortest sampling time (50 nsec) which was available in the transient memory; then, the error is estimated to be less than 1.0%.

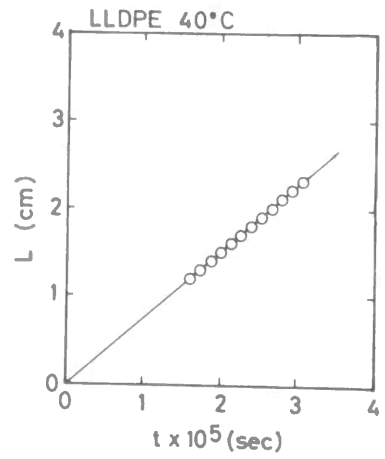

Fig.2-3 *Plot of traveling distance of ultrasonic waves against traveling time t. The figure was obtained for linear low density polyethylene films at 40° C.*

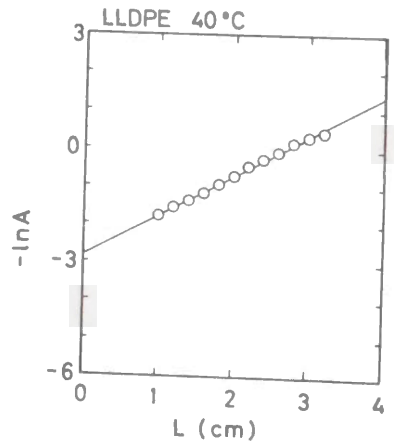

Fig.2-4 *Plot of the logarithm of the ultrasonic amplitude against traveling distance of ultrasonic waves. The figure was obtained for linear low density polyethylene films at 40° C.*

The attenuation coefficient α describes the absorption of the amplitude with distance and is expressed by

$$\alpha = \frac{1}{L} \ln \frac{A_0}{A} \qquad (2\text{-}2)$$

where A is the amplitude of the ultrasonic wave at a propagation distance L and A_0 the amplitude at L=0. As is evident from the equation, one can determine the attenuation coefficient as a ratio of the amplitude at a given distance to the amplitude at a reference distance. The amplitudes were estimated from the peak height of the ultrasonic wave, as indicated in Fig.2-2.

Fig.2-4 presents an example of the distance between two transducers plotted against the logarithmic amplitude of the ultrasonic wave at 40° C for LLDPE films. All the points fall on a straight line as Eq.(2-2) predicts, in which the slope gives the attenuation coefficient at 40° C. An intrinsic error in the attenuation coefficient may be caused by the incompleteness of bond coupling between transducer and material. Taking great care of bond coupling, the error was reduced to be less than 3.0 %.

1) Temperature Dependence of Ultrasonic Properties. The variations of ultrasonic velocity with temperature were estimated from the variations of the traveling time Δt with temperature at a fixed traveling distance L. The temperature dependence of attenuation coefficient $\alpha(T)$ was determined from the amplitude $A(T)$ at a given temperature, the amplitude $A(T_0)$ at a reference temperature T_0, and the attenuation coefficient using the following equation.

$$\alpha(T) = \alpha(T_0) + \frac{1}{L} \ln \frac{A(T_0)}{A(T)} \qquad (2\text{-}3)$$

$\alpha(T_0)$ was separately determined from the logarithmic plot of the amplitude against traveling distance at temperature T_0.

2) Strain Dependence of Ultrasonic Measurements. The ultrasonic properties were measured under a dynamic (cyclic) strain and a constant rate of strain. The velocity $v(\gamma)$ at a given strain were determined from $\Delta t(\gamma)$ at a given

strain:

$$v(\gamma) = \frac{L \cdot (1+\gamma)}{\Delta t(\gamma)} \qquad (2\text{-}4)$$

where γ is the strain and L the traveling distance at $\gamma = 0$.. The attenuation coefficient $\alpha(\gamma)$ were determined from the measurements of the amplitude at a given strain using following equation:

$$\alpha(\gamma) = \frac{\alpha_0}{1+\gamma} + \frac{1}{L \cdot (1+\gamma)} \ln \frac{A(0)}{A(\gamma)} \qquad (2\text{-}5)$$

where α_0 is the attenuation coefficient at $\gamma = 0$.

The ultrasonic properties under a cyclic strain were analyzed using a Fourier expansion method. Details will be presented in the next chapter.

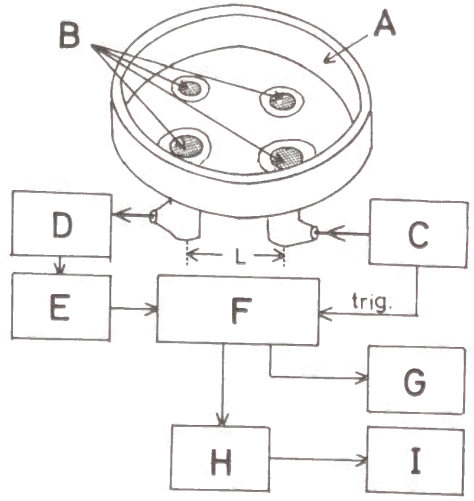

Fig.2-5 *Block diagram of the apparatus for measuring ultrasonic velocity and amplitude under solvent evaporating process: (A) cell; (B) transducer; (C) function generator; (D) differential preamplifier; (E) discriminator; (F) transient memory; (G) oscillator; (H) computer; and (I) printer*

3) Ultrasonic Properties under Solvent Evaporation. The molecular aggregation in polymer solutions during solvent evaporation were examined using ultrasonic measurements (Chapters 7 to 9). The equipment is shown in Fig.2-5. Four transducers are fixed in the bottom of the teflon cell so that the measurements can be carried out at six different distances (1.4 to 3.8 cm). The ultrasonic properties were measured as a function of the concentration. The concentration of the solution was calculated from the weight of both the cell and the solution.

REFERENCES

1. G. W. Pierce, *Proc. Am. Acad. Arts Sci.*, **60**, 271 (1925).
2. M. Greenspan, *J. Acoust. Soc. Am.*, **22**, 568 (1950).
3. M. Greenspan and M. C. Thompson, *ibid.*, **25**, 92 (1953).
4. L. Brillouin, *Annls. Phys.*, **17**, 88 (1922).
5. Y. Y. Haung and C. H. Wang, *J. Chem. Phys.*, **64**, 4847 (1947).
6. G. D. Patterson, *J. Polym. Sci., Polym. Phys. Ed.*, **15**, 455 (1979).
7. G. Fytas, Y. H. Lin, and B. Chu, *J. Chem. Phys.*, **74**, 3131 (1981).
8. P. I. Roderick and R. Truell, *J. Appl. Phys.*, **23**, 267 (1952).
9. B. D. Simmons and R. I. Urick, *J. Acoust. Soc. Am.*, **21**, 633 (1948).
10. H. Seki, A. Granats, and R. Truell, *ibid*, **28**, 230 (1956).
11. C. Kittel, "*Introduction to Solid State Physics*," 4th Ed., John Wiley & Sons, New York (1971).
12. D. R. Bland, "*Wave Theory and Applications*," Oxford Univ. Press, London (1988).
13. J. B. Marion, "*Classical Dynamics of Particles and Systems*," Academic Press, New York (1965).
14. R. Truell, C. Elbaum, and B. B. Chick, "*Ultrasonic Methods in Solid State Physics*," Academic Press, New York (1969).
15. O. R. Gericke, *J. Acoust. Soc. Am.*, **35**, 364 (1963).
16. A. F. Brown, "*Ultrasonic Testing*," John Wiley & Sons, New York (1982).

PART II

CHAPTER 3

DYNAMIC ULTRASONIC WAVE VELOCITY AND ATTENUATION

3-1 Introduction

Polymeric solids, in particular crystalline ones, exhibit nonlinear viscoelasticity even at small strains, which is one of indispensable properties of materials for practical use. With rapidly growing use of polymers, there appears to be a need for systematic studies of the nonlinear viscoelasticity. In past two decades, rheo-optical studies such as simultaneous measurements of dynamic mechanical properties with dynamic optical properties such as dynamic birefringence[1-6] and dynamic wide angle X-ray diffraction[7-10] have been applied to investigate the nonlinear viscoelasticity. The previous studies suggested that the nonlinear viscoelastic behavior is ascribed mainly to plastic deformation such as void-opening, dislocation, slippage, and crystal defects.[1-18] Thus, for a precise understanding of the nonlinearity, it is desirable to measure the physical quantity related more directly to the plastic deformation. Hence, the author designed a new apparatus in such a way that the ultrasonic velocity and attenuation can be measured under an oscillatory deformation.

The ultrasonic wave travels by molecular interaction and therefore it is sensitive to minute changes in the material structure. Actually, Pethrick *et al.*[19,20] evaluated the molecular orientation and the crystallinity from the ultrasonic velocity data and also the amount of voids from the ultrasonic attenuation data. Thus, ultrasonic measurements will provide us more direct information about

the plastic deformation.

The purpose of this chapter is as follows: (1) to present the experimental method for measurements of ultrasonic velocity and attenuation under oscillatory deformation, *i.e.* the dynamic ultrasonic velocity and the dynamic ultrasonic attenuation, (2) to demonstrate that the change in the density under oscillatory deformation, as referred to the dynamic density, can be determined from the dynamic velocity and dynamic modulus data, and finally (3) to demonstrate the potential utility in the study of the nonlinear viscoelastic properties of polymeric solids.

3-2 Apparatus and Analysis Method

A set of acoustic apparatus was attached to Rheovibron Model DDVIIIc (Toyo Baldwin Co.,Ltd.). The block diagram of the apparatus is shown in Fig.3-1 (the sample specimen shown as the hatched portion). In the Rheovibron, an oil pressure pump drives tensile deformation, and the displacement acceptable is up to ca.16 mm. Moreover, the displacement is adjusted by servo system to balance the signal of an oscillator, and therefore one can choose various types (sinusoidal, triangular, square etc) of deformation. In this study, the sinusoidal deformation was chosen. (In the case of examining the ultrasonic properties under a constant rate of strain, the triangular deformation was chosen.) Furthermore, the apparatus is combined with a birefringence apparatus so that the birefringence can also be simultaneously measured. The direction of wave propagation was parallel to the draw direction, unless one gives notice additionally.

The analytical procedure of the dynamic ultrasonic properties will be presented below. Here, only the procedure for the attenuation coefficient is described, because the procedure for the dynamic ultrasonic velocity is quite analogous to that for the attenuation coefficient.

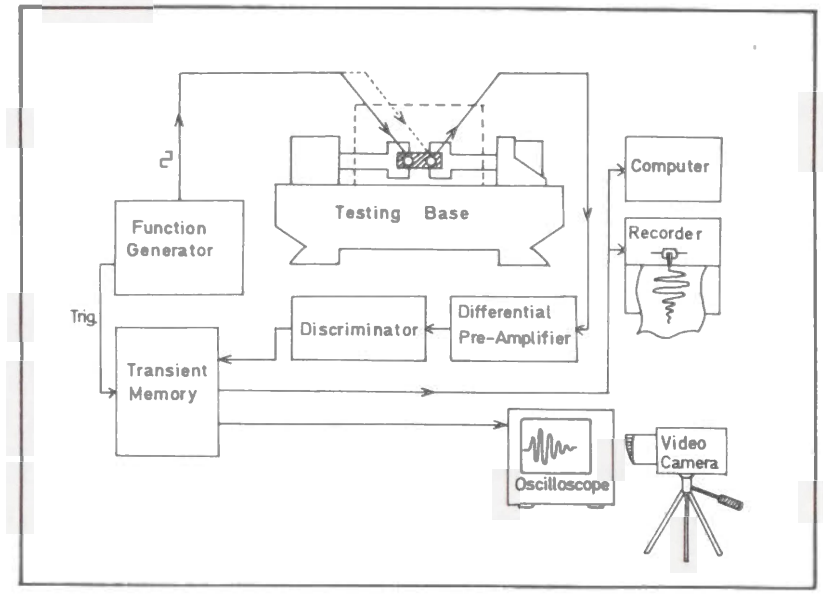

Fig.3-1 *Block diagram of the apparatus for measurements of the ultrasonic velocity and attenuation coefficient under an oscillatory deformation.*

Consider sinusoidal strain superimposed onto prestrain (*i.e.* static strain):

$$\gamma(t) = \gamma_s + \gamma_d \sin \omega t \tag{3-1}$$

where $\omega(=2\pi f)$ is the angular frequency, f the frequency in Hz, γ_s the static strain, and γ_d the dynamic strain amplitude. Then the attenuation coefficients are presumably expressed by a Fourier series as follows:

$$\alpha(t) = a_0/2 + a_1 \sin \omega t + a_2 \sin 2\omega t + \cdots\cdots$$
$$+ b_1 \cos \omega t + b_2 \cos 2\omega t + \cdots\cdots \tag{3-2}$$

The coefficients, a_o, a_n, and b_n can be calculated by Eqs.(3-3), (3-4), and (3-5), respectively.

$$a_o = \frac{\omega}{\pi} \int_0^{2\pi/\omega} \alpha(t)\, dt \tag{3-3}$$

$$a_n = \frac{\omega}{\pi} \int_0^{2\pi/\omega} \alpha(t) \sin n\omega t\, dt \tag{3-4}$$

$$b_n = \frac{\omega}{\pi} \int_0^{2\pi/\omega} \alpha(t) \cos n\omega t\, dt \tag{3-5}$$

For the fundamental component (n=1), the absolute value, in-phase, and out-of-phase of the complex attenuation coefficient, *i.e.* $|\alpha_1^*|$, α_1', and α_1''; moreover the phase difference δ_{A1} are defined by the following equations. Positive δ_{A1} means that the strain is behind the attenuation coefficient by a phase angle δ_{A1}.

$$|\alpha_1^*| = \frac{\sqrt{a_1^2 + b_1^2}}{\gamma_0} \tag{3-6}$$

$$\alpha_1' = |\alpha_1^*| \cos\delta_{A1} \tag{3-7}$$

$$\alpha_1'' = |\alpha_1^*| \sin\delta_{A1} \tag{3-8}$$

$$\delta_{A1} = \cos^{-1}\left[\frac{a_1}{\sqrt{a_1^2 + b_1^2}}\right] \tag{3-9}$$

Furthermore, the nonlinear parameter P_α of attenuation coefficient was introduced by Eq.(3-10).

$$P_\alpha = \frac{\Delta S}{\sqrt{a_1^2 + b_1^2}} \tag{3-10}$$

where ΔS is determined as the total deviation of experimental value from the fundamental wave over one cycle, which will be shown later.

The similar dynamic coefficients for the velocity were also determined in the same procedure and they are defined as follows:

$$|v_1^*| = \frac{\sqrt{a_1'^2 + b_1'^2}}{\gamma_0} \tag{3-11}$$

$$v_1' = |v_1^*| \cos\delta_{A1} \tag{3-12}$$

$$v_1'' = |v_1^*| \sin\delta_{A1} \tag{3-13}$$

$$\delta_{v1} = \cos^{-1}\left[\frac{a_1'}{\sqrt{a_1'^2 + b_1'^2}}\right] \tag{3-14}$$

$$P_v = \frac{\Delta S}{\sqrt{a_1'^2 + b_1'^2}} \tag{3-15}$$

where a_1' and b_1' are fundamental components of Fourier series for the dynamic velocity.

The dynamic experiment was usually carried out as follows: First, a given level of static strain (5%) was applied to the film specimen. After the specimen was allowed to relax for a long time, a sinusoidal strain (1-4%) was superimposed on the static strain. The frequency of the dynamic strain was 0.05 Hz. After stationary state was attained (usually about 20 cycles was required), the dynamic measurements were carried out.

3-3 Preliminary Results

In Fig.3-2, are shown examples of the attenuation coefficient plotted against the phase angle $\theta(=\omega t)$ of the dynamic strain at different levels of the dynamic strain amplitude. Quenched films of linear low density polyethylene were used.

In the figure, scattered points denote attenuation coefficients over several cycles, each of which was determined from one intermittent shot of impulsive ultrasonic wave. The ultrasonic wave usually travels between two transducers within a order of 10^{-5} sec; that is, each point is obtained instantaneously as compared with the time scale of the cyclic deformation (0.05 Hz). Hence, each attenuation coefficient can be regarded as the attenuation coefficient at a given phase angle of the sinusoidal strain. Open circles denote the average attenuation coefficient in a given interval of phase angle, and solid lines the fundamental component in the Fourier expansion.

Some characteristics are seen in Fig.3-2. First, the attenuation coefficients varied almost sinusoidally with the phase angle of strain. Second, some

phase differences were recognized between the dynamic attenuation. Third, the absolute value of the complex dynamic attenuation coefficient of the fundamental component, which is the amplitude of the change in the solid line, increased with increase in the amplitude of dynamic strain. Finally, the attenuation amplitude increased nonlinearly with respect to the strain amplitude. The nonlinear characteristics were also found in nonlinear parameter ;that is, P_αs were relatively high over the entire region of dynamic strain amplitude, and it was highest at γ_d=1.96 %.

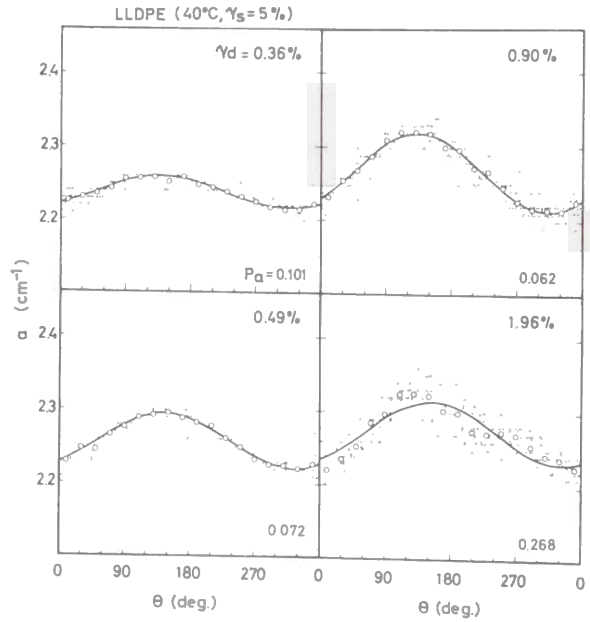

Fig.3-2 *Variation of the attenuation coefficient α with phase angle of the dynamic strain θ for LLDPE films. Points indicate attenuation coefficients obtained from each of intermittent shots; open circles indicate the average attenuation coefficients in a given interval of the phase angle, and solid lines indicate the fundamental components of Fourier expansion. P_α denotes the nonlinear parameter of the dynamic attenuation coefficient.*

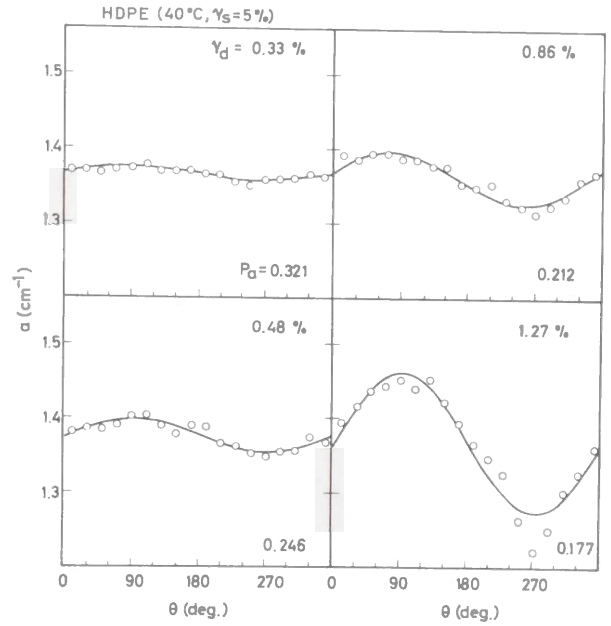

Fig.3-3 *Variation of the attenuation coefficient α with the phase angle of the dynamic strain θ for HDPE films. Open circles indicate the average attenuation coefficients in a given interval of the phase angle, and solid lines indicate the fundamental components of Fourier expansion. P_α denotes the nonlinear parameter of the dynamic attenuation coefficient.*

In Fig.3-3 are shown the analogous plots for high-density polyethylene (HDPE) films. The phase differences of the dynamic attenuation with respect to the dynamic strain were different from those for LLDPE films, as seen in comparison

with Fig.3-2. The phase differences for HDPE films were close to zero, whereas those of LLDPE films were in the fourth quadrant (270 to 360 degrees). In other words, the dynamic attenuation coefficient for HDPE films responds almost elastically with the dynamic strain, whereas that for LLDPE films lags the dynamic strain somewhat.

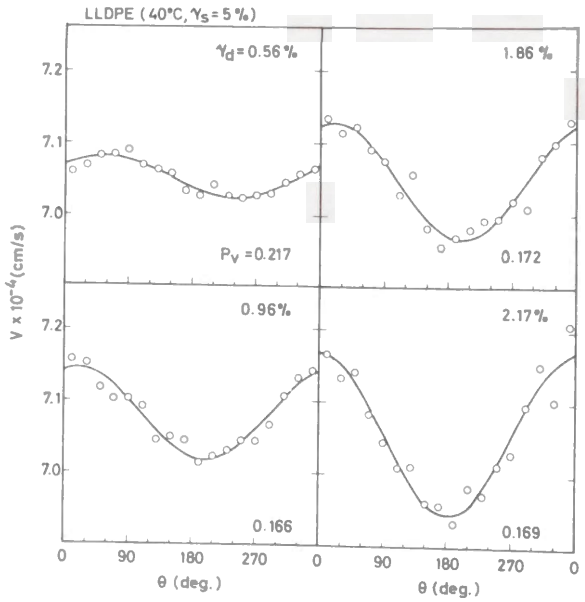

Fig.3-4 *Variation of the ultrasonic velocities v with the phase angle of the dynamic strain θ for LLDPE films. Open circles indicate the velocities at a given interval of the phase angle, and solid lines indicate the fundamental components of Fourier expansion. P_v denotes the nonlinear parameter of the dynamic velocity.*

Figs.3-4 and 3-5 show the ultrasonic velocity plotted against the phase angle of dynamic strain for LLDPE and HDPE films, respectively. As is seen in the figures, the ultrasonic velocity for both films varied sinusoidally with the dynamic strain, and the phase differences for both the films lies in the first quadrant. But a few differences are seen between the two films. First, the phase differences were close to zero for HDPE films, but not for LLDPE films. Second, the increase in the amplitude of the sonic velocity with the dynamic strain for HDPE films is larger than that for LLDPE films.

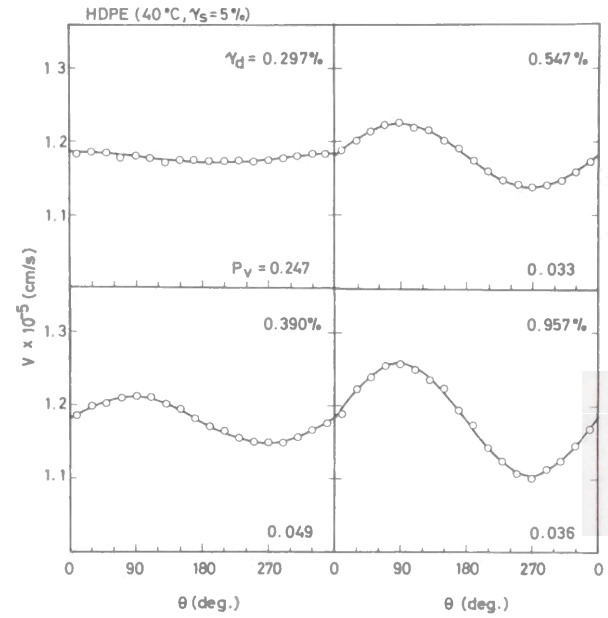

Fig.3-5 *Variation of the ultrasonic velocity v with the phase angle of the dynamic strain θ for HDPE films. Open circles indicate the velocities at a given interval of the phase angle, and solid lines indicate the fundamental components of Fourier expansion. P_v denotes the nonlinear parameter of the dynamic velocity.*

3-4 Positive and Negative Mechanism

From the physical point of view, whenever materials are subjected to cyclic deformations, all the structural changes should respond with a phase difference between 0 and 90 degrees (in the first quadrant) with respect to the strain. As is often the case, however, the phase difference does not always lie in the first quadrant. This can be explained as follows: In the case of which the phase difference is out of the first quadrant, there might exist at least two kinds of deformation mechanism contributing to a given parameter. One mechanism causes increase in the parameter with increasing strain (we call this the positive mechanism). Another causes a decrease in the parameter (we call this the negative mechanism). If only positive mechanism contributes to the quantity during the sinusoidal strain, the phase difference should be between 0 to 90 degrees. On the contrary, if only negative mechanism contributes, then the phase difference should be between 180 to 270 degrees. If both positive and negative mechanism contributes, the phase difference possibly lies at any angle, as suggested in the following equations. Total variation of the parameter $F(t)$ is assumed to be expressed by the sum of positive and negative contributions during cyclic strain, then

$$F(t) = \phi \sin(\omega t + \delta_p) - (1-\phi)\sin(\omega t + \delta_n) \tag{3-16}$$

$$= [\phi \cos\delta_p - (1-\phi)\cos\delta_n]\sin\omega t + [\phi\sin\delta_p - (1-\phi)\sin\delta_n]\cos\omega t \tag{3-17}$$

$$= \sqrt{R^2+I^2}\sin(\omega t + \delta) \tag{3-18}$$

where

$$R = \phi\cos\delta_p - (1-\phi)\cos\delta_n \tag{3-19}$$

$$I = \phi\sin\delta_p - (1-\phi)\sin\delta_n \tag{3-20}$$

$$\cos\delta = \frac{R}{\sqrt{R^2+I^2}} \tag{3-21}$$

δ_p and δ_n denote the phase differences of positive and negative mechanism, respectively, and ϕ the fraction of the positive mechanism.

In Fig.3-6, four typical examples of superposed waves are shown. The thin solid and broken lines show the waves caused by the positive and negative mechanism, respectively and the thick lines show the superposed wave. Fig.3-6a shows the case in which small amounts of negative mechanism having some phase differences (*i.e.* viscoelastic) were superimposed onto large amounts of positive mechanism having the phase difference of 0 degrees (*i.e.* elastic). This gives a phase angle in the fourth quadrant. Fig.3-6b shows the case in which small

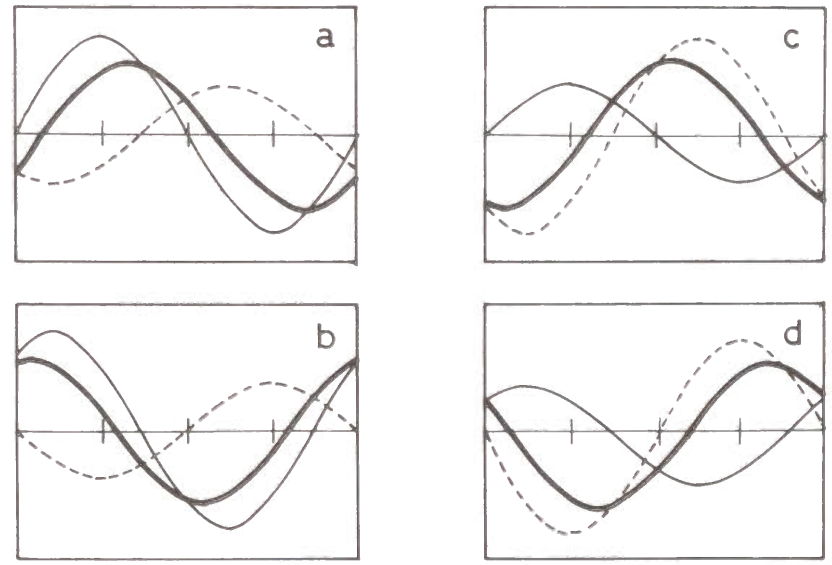

Fig.3-6 *Four typical patterns of the superposition of waves resulting from positive and negative mechanism. Solid lines show the response wave from positive mechanism; broken lines show one from the negative mechanism; and bold lines show the superposition waves.*

amounts of negative and elastic contribution were superimposed onto large amounts of positive and viscoelastic contribution. This gives a phase difference in the first quadrant. Fig.3-6c shows the case in which small amounts of positive and elastic mechanism were superimposed onto large amounts of negative and viscoelastic mechanism. This gives a phase difference in the third quadrant. Fig.3-6d shows the case of which small amounts of positive and viscoelastic contribution were superimposed onto large amounts of negative and elastic mechanism. This gives a phase difference in the second quadrant.

As described above, the phase difference of the dynamic attenuation coefficient of HDPE films was in the first quadrant. This suggests that the attenuation coefficient of the HDPE films is governed mostly by positive mechanism. The positive mechanism may be plastic deformation such as the dislocation and the formation of the crystal defects and/or voids. The generation of such plastic deformation is possibly explained by the fact that the HDPE films consist of well-organized spherulites and that they are difficult to elongate without disruption of the spherulitic structure. On the other hand, the phase difference for the LLDPE films was found in the fourth quadrant, suggesting that the attenuation coefficient is influenced not only by positive mechanism but also negative one. The negative mechanism could be orientations of lamellae, crystallites, and amorphous chains, which cause an enhancement of ultrasonic propagation and result in the decrease in the attenuation coefficient. Also, the contribution of the positive mechanism must be much smaller than that for HDPE films. this small contribution of positive mechanism can be expected from a morphological feature of LLDPE films. That is, ethyl and longer branches are not readily accommodate in the polyethylene unit cell, leading to the formation of a less-organized (disordered or incomplete) spherulitic structures. Accordingly, the crystallites orient more than the lamellae do without producing a lot of defects or voids by drawing.

The change in the dynamic velocity can be caused by the orientations of the lamellae, crystallites and amorphous chains. According to the previous rheo-

optical studies,[21,22] the orientations of lamellae and amorphous chains respond quickly to the dynamic strain (*i.e.* elastic), while that of crystallites responds with a phase lag (*i.e.* viscoelastic). In addition, the orientation of amorphous chains will contribute little in the strain range in this study. Thus, the relatively large and elastic change in the dynamic velocity for HDPE films can be ascribed mainly to the lamellae orientation, which results from the affine deformation of spherulitic structures. The relatively small and viscoelastic change in the dynamic velocity for LLDPE films can be ascribed to the orientation of crystallites. Accordingly, the effect of lamellae orientation to the dynamic velocity is larger than that of crystallites orientation. Moreover, the phase difference in the first quadrant suggests that negative mechanism such as defect and void formation contribute little to the change in the velocity under an oscillatory deformation. These observation and their interpretation are also consistent with the morphological features; that is, less-organized spherulites are formed in the HDPE films and less-organized spherulites are formed in LLDPE films.

A new apparatus in which ultrasonic velocity and attenuation coefficient can be measured under an oscillatory deformation was designed. It was found that the dynamic ultrasonic parameters were obtained with enough accuracy using the apparatus, and that the method has potential as a new tool for the study of plastic deformation in solid polymers.

3-5 Evaluation of Dynamic Density

3-5-1 Background

Density is directly related to the degree of crystallinity[23] which affects properties such as the elastic moduli, the impact strength, and the melting point. Thus, density has always been a criterion for characterizing materials.

It can be expected that density varies with deformation. An examination of the density change can be very meaningful for studies on the deformation mecha-

nism of polymeric solids. However, the change in density during deformation can not be obtained by usual methods such as density gradient sedimentation[24] or flotation.[25]

As is well known, the sonic velocity is related to the modulus and the density of the materials[26,27](see Eq.(1-3)). On the basis of that relation, there have been a number of studies in which the sonic moduli of polymeric solids have been evaluated from the sonic velocity data.[28-33] Some investigators have found a correlation between the sonic velocity and density for particular polymer systems.[19,34-39] To my knowledge, however, there has been no report in which density has been determined from the modulus and the sonic velocity. The lack of such a report may be due to the difficulty of the determination of the sonic velocity and the modulus on the same time scale. Otherwise, it may also be due to the large difference between the magnitude of deformation mechanism involved in the mechanical tests and that in the sonic velocity tests, which makes the estimation ambiguous.[36]

In this section, a method for evaluating density from the simultaneous measurements of the modulus and the sonic velocity under an oscillatory deformation will be proposed.

3-5-2 Theoretical Consideration

Consider a model composed of identical particles (oscillators) of mass M (see Fig.3-7). In the figure, a is the equilibrium separation between neighboring particles in the direction of propagation of an ultrasonic wave. Usually a is much shorter than the wavelength of the ultrasonic wave, and the width of the sound source is longer than the wavelength of the ultrasonic wave. Hence, the sonic wave can be regarded as a plane wave.[26,41] Let the spring constant and friction constant between nearest particles be K and ζ, respectively; then, the equation of motion for the n-th oscillator is as follows:

$$M\frac{\delta^2\Psi_n}{\delta t^2}=K a^2\ [\Psi_{n+1}+\Psi_{n-1}-2\Psi_n] + \zeta a^2\ [\dot{\Psi}_{n+1}+\dot{\Psi}_{n-1}-2\dot{\Psi}_n] \qquad (3\text{-}22)$$

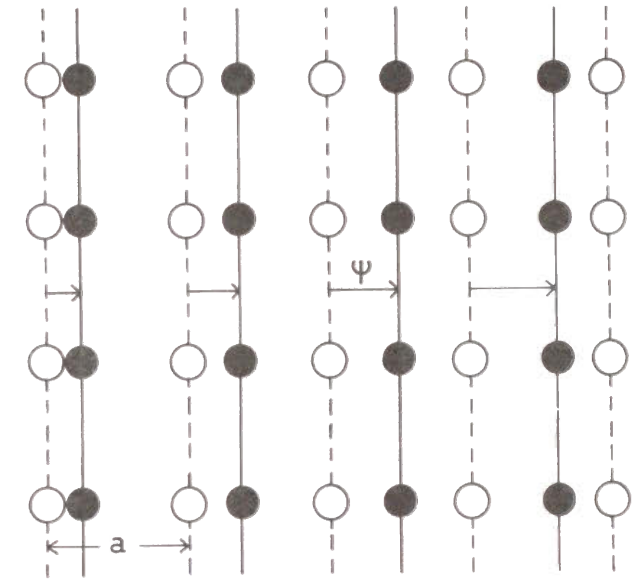

Fig.3-7 Lattice model composed of identical particles. Broken lines show the planes of particles when in equilibrium whereas solid ones show those when particles are displaced as for a longitudinal wave. a is the spacing between planes when in equilibrium, and ψ the displacement of the plane at a given distance.

where Ψ_n is the displacement (wave function) of the n-th oscillator and $\dot{\Psi}_n$ the first differentiation with respect to t. If Ψ_n does not change much from one particle to the next, then one can use the continuum approximation, and the equation of motion for $\Psi(x,t)$ is

$$M\frac{\delta^2}{\delta t^2}\Psi(x,t)=K a^2\ \left[1+\frac{\zeta}{K}\cdot\frac{d}{dt}\right]\ \frac{\delta^2}{\delta x^2}\Psi(x,t) \qquad (3\text{-}23)$$

The above equation is the wave equation for viscoelastic body. As described in the Chapter 1, if a is constant and independent of time, the solution of Eq.(3-23) is $\Psi(x,t)=\Psi_0\exp\ [i(\omega_s t-k^* x)]$, in which ω_s and k^* are the angular frequency and the wave vector, respectively. The wave vector k^* will be a complex value for viscoelastic body. Therefore, the velocity v must be a complex value ($v^*=\omega_s/k^*$). However, the imaginary part can usually be neglected. Then the sonic velocity v can be expressed by the following equation :

$$v=\sqrt{\frac{K}{M}}a \tag{3-24}$$

Thus, the sonic velocity is found to be independent of frequency. In fact, it has been found that the sonic velocity depends little on the frequency as long as the sonic frequency is not too high.[26,41] This point was confirmed experimentally. Fig.3-8 shows a plot of the traveling distance of ultrasonic wave against the traveling time for HDPE films. In the figure, data obtained using ultrasonic wave having frequency of 150 kHz and 1.4 MHz are involved. All the points fall on a straight line, the slope of which gives the ultrasonic velocity. This plot indicates that the sonic velocity is independent of frequency.

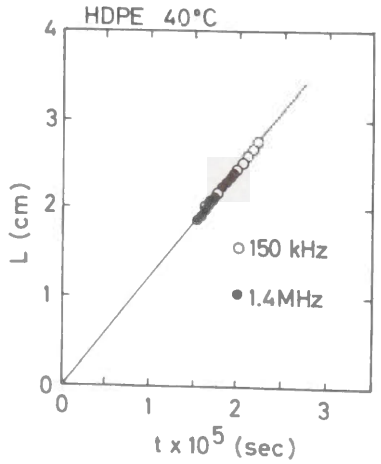

Fig.3-8 *Plot of traveling distance L of ultrasonic waves against traveling time t. The figure was obtained for HDPE films at 40° C. Open circles show the data obtained using the ultrasonic wave of 150 kHz and closed circles the data of 1.4 MHz.*

The density ρ and the modulus E of the model system can be written as in the following equations:

$$\rho=\frac{M}{Aa} \tag{3-25}$$

and

$$E=\frac{Ka}{A} \tag{3-26}$$

where A is the area of cross section that is occupied by one particle in the direction perpendicular to the propagation direction. Using Eqs.(3-25) and (3-26), the Eq.(3-24) is reduced to the well known formula: $v=\sqrt{E/\rho}$.

When the system is subjected to a sinusoidal strain:

$$\gamma=\gamma_0\exp(i\omega_0 t) \tag{3-27}$$

the distance a is also expressed by sinusoidal function with the same angular frequency ω_0:

$$a^*=\ a(i\omega_0)\gamma_0\exp(i\omega_0 t) \tag{3-28}$$

Generally speaking, when a depends on time, one can not solve the Eq.(3-23). However, when the frequency of the strain is much lower than the frequency of the sonic velocity, Eq.(3-23) can be solved by assuming that a is constant at each instant of the deformation. That is, the sonic velocity at each instant of the deformation can be determined by Eq.(3-24). Then, the dynamic velocity v^* can be expressed by substituting Eq.(3-28) into Eq.(3-24);

$$v^*=\frac{K}{M}a^*=\frac{K}{M}a(i\omega_0)\gamma_0\exp(i\omega_0 t) \tag{3-29}$$

Accordingly, the velocity varies sinusoidally in response to sinusoidal change of the strain. This point was also confirmed experimentally. As already shown in Figs.3-4 and 3-5. As is expected from Eq.(3-29), the dynamic velocity varied almost sinusoidally with the sinusoidal strain and the amplitude of the velocity

increased with increasing strain amplitude.

The stress can be also expressed by sinusoidal function with the angular frequency ω_0:

$$\sigma^* = \frac{K}{A} a^* = \frac{K}{A} a(i\omega_0)\gamma_0 \exp(i\omega_0 t) \tag{3-30}$$

The dynamic modulus can be expressed by the following equation.

$$E^* = \frac{K}{A} a(i\omega_0) \tag{3-31}$$

It should be noted that the stress does not depend on the mass of oscillator M (an inertia term), but that the sonic velocity does. The mass appears to change with the dynamic deformation. That is, the apparent changes in the mass may be caused by generation of defects such as cracks, dislocations, and microvoids, and also by orientation of lamellae, crystallites, and amorphous chains. The generation of defects may cause decrease in M, whereas the orientation of polymer chains may cause increase in M. Hence, M should be treated as a complex quantity.

Consequently, the dynamic density ρ^* can be defined as in the following equation:

$$\frac{\rho^*}{\gamma_0} = \frac{M^*}{Aa(i\omega_0)} \tag{3-32}$$

The magnitude of the dynamic density can be calculated from those of the modulus Eq.(3-31) and the dynamic velocity Eq.(3-24) as follows;

$$\frac{|\rho^*|}{\gamma_0} = \frac{|E^*|}{(|v^*|/\gamma_0)^2} \tag{3-33}$$

and the phase difference of the dynamic density has the form:

$$\tan\delta_D = \tan(\delta - 2\delta_v) \tag{3-34}$$

where δ and δ_v are the phase differences of the dynamic stress and sonic velocity with respect to the dynamic strain, respectively.

It should also be pointed out that the dynamic density thus obtained

represents the dynamic density in the direction of sonic wave propagation (or strain). The measurement of the dynamic velocity perpendicular as well as parallel to the strain direction enables us to estimate the dynamic Poisson's ratio. For the purpose, however, it is necessary to use a transient memory with which one can observe the ultrasonic wave in a time interval less than 0.1 nsec, or to use a very thick sample specimen.

Some conditions are required for the determination of the dynamic density, resulting from above discussions. The requirements are summarized as follows: (1) The diameter of the acoustic beam is sufficiently large in comparison with the wavelength of sonic waves and is comparable with the width of specimen films. Plane sonic wave is necessary in this approach. If the sonic wave is a plane wave, the corresponding modulus is Young's modulus. (2) The frequency of sonic waves is sufficiently high in comparison with that of the dynamic strain. (3) The sonic wave must be a longitudinal elastic wave which depends little on the frequency.

In this study, the diameter of transducer was 0.72 cm, the width of the specimen 1.0 cm, the frequency of sonic waves 150 kHz, and dynamic strain 0.05 Hz. This experimental condition satisfies requirements (1) and (2). It was experimentally confirmed that the velocity was independent of the frequency, as mentioned above. The velocity was determined by the traveling time of the first wave which has arrived at transducer after traveling through the sample specimen. The first wave must be longitudinal wave as is verified by theoretical consideration[26] (see Chapter 1). The theory says that longitudinal waves are faster than all other waves such as the shear and Rayleigh waves in solids. Furthermore, the sonic velocities of polyethylenes obtained in this study were comparable to those of polyethylenes obtained by Davidse *et al.*[38] who measured the ultrasonic velocity of low frequency longitudinal oscillations by a resonance method. Thus, the requirement (3) is also satisfied.

REFERENCES

1. S. Onogi, D. A. Keedy, and R. S. Stein, *J. Polym. Sci.*, **50**, 153 (1961).
2. R. S. Stein, S. Onogi, and D. A. Keedy, *ibid.*, **57**, 801 (1962).
3. R. S. Stein, S. Onogi, K. Sasaguri, and D. A. Keedy, *J. Appl. Phys.*, **34**, 80 (1963).
4. R. Yamada and R. S. Stein, *ibid.*, **36**, 10 (1965).
5. D. G. LeGrand and P. F. Erhart, *Trans. Soc. Rheol.*, **6**, 301 (1962).
6. R. Yamada, C. Hayashi, S. Onogi, and M. Horio, *J. Polym. Sci.*, **C5** 123 (1964).
7. H. Kawai, T. Itoh, D. A. Keedy, and R. S. Stein, *J. Polym. Sci. Polym. Lett. Ed.*, **2**, 1075 (1964).
8. T. Kawaguchi, T. Itoh, H. Kawai, and R. S. Stein, *Macromolecules*, **1**, 126 (1968).
9. A. Tanaka, E. P. Chang, B. Delf, I. Kimura, and R. S. Stein, *J. Polym. Sci. Polym. Phys. Ed.*, **11**, 1683 (1973).
10. S. Suehiro, T. Yamada, H. Inagaki, T. Kyu, S. Nomura, and H. Kawai, *ibid.*, 17, 763 (1979).
11. A. Tanaka, M. Fukuda, H. Nagai, and S.Onogi, *Repts. Progr. Polym. Phys. Japan*, **22**, 297 (1979).
12. A. Tanaka, H. Nagai, and S.Onogi, *ibid.*, **22**, 451 (1979).
13. A. Tanaka, H. Nagai, M. Shinohara, and S.Onogi, *ibid.*, **24**, 297 (1981).
14. A. Tanaka, M. Shinohara, and S.Onogi, *ibid.*, **25**, 367 (1982).
15. A. Tanaka, H. Nagano, and S. Onogi, *ibid.*, **25**, 361, 363, & 369 (1982).
16. A. Tanaka, and S. Onogi, *Polym. Eng. Rev.*, **3**, 235 (1983).
17. A. Tanaka, M. Fukuda, H. Nagai, and S.Onogi, *J. Polym. Sci. Polym. Phys. Ed.*, **27**, 2283 (1989).
18. A. Tanaka, H. Nagano, M. Shinohara, and S. Onogi, *Polym. J.*, **20**, 987 (1988).
19. K. Adachi, G. Harrison, J. Lamb, A. M. North, and R. A. Pethrick, *Polymer*, **22**, 1026 (1981).
20. R. A. Pethrick, *Prog. Polym. Sci.*, **9**, 197 (1983).
21. S. Onogi, A. Tanaka, Y. Ishikawa, and T. Igarashi, *Polymer J.*, **7**, 467 (1975).

22. A. Tanaka, E. P. Chang, B. Delf, I. Kimura, and R. S. Stein, *J. Polym. Sci., Polym. Phys. Ed.*, **11**, 1891 (1973).
23. S. Kavesh and J. M. Shultz, *Polym. Eng. Sci.*, **9**, 331 (1969).
24. M. S. Meselson, F. W. Stahl, and T.Vinogard, *Proc. Natl. Acad. Sci.*, **43**, 581 (1957).
25. R. M. Roberts, J. C. Gilbert, L. B. Rodeward, and A. S. Wingrove, "*An Introduction to Modern Experimental Organic Chemistry*," Halt, Rinehalt and Winston Inc. New York, 1969.
26. L. D. Landau and E. M. Lifshitz, "*Theory of Elasticity*," Addison-Wesley, Reading, Mass. 1964, Ch.1 and 3.
27. J. W. Ballou and S. Silverman, *Textile Research J.*, **14**, 282 (1944).
28. W. W. Moseley, *J. Appl. Polym. Sci.*, **3**, 266 (1960).
29. O. K. Chen, F. C. Chen, C. L. Choy, and I. M. Ward,, *J. Phys. D.*, **11**, 617 (1978).
30. J. C. Seferis and R. J. Samuels, *Polym. Eng. Sci.*, **19**, 975 (1979).
31. W. P. Leung, F. C. Chen, C. L. Choy, A. Richardson, and I. M. Ward, *Polymer*, **25**, 447 (1984).
32. A. M. Ibrahim, A. R. Wedgewood, and J. C. Seferis, *Polym. Eng. Sci.*, **26**, 593 (1986).
33. G. Hinrichsen, S. M. Sdat-Darbandi, and A. Al-Irobaidi, *Polym. Bull.*, **13**, 15 (1985).
34. R. J. Urick, *J. Polym. Sci.* A-2., **3**, 1741 (1978).
35. H. A. Waterman, *Kolloid Z.*, **192**, 9 (1975).
36. P. D. Davidse, H. I. Waterman, and J. B. Westerdijk, *J. Polym. Sci.*, **59**, 389 (1962).
37. J. Schuyer, *J. Polym. Sci.*, **36**, 475 (1959).
38. A. Levene, W. J. Pullen, and J. Roberts, *J. Polym. Sci.* Part A., **3**, 697 (1965).
39. L. Piché, *Polym. Eng. Sci.*, **24**, 1354 (1984).
40. W. P. Mason, "*Physical Acoustics and the Properties of Solids*," Van Nostrand Co. New York (1958).
41. A. B. Bhatia, "*Ultrasonic Absorption*," Oxford Univ. Press, London 1967.

CHAPTER 4

DYNAMIC ULTRASONIC STUDIES OF MECHANICAL NONLINEARITY
(1) UNDRAWN POLYETHYLENE FILMS

4-1 Introduction.

When a polymeric specimen is subjected to a sinusoidal strain, the resulting stress is not sinusoidal. The deviations from a linear response is greater in particular for crystalline polymers. The mechanical nonlinearity can be attributed to plastic deformation caused by disruption of their superstructure.[1] Therefore, the nonlinearity depends largely on molecular aggregation states in the superstructure. The aim of this chapter is to elucidate the nature of the nonlinear behavior for undrawn polyethylene films having spherulitic structure from structural points of view. For the purpose, the dynamic deformation mechanism in the nonlinear regions was investigated using the dynamic ultrasonic measurements. In this chapter, the nonlinearity is restricted to that observed at rather small strains under which macroscopic necking cannot be recognized, and also above room temperature, that is, in the alpha dispersion region. The nonlinearity under large scale deformation will be discussed in the Chapter 6.

Many morphological studies have been carried out on polyethylene films. The morphology of the bulk-crystallized polyethylene is briefly described below. The superstructure of the polyethylene is usually spherulitic[2] with the b-axis directed along the radius and with the a- and c-axes helicoidally oriented perpendicular to the b-axis with more-or-less radial order.[3] The b-axis is believed to lie in the direction of the extension of the lamellae. The stretching of polyeth-

ylene is accompanied by deformation of spherulites.[4] The deformation is not simply affine. It involves crystal reorientation within the deformed spherulite. The reorientation process is not the same throughout the spherulite. The principal mechanism at small deformation in the equatorial part of the spherulite has been postulated to be a twisting of the lamellae about their *b*-axis so as to turn the *c*-axis (chain direction) toward the stretching direction.[5-9] In the 45°to polar parts of the spherulite, shearing of the lamellae leads to chain tilt with respect to the lamellar plane.

It is expected that plastic deformation in polyethylene will be influenced by the aggregation state of crystallites in spherulites. The aggregation state depends largely on short branches in polyethylene molecules.[10,11] Hence, the blend films of high density and linear low density polyethylenes were employed.

4-2 Experimental

4-2-1 Materials

High density (linear) polyethylene (HDPE) and linear low density polyethylene (LLDPE), ethylene/butene-1 copolymer, were supplied from Mitsui Petrochem. Inc. Ltd. The number and weight average molecular weights, and their ratio were 1.3×10^4, 7.0×10^4, and 5.4 for the HDPE, and 1.4×10^4, 1.0×10^5, and 7.6 for the LLDPE. The LLDPE polymers contain ethyl branches of about 3.7 per 100 backbone carbon atoms.

Pellets of the two polymers were blended with various proportions in a solution of xylene at 110° C. The polymers were precipitated in methyl alcohol and dried in a vacuum oven at room temperature. They were melt pressed in a laboratory press for 10 min. at ca. 200℃ and ca. 100 kg/cm². The films prepared by quenching the polymer melts into ice-water bath (0° C) was provided for the measurement. The following compositions were employed: A100/C0, A75/C25, A50/C50, A25/C75, and A0/C100. (Code A denotes the HDPE, code C the LLDPE, and numeral the percentage by weight of the materials.)

4-2-2 Characterization of Film Specimen

Density of the quenched films was determined by a flotation method.[12] The binary medium prepared from various ratios of distilled water and ethyl alcohol was used. The densities of A100/C0, A75/C25, A50/C50, A25/C75, and A0/C100 were 0.943, 0.930, 0.925, 0.920, and 0.912 g/cm³, giving the degrees of crystallinity[13-15] of 60.7, 51.7, 48.7, 44.8, and 39.3 %, respectively.

Light scattering pictures were taken using a photographic camera under the Hv polarization condition (polarization direction is vertical with an analyzer in horizontal direction). A He-Ne laser of wavelength 632.8 nm was used. The Hv-light scattering pictures showed the so-called "*four-leaf clover*" pattern for all the films (see Fig.4-1), indicating the formation of spherulites. The pattern of HDPE films was clear and intense, indicating that spherulites are well-organized.

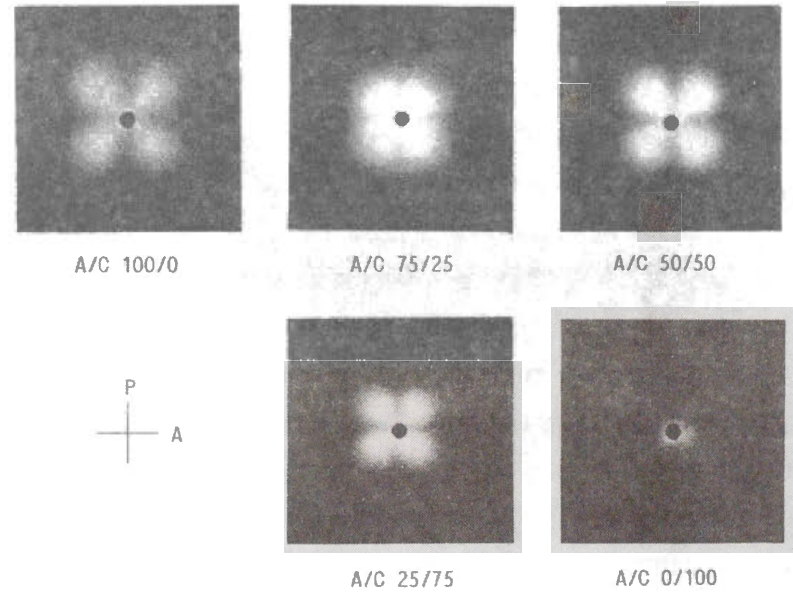

Fig.4-1 *Hv-light scattering patterns for HDPE(A), LLDPE(C), and their blend films at room temperature.*

On the other hand, the pattern of LLDPE films was faint and diffused, indicating that spherulites are less-organized (incomplete or disordered). The observations are consistent with the previous findings[16]: ethyl or longer branches are not accommodated in the polyethylene unit cell.

Hv patterns of A75/C25 and A25/C75 films showed overlapping of two sizes of four-leaf clover patterns. This dual pattern may result from two different sizes of spherulites. Such a dual pattern was not seen in A50/C50 films. It should be mentioned that the observation of a single four-leaf clover pattern is not an adequate proof of cocrystallization. That is, if separate crystals are formed between the components, there is a possibility that these crystals may be incorporated in a single kind of spherulite, as demonstrated by Stein *et al.*[16-18]

Dynamic mechanical properties were determined with a direct-reading dynamic viscoelastometer, Rheovibron Model DDVIIc (Toyo Baldwin Co. Ltd.). Measurements were conducted at 110Hz between -150° and ca.100° C. The sample specimen was cooled from room temperature to -150°C and subsequently slowly heated up at a rate of ca. 1° C/min. In the measurement, both static and dynamic strain are quite small; consequently, the viscoelastic properties of materials behave linearly.

Figs.4-2 and 4-3 show the temperature dependence of the dynamic modulus E', the loss modulus E'', and the loss tangent tan δ for all the films. As is apparent from the figures, three dispersion peaks, namely the alpha, beta, and gamma dispersion, are seen. On the gamma peak appearing at the lowest temperature (ca -110° C), no significant difference is seen among the films. This is plausible since the gamma dispersion is associated with a minute vibration of local elements of the chain-segmental motion.[19,20] On the beta dispersion appearing at ca. -20°C for all other films except A100/C0 films, its magnitude increases with increasing the content of LLDPE. This is consistent with the previous suggestion[21,22]: the beta dispersion is associated with the rotational isomerism of movement of branches. On the alpha dispersion, the temperature at its maximum changed widely with HDPE/LLDPE component. For LLDPE films, the alpha dispersion appears at ca. 40°-50°C, that for HDPE films at ca. 80°-110°C, and that for blend films at

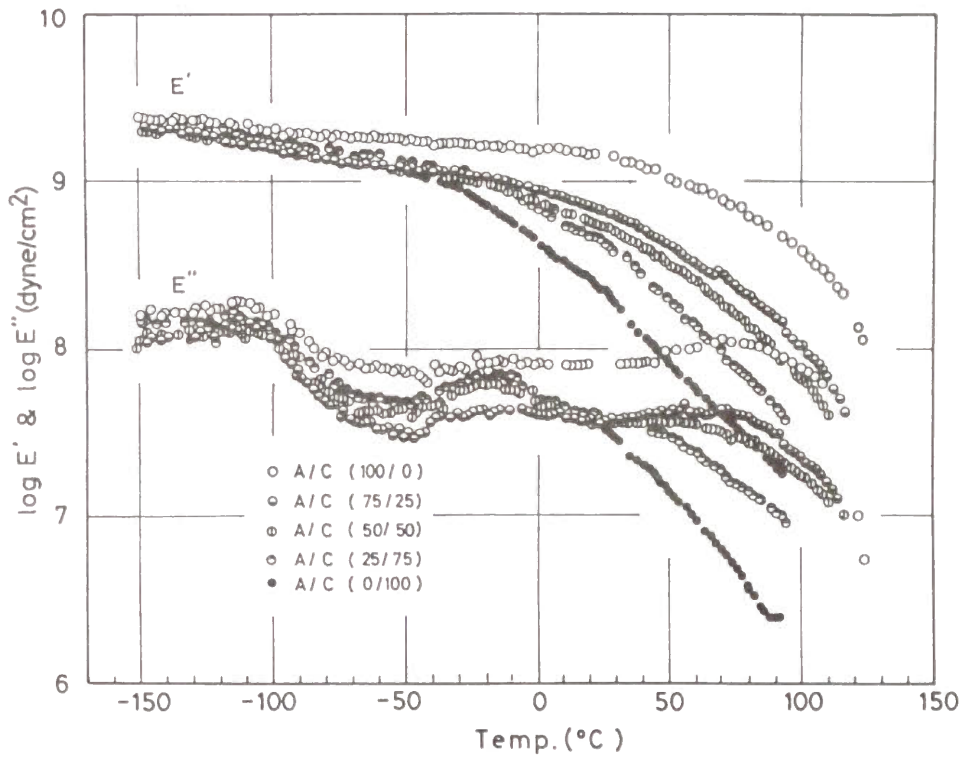

Fig.4-2 *Variation of the mechanical storage modulus E' and loss modulus E'' with temperature for the HDPE(A), LLDPE(C), and their blend films. The frequency used was 110 Hz.*

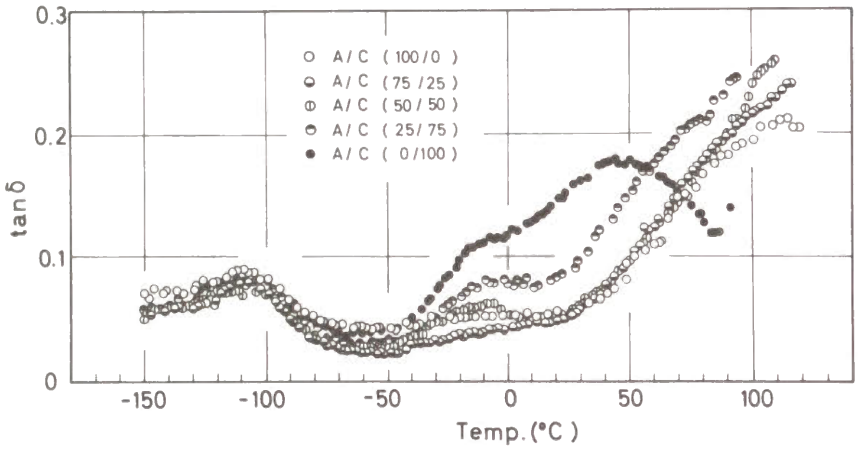

Fig.4-3 *Variation of mechanical loss tangent tan δ with temperature for HDPE(A), LLDPE(C), and their blend films. The frequency used was 110 Hz.*

the intermediate temperatures. The alpha dispersion is considered to be associated with the deformation of crystallites such as tilting of crystallites and twisting of lamellae.[23-28] Such deformation can be strongly influenced by the alignment (or packing) of crystallites in the spherulites. Thus, it is suggested that the crystallites align (or pack) in the different manners among the films.

Tensile tests were also carried out at room temperature using Tensilon UTM-4L (Toyo Baldwin Co. Ltd.) (see Fig.4-4). The drawing speed was 2 cm/min. A significant yield appeared on the stress-strain curves of A100/C0 and A75/C25 whereas no yield on the curves of A25/C75 and A0/C100. The curve of A50/C50 showed the intermediate shape and magnitude between the two curves.

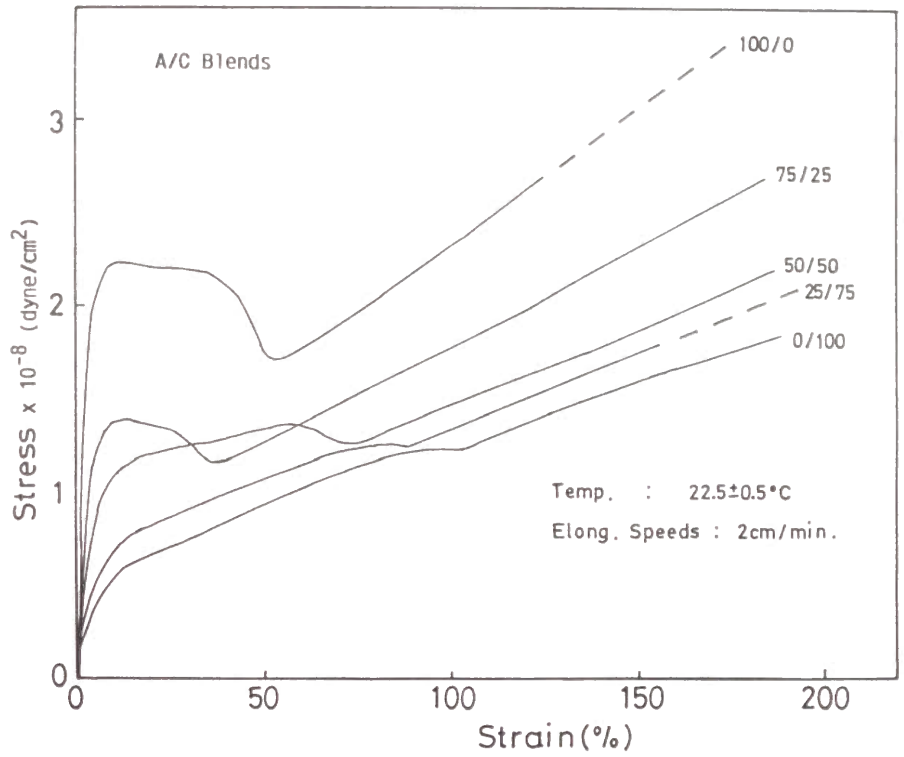

Fig.4-4 *Stress-Strain curve for HDPE(A), LLDPE(C), and their blend films at room temperature.*

The ultrasonic attenuation coefficient and the velocity were measured in the temperature range between room temperature and 100°C (see Figs.4-5 and 4-6). The attenuation coefficient increases with increasing temperature for all the films. The more the LLDPE content, the higher the attenuation coefficient is. The ultrasonic velocity, on the other hand, decreases with increasing temperature for all the films. The more the LLDPE content, the lower the velocity is.

The increase in attenuation and the decrease in velocity result from the "softening" due to the increase in temperature and/or in LLDPE components. The softening effect was also seen in the linear dynamic mechanical and tensile properties.

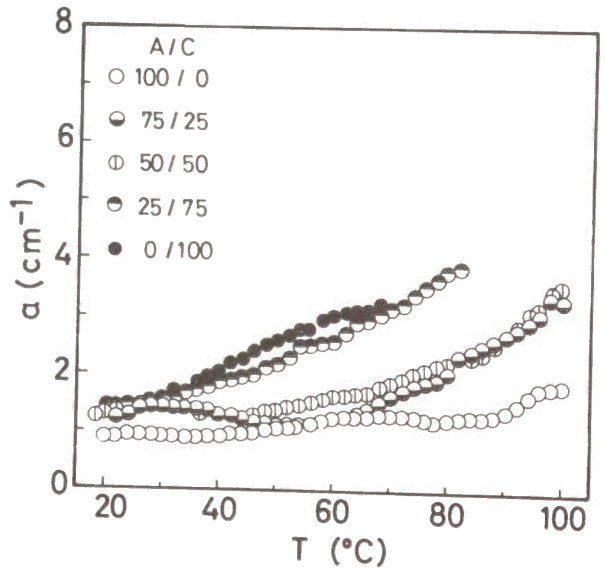

Fig.4-5 *Temperature dependence of attenuation coefficient for HDPE(A), LLDPE(C), and their blend films.*

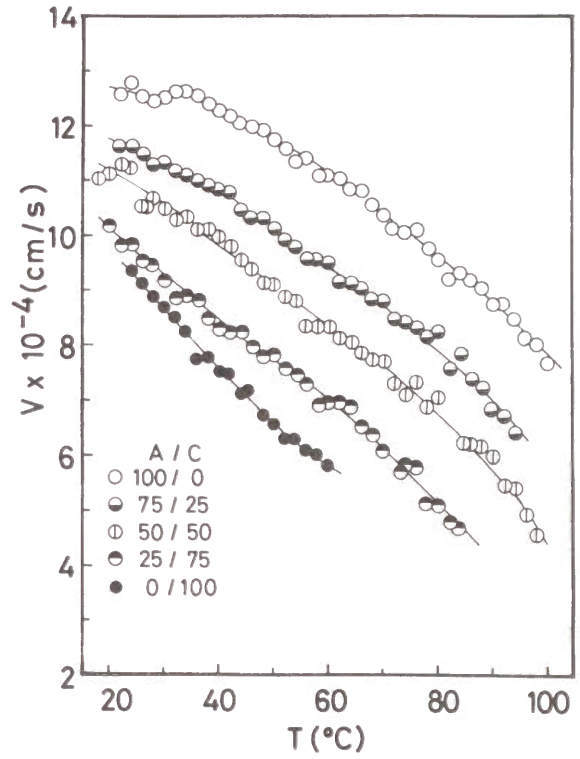

Fig.4-6 *Temperature dependence of ultrasonic velocity for HDPE(A), LLDPE(C), and their blend films.*

4-2-3 Dynamic Mechanical and Optical Coefficients

The dynamic mechanical properties and the dynamic birefringence were measured at 30°, 40°, and 50°C simultaneously with the dynamic ultrasonic velocity and attenuation. The dynamic parameters were determined from the first harmonic term in the Fourier expansion of these dynamic responses, as described in

Chapter 3. The amplitude of the complex modulus $|E_1^*|$ and the phase difference δ_1 were determined from the dynamic mechanical measurements. The amplitude of the complex strain optical coefficient $|K_1^*|$ and the phase difference δ_{B1} were determined from the dynamic birefringence measurements. Positive δ_1 or δ_{B1} means that the strain lags the stress or birefringence by the phase angle δ_1 or δ_{B1}, respectively. Also, the mechanical and optical nonlinear parameters P_σ and P_Δ were introduced as a measure of mechanical and optical nonlinearities, respectively.[27] The nonlinear parameter is defined as the total deviation of experimental stress wave (or birefringence wave) from the fundamental wave of stress (or birefringence) over one cycle. The dynamic response is always nonlinear when the nonlinear parameter is not zero; however, the response is not always linear when the nonlinear parameter is zero because the parameter becomes zero whenever the time-dependent and strain-dependent response terms are separable and at least one term is linear.

Birefringence meaurements were carried out using a He-Ne laser (632.8 nm). The laser beam is polarized by a polarizer at 45° to the stretching direction, passes through the sample and an analyzer oriented perpendicular to the polarizer, and passes into a photomultiplier. The transmitted intensity is recorded by a pen recorder or a transient computer memory and is then converted to birefringence by the following equations:

$$T = A \sin^2(\Gamma/2) \tag{4-1}$$

where T and Γ are the transmitted intensity and the retardation, and A the arbitrary constant.

$$\Delta n = (\lambda \Gamma)/(2\pi d) \tag{4-2}$$

where Δn is the birefringence, λ the wavelength of light, and d the thickness of film specimen.

4-3 Results and Discussion

4-3-1 Dynamic Mechanical and Optical Properties

In Fig.4-7, the dynamic mechanical coefficients for all the films are plotted against the dynamic strain amplitude. The absolute value of complex modulus $|E_1^*|$ increased with increasing HDPE content at each temperature, and it decreased with increasing temperature. Furthermore, the $|E_1^*|$ decreased with increasing the dynamic strain amplitude and the decrease in $|E_1^*|$ was greater for films having higher HDPE contents. This indicates that the strain-dependent nonlinearity is greater for HDPE-rich films. However, the nonlinear parameters P_σ's were extremely small and almost independent of γ_d except those of the A100/C0 and A75/C25 films at 30°C. The low P_σ means that the time-dependent nonlinearity is low.

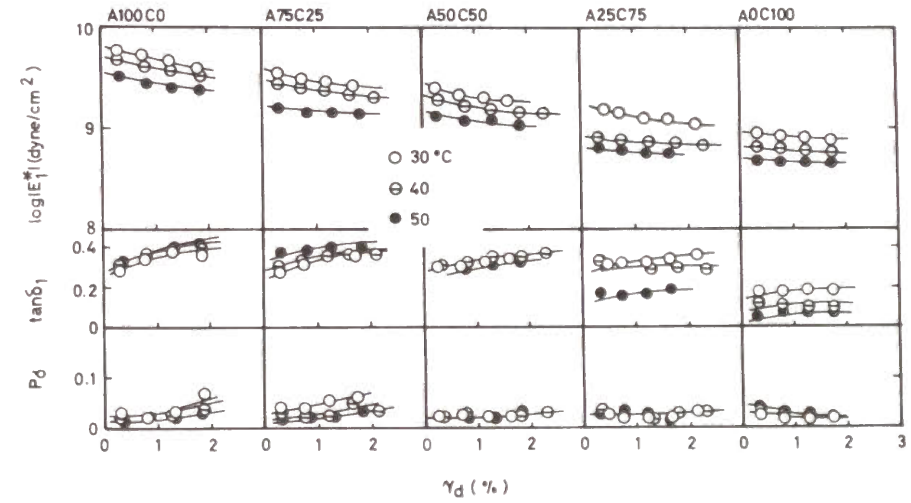

Fig.4-7 *Dynamic strain dependence of* $|E_1^*|$, $\tan\delta_1$, *and* P_σ *at different temperatures for HDPE(A), LLDPE(C), and their blend films.*

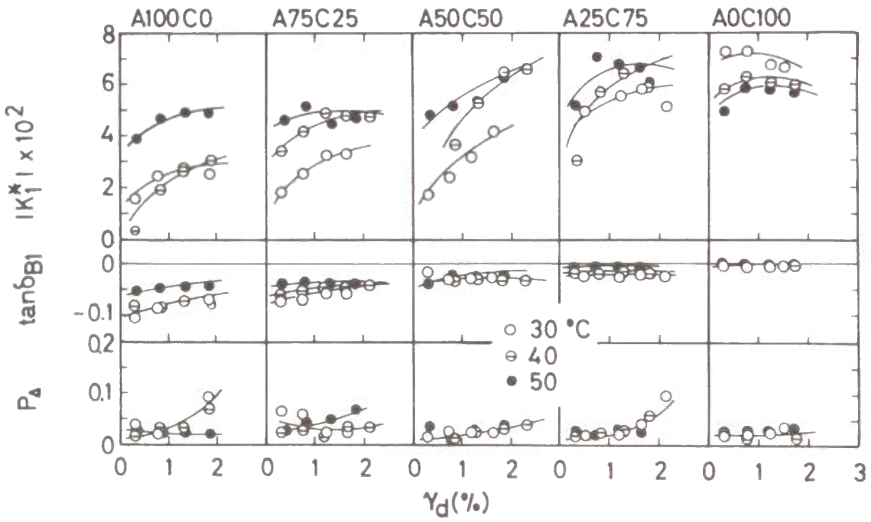

Fig.4-8 *Dynamic strain dependence of* $|K_1^*|$, $\tan\delta_{B1}$, *and* $P\Delta$ *at different temperatures for HDPE(A), LLDPE(C), and their blend films.*

In Fig.4-8, the optical coefficients are plotted against the dynamic strain amplitude. As the LLDPE content increases, the absolute value of the complex strain-optical coefficient $|K_1^*|$ increases, reflecting better orientation of crystallites and amorphous chains.

It should be noted that $\tan\delta_{B1}$ was negative for all the films and it approached zero as the LLDPE-content increased or as the temperature increased. The negative $\tan\delta_{B1}$ indicates that the birefringence lags behind the applied sinusoidal strain. This is interpreted as follows: When polyethylene films having spherulites, which consist of lamellae grown in the radial direction, are stretched,

the elastic orientation of lamellae in addition to the viscoelastic orientation of crystallites within lamellae and amorphous chains will occur.[5,28-32] The lamellae orientation leads to a negative birefringence because of the orientation of *b*-axis. The orientations of crystallites and amorphous chains, on the other hand, lead to the positive birefringence as a consequence of the orientation of *c*-axis. The superposition of positive and negative contributions causes the phase lag with the strain, *i.e.* a negative $\tan\delta_{B1}$, (see Fig.3-6a). Thus considered, the negative $\tan\delta_{B1}$ can be related to the completeness of the spherulitic structure, Accordingly, the results for $\tan\delta_{B1}$ indicate that the spherulitic structure becomes more complete as the HDPE content increases.

The optical nonlinear parameter $P\Delta$ depended little on γ_d and was close to zero for all the films in spite of the fact that $|K_1^*|$ extremely increased with increasing γ_d. The higher the HDPE content, the greater the dependence of the dynamic strain on $|K_1^*|$ was. These results suggest that the optical nonlinearity is not time-dependent but strain-dependent and also that the strain-dependent nonlinearity are greater as the HDPE content increases.

In conclusion, the mechanical and optical nonlinearities became greater for the films having higher HDPE content. The nonlinearities were considered to be dependent of the completeness of the crystallites alignment in spherulites.

4-3-2 Dynamic Attenuation Coefficient

Figs.4-9 shows two typical variations of the amplitude of dynamic attenuation coefficient with respect to the dynamic strain amplitude at different temperature. One is for the A75/C25 films (a), and another for the A25/C75 films (b). As is obvious from the figures, $|\alpha_1^*|$ increases nonlinearly with γ_d for both films: $|\alpha_1^*|$ curved downward in the low γ_d range, and then increases linearly in the high γ_d range. The temperature dependence, however, was classified into two cases, depending on the HDPE content. For the A75/C25 films, $|\alpha_1^*|$ becomes lower with increasing temperature, as shown in Fig.4-9a. This temperature

(a)

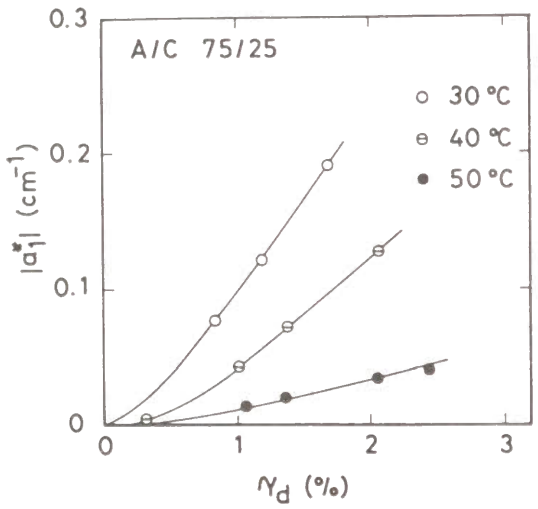

(b)

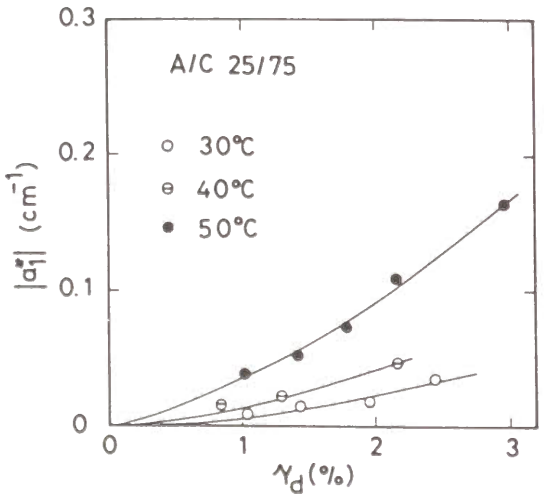

Fig.4-9 *Variation of* $|\alpha_1^*|$ *with dynamic strain amplitude* γ_d *for A75/C25 and A25/C75 films.*

dependence was also seen in the A100/C0 and A50/C50 films. For the A25/C75 films, on the other hand, $|\alpha_1^*|$ becomes greater with increasing temperature, as shown in Fig.4-9b. This temperature dependence was also seen in the A0/C100 films. This difference in temperature dependence of $|\alpha_1^*|$ is clearly demonstrated in Fig.4-10. The figure shows the values of $|\alpha_1^*|$ at γ_d=1.2 % plotted against the blend ratio at different temperatures. Also, as shown in Fig.4-10, the more the HDPE content, the higher $|\alpha_1^*|$ becomes.

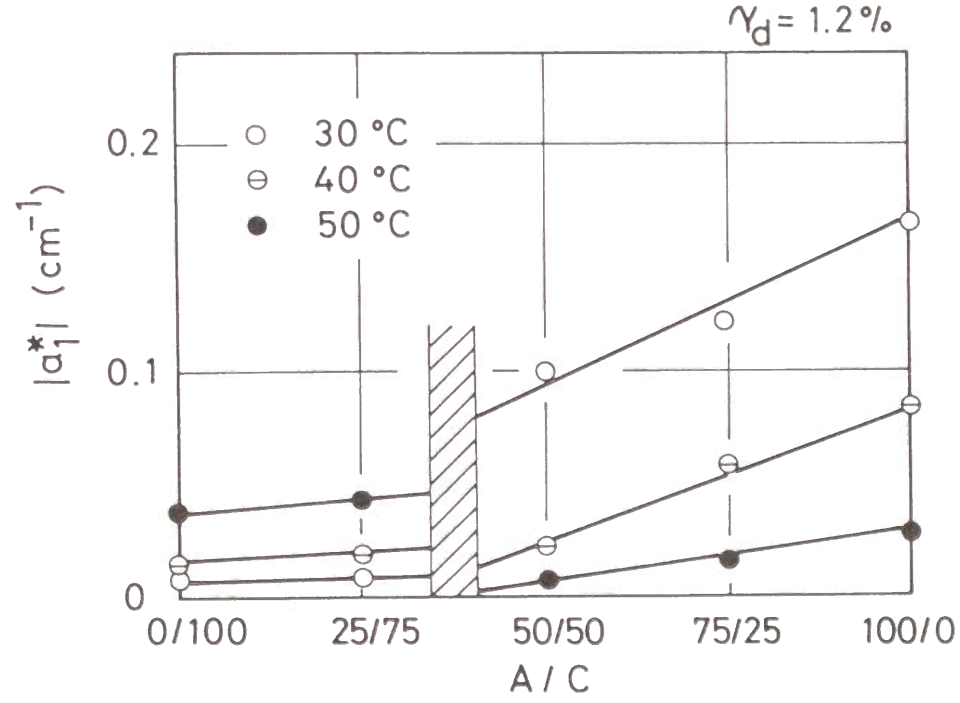

Fig.4-10 *Variation of* $|\alpha_1^*|$ *with blend ratio at* γ_d *of 1.2 % at different temperatures.*

Fig.4-11 shows the variation of the phase difference of the dynamic attenuation coefficient with respect to the dynamic strain amplitude at different temperatures. In the figure, the dynamic strain amplitude γ_d is taken in the radial direction and the phase angle δ_{A1} is taken in the counter-clockwise direction.

As is seen from Fig.4-11, δ_{A1}'s of A100/C0 and A75/C25 films, *i.e.* HDPE-rich films, are around zero degrees, indicating that the attenuation coefficient increases almost in phase with the dynamic strain. Those of LLDPE-rich films, on the other hand, in particular for A25/C75 are around 180 degrees, indicating that the attenuation coefficient decreases almost in phase with the dynamic strain. As mentioned in Chapter 3, the increase in the attenuation coefficient will be ascribed to scattering associated with crystal defects and/or microvoids which are caused on the stretching process during a cycle deformation. The decrease in the attenuation will be ascribed to the orientation of lamellae, crystallites, and amorphous chains, since the orientation enhances the ultrasonic wave propagation.

These points will be approved by the morphological feature whether tightly or loosely crystallites align in the spherulites. In the case of HDPE-rich films in which crystallites align tightly or well-organized, spherulitic structure disrupts, when the spherulites deform. The disruption accompanies the formation of crystal defects and microvoids. The greater $|\alpha_i^*|$ at lower temperatures may be ascribed to better formation of defects and microvoids at lower temperatures. In the case of LLDPE-rich films in which crystallites align loosely, on the other hand, the crystallites and/or molecular chains can orient without disrupting spherulites. As a result, the attenuation coefficient decreases on stretching process. The greater $|\alpha_i^*|$ at higher temperatures may be ascribed to better orientation at higher temperatures.

Some δ_{A1}'s lie in the second and fourth quadrant. The phase difference indicates that both positive and negative deformation mechanism contribute to the attenuation coefficient: one is the positive deformation mechanism by which the attenuation coefficient is enhanced, and the other the negative deformation

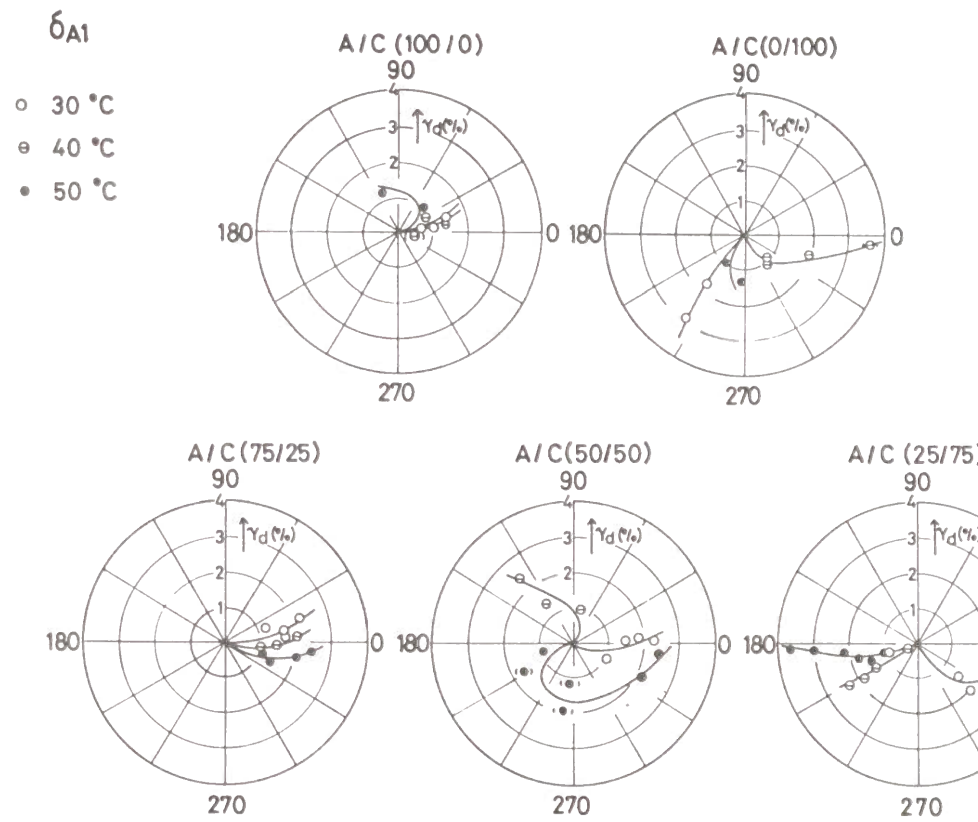

Fig.4-11 *Variation of the phase difference of the dynamic attenuation coefficient with dynamic strain amplitude at different temperatures. The dynamic strain amplitude γ_d is taken in the radial direction and the phase difference δ_{A1} is taken in the counter-clockwise direction.*

mechanism by which the attenuation coefficient is lowered. This point is revealed on the plot of the attenuation coefficient vs. the phase angle of dynamic strain at 50°C for the A50/C50 films (see Fig.4-12). In Fig.4-2, the open circle indicates the average attenuation coefficients in a given interval of phase angle θ, and solid lines the fundamental component in Fourier expansion.

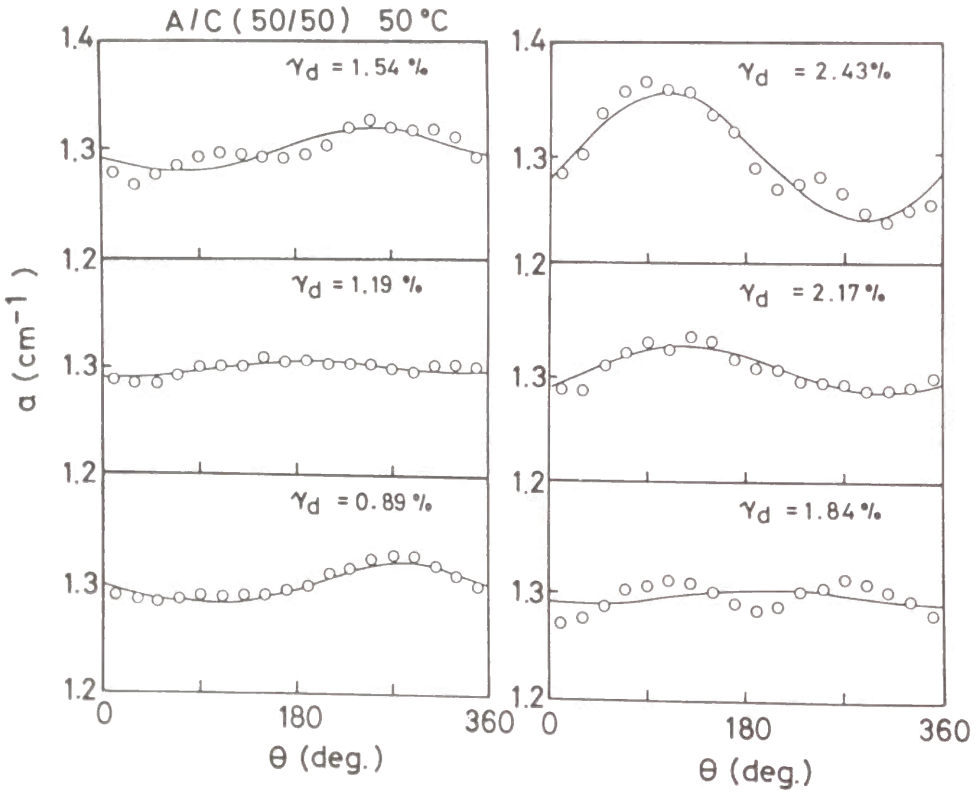

Fig.4-12 *Variation of attenuation coefficient α with phase angle of the dynamic strain for A50/C50 films at different dynamic strain amplitude. The open circles indicate the average attenuation coefficients in a given interval of the phase angle, and solid lines indicate the fundamental components in Fourier expansion.*

The attenuation coefficient varies behind about 180 degrees with respect to the dynamic strain at lower dynamic strain amplitudes; on the other hand, the attenuation varies in phase at higher dynamic strain amplitudes. In the intermediate dynamic strain range (γ_d = 1.54 to 1.84 %), the attenuation had two maxima in one cycle. These results suggest that the deformation mechanism gradually changes from negative one (plastic deformation) to positive one (orientation) with increasing the dynamic strain amplitude.

4-3-3 Dynamic Ultrasonic Wave Velocity.

Fig.4-13 shows the variations of the amplitude of the dynamic ultrasonic velocity $|v_1^*|$ with the dynamic strain amplitude at 40° C for all the films. As is obvious from the figure, $|v_1^*|$ increases linearly with γ_d, in which the slope of line increases with increasing HDPE content. The slope was also found to be greater at lower temperatures, although the figures are not shown here. The high value of $|v_1^*|$ at lower temperatures for HDPE-rich films can be related to their high modulus (see Fig.4-7).

In Fig.4-14, the phase difference of the dynamic velocity with respect to the dynamic strain are plotted against the dynamic strain amplitude. As is shown in the figure, δ_{v1} lies in the first quadrant (0 to 90 degrees) for all the films. For HDPE-rich films, δ_{v1} is near 0 degrees in whole γ_d range and at all temperatures, whereas for LLDPE-rich films it tends to approach 90 degrees as γ_d increases. The tendency is more pronounced at higher temperatures. This indicates that the dynamic velocity for HDPE-rich films responds elastically to dynamic strain, whereas that for LLDPE-rich films responds viscoelastically.

The increase in the velocity is indicative of the increase in ultrasonic modulus due to the orientation of lamellae, crystallites, amorphous chains, and so on. As described in the previous chapter (see section 3-3), the orientation of lamellae affects predominantly the ultrasonic velocity. In the case of the films having higher HDPE content (or at lower temperature), the lamellae in which dynamic velocity responds elastically. In the case of the films having higher

LLDPE content (or at higher temperatures), on the other hand, the lamellae in which crystallites are loosely packed orient with a phase lag; therefore, the dynamic velocity responds viscoelastically.

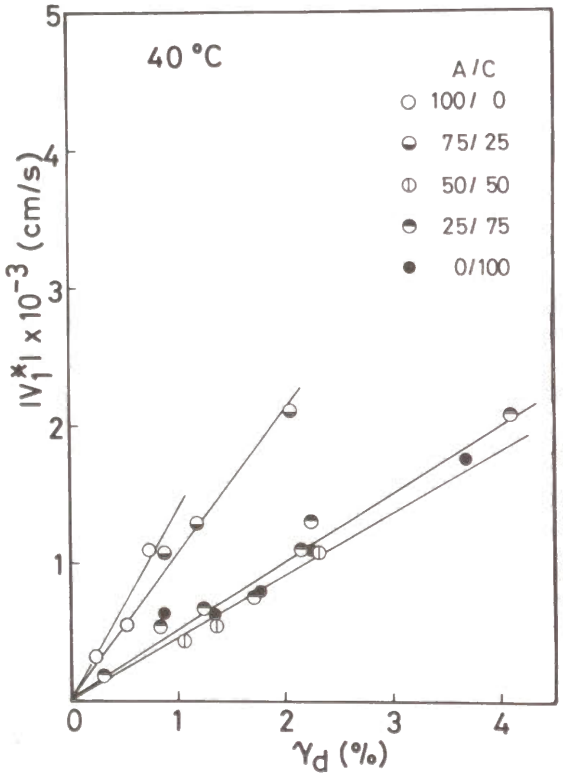

Fig.4-13 *Variation of* $|v_1^*|$ *with dynamic strain amplitude,* γ_d *at 40 C for HDPE(A), LLDPE(C), and their blend films.*

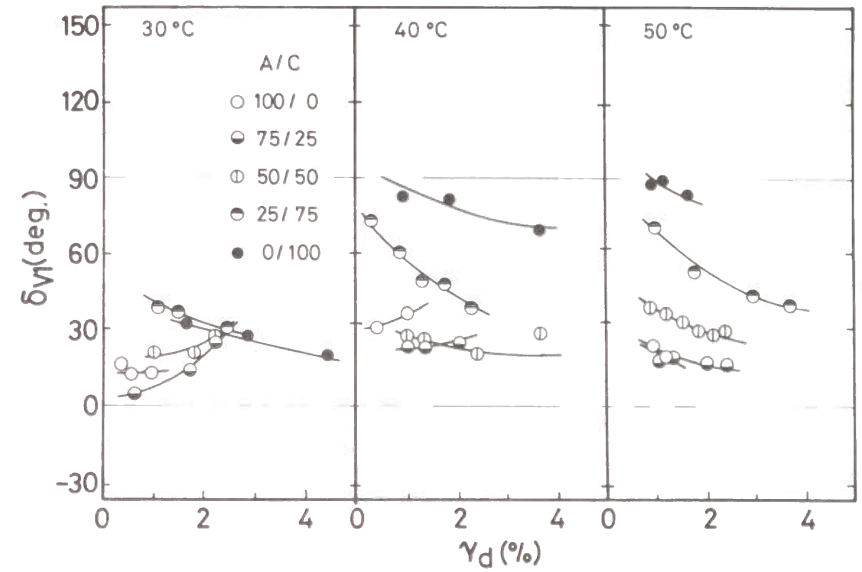

Fig.4-14 *Variation of the phase difference of dynamic ultrasonic velocity with the dynamic strain for HDPE (A)/LLDPE (C) blend films at 30°, 40°, and 50° C.*

4-3-4 Dynamic Density

As is reported in the previous chapter, the dynamic changes in density during a sinusoidal deformation, can be evaluated from the dynamic ultrasonic velocity and the dynamic modulus. In Fig.4-15, the amplitude of the dynamic density per unit dynamic strain, $|\rho_1^*|/\gamma_d$ is plotted against the dynamic strain amplitude for all the films. As is obvious from the

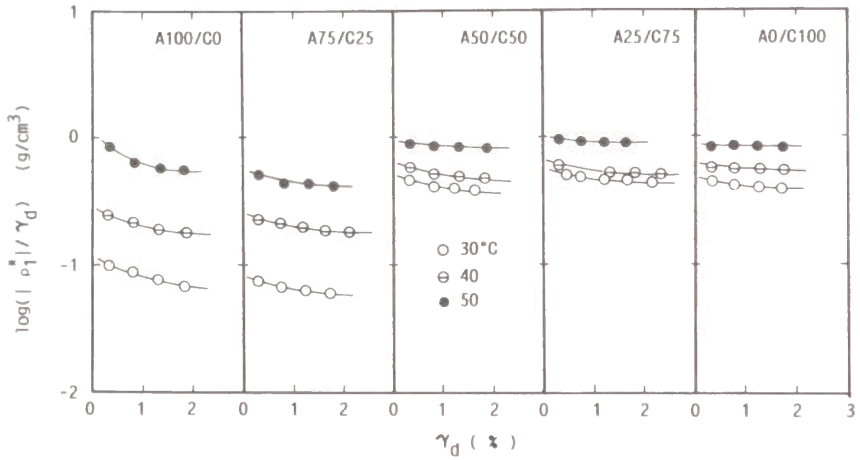

Fig.4-15 *Variation of dynamic density amplitude per unit dynamic strain amplitude* $|\rho_1^*|/\gamma_d$ *with dynamic strain* γ_d *for HDPE (A), LLDPE (C), and their blend films at 30°, 40°, and 50° C.*

figure, the magnitude of the dynamic density $|\rho_1^*|/\gamma_d$ had an order of 10^{-2} g/cm³. The dynamic density decreases with increasing dynamic strain amplitude for all the films. The decrease for the HDPE-rich films is greater than that for the LLDPE-rich films.

In Fig.4-16, the phase difference of the dynamic density with respect to the dynamic strain is plotted against the dynamic strain amplitude for all the films. As is obvious from the figure, δ_{D1} for HDPE-rich films is around 180 degrees, whereas that for the LLDPE-rich films 90 to 180 degrees at 30° C and 0 to 90 degrees at higher temperatures. The phase difference of 180 degrees indicates that

the density decreases elastically (or in phase) with the dynamic strain. The decrease in the density can be ascribed to the formation of crystal defects and microvoids, because their formation leads to volume expansion in the stretching direction. The phase difference of 0 degrees, on the other hand, indicates that the density increases in phase with the dynamic strain. The increase in density can be ascribed to the orientation of lamellae, crystallites, and/or amorphous chains, because their orientations lead to the increase in the mass in the stretching direction.

It is concluded from above discussion that the predominant mechanism for the HDPE rich films must be the formation of crystal defects and microvoids whereas predominant ones for the LLDPE-rich films must be the molecular orientation. This is consistent with the results of dynamic attenuation coefficient and dynamic velocity measurements.

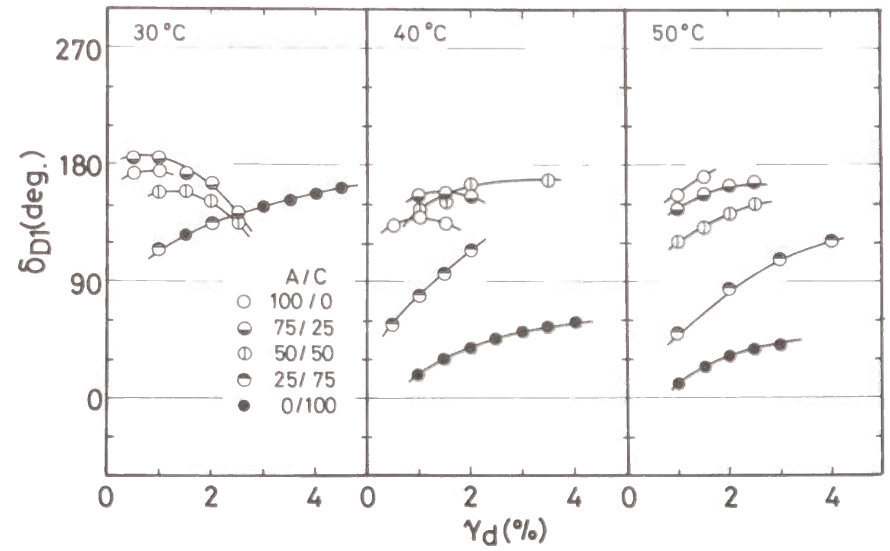

Fig.4-16 *Variation of the phase difference of dynamic density with dynamic strain* γ_d *for HDPE (A)/LLDPE (C) blend films at 30°, 40°, and 50° C.*

4-4 Summary

In this chapter, the nonlinear viscoelastic properties of undrawn polyethylene films having spherulitic structures were investigated using the dynamic ultrasonic measurements. The quenched films of HDPE, LLDPE, and their blends were used in this investigation. The higher the content of HDPE, the greater the nonlinearity of the dynamic mechanical properties was. The change in the dynamic ultrasonic quantities for HDPE-rich films was found to be caused by the plastic deformation such as the formation of micro-voids and crystal defects; on the other hand, that for LLDPE-rich films by the orientation of lamellae and/or crystallites. Thus, the less nonlinearity in LLDPE-rich films can be ascribed to the fact that lamellae and/or crystallites can orient without disrupting spherulitic structure. The results were consistent with the morphological features of polyethylene films.

REFERENCES

1. A. Tanaka, E. P. Chang, B. Delf, I. Kimura, and R. S. Stein, *J. Polym. Sci., Polym. Phys. Ed.*, **11**, 1891 (1973).
2. P. H. Geil, "*Polymer Single Crystal*," John Wiley Sons, New York,(1963).
3. I. L. Hey and Keller, *Kolloid-Z*, **204**, 43 (1965).
4. K. Kobayashi and T. Nagasawa, in *US-Japan Symposium on Polymer Phys.*, R. S. Stein and S. Onogi, Eds., Interscience, New York, pp.163, (1967).
5. K. Sasaguri, S. Hoshino, and R. S. Stein, *J. Appl. Phys.*, **35**, 47 (1964).
6. K. Sasaguri, R. Yamada, and R. S. Stein, *ibit.*, **35**, 3188 (1964).
7. K. Fujino, H. Kawai, T. Oda, and H. Maeda, *Proceedings of the Fourth International Congress on Rheologypn*, Interscience, New York, Part 3, pp.501 (1965).
8. T. Oda, S. Nomura, and H. Kawai, *J. Polym. Sci.*, **A-3**, 1993 (1965).
9. T. Oda, N. Sakaguchi, and H. Kawai, in *US-Japan Symposium on Polymer Phys.*, R. S. Stein and S. Onogi, Eds., Interscience, New York, pp.223, (1967).
10. L. Mandelkern and J. Maxfield, *J. Polym. Sci., Polym. Phys. Ed.*, **17**, 1913 (1979).
11. L. Mandelkern, M. Boltin, and R. A. Benson, *Macromolecules*, **14**, 1479, (1981).
12. R. M. Roberts, and J.C. Gilbert, L. B. Rodgeward, and A. S. Wingrove, "*An Introduction to Modern Experimental Organic Chemistry*," Halt, Renehalt and Winston Inc. New York,(1969).
13. M. J. Richardson, P. J. Flory, and J: B. Jacson, *Polymer*, **4**, 221 (1963).
14. B. Wunderloch, "*Macromolecular Physics*," Vol.1; "*Crystal Structure, Morphology and Defects*," Acad. Press., New york, Ch.3, (1973).
15. G. T. Davis, R. K. Eby, and G. M. Martin, *J. Appl. Phys.*, **39**, 4973 (1968).
16. S. R. Hu, T. Kyu, and R. S. Stein, *J. Polym. Sci., Polym. Phys. Ed.*, **25**, 71 (1987).
17. T. Kyu, R. S. Hu, and R. S. Stein, *ibid.*, **25**, 89 (1987).
18. M. Ree, T. Kyu, and R. S. Stein, *ibid.*, **25**, 105 (1987).

19. R. H. Boyd, *Polymer*, **26**, 323 (1985).
20. R. H. Boyd, *ibid.*, **26**, 1123 (1985).
21. M. Mansfield and R. H. Boyd, *J. Polym. Sci., Polym. Phys. Ed.*, **16**, 1227 (1978).
22. C. R. Ashcraft and R. H. Boyd, *J. Polym. Sci., Polym. Phys. Ed.*, **14**, 2153 (1976).
23. L. Mandelkern, M. Glotin, and R. Poli, *J. Polym. Sci., Lett. Ed.*, **19**, 435 (1981).
24. T. Kyu, M. Yamada, S. Suehiro, and H. Kawai, *Polym. J.*, **12**, 809, (1980).
25. G. Williams, J. I. Lauritzen, and J. D. Hoffman, *J. Appl. Phys.*, **38**, 4203 (1967).
26. J. L. Skinner and P. G. Wolynes, *J. Chem. Phys.*, **73**, 4022 (1980).
27. A. Tanaka, M. Fukuda, H. Nagai, M. Shinohara, and S. Onogi, *J. Polym. Sci., Polym. Phys. Ed.*, **27**, 2283 (1989).
28. R. Yamada and R. S. Stein, *J. Appl. Phys.*, **36**, 3005 (1965).
29. S. Onogi, A. Tanaka, Y. Ishikawa, and T. Igarashi, *Polym. J.*, **7**, 467 (1975).
30. A. Tanaka, H, Nagano, M. Shinohara, and S. Onogi, *Polym. J.*, **20**, 987, (1988).
31. A. Tanaka and S. Onogi, *Polym. Eng. Rev.*, **3**, 235 (1983).
32. A. Tanaka, M. Fukuda, H. Nagai, M. Shinohara and S. Onogi, *J. Polym. Sci., Polym. Phys. Ed.*, **27**, 2283 (1989).

CHAPTER 5

DYNAMIC ULTRASONIC STUDIES ON MECHANICAL NONLINEARITY (2) DRAWN POLYETHYLENE FILMS

5-1 Introduction

In the preceding chapter, ultrasonic properties of undrawn films of high density polyethylene (HDPE), and linear low density polyethylene (LLDPE), and their blends, all of which have spherulitic structure, were measured under oscillatory deformation and the nonlinear viscoelasticity was examined. The nonlinearity appearing on HDPE and HDPE-rich films was found to be ascribed to plastic deformation such as formation of microvoids and crystal defects caused by disruption of spherulites. The dynamic mechanical properties for LLDPE and LLDPE-rich films, on the other hand, was rather linear. This linear behavior was understood in terms of deformation mechanism which lead to lamellae and/or crystallites orientation without disrupting spherulitic structures.

The mechanical nonlinearity also appears on drawn films of HDPE, LLDPE, and their blends. However, the nonlinearity will be different from that found in undrawn films since uniaxal drawn polyethylene films have a different type of superstructure (*i.e.* fibrous structure).[1-6] The purpose of this study is to characterize the mechanical nonlinearity appearing on drawn films by means of dynamic ultrasonic measurements.

5-2 Experimental

5-2-1 Preparation of Drawn Films

HDPE and LLDPE polymers used in this study were identical to those in the previous chapter. Details of the materials, blending method, and the preparation of quenched-films have already been described in Chapter 4. As-quenched films were uniaxially drawn at 50° C by a hand stretcher until a major portion of the film specimen was necked. The drawn films had been kept at room temperature for more than three weeks before the dynamic measurements were carried out. The draw ratios of the drawn films thus obtained were 1000% for A100/C0 (HDPE), 700% for A75/C25, 600% for A50/C50, 450% for A25/C75, and 450% for A0/C100 (LLDPE), approximately.

5-2-2 Characterization of Film Specimen

Dynamic mechanical properties of drawn films were measured with Rheovibron Model DDV-IIc (Toyo Baldwin Co.,Ltd.). The measurement was carried out at 110 Hz between -150° and 110°C. Figs.5-1 and 5-2 show the temperature dependence of the dynamic modulus E', the loss modulus E'', and the loss tangent tan δ for all the drawn films. As is obvious from the figures, only the two dispersion, the gamma and alpha dispersions are seen and the beta dispersion disappears. Moreover, it is noted that the alpha dispersion has a more symmetrical shape in drawn films than in the undrawn films (see Fig.4-3).

As is well known, folded chains in the undrawn films are transformed into a fibrous structure by drawing. Thus, the drawing process induces a large scale chain reorganization: amorphous chains are incorporated into the micro-fibrous structure. Consequently, the beta dispersion which is associated with amorphous chains is depressed by drawing. The complex shape of the alpha dispersion peak in undrawn films indicates that the distribution of relaxation time is broad; in other words, different kinds of deformation mechanism associated with amorphous and/or crystalline parts will be involved. Symmetric peak in the alpha dispersion for drawn films can be ascribed to a narrow distribution of relaxation time.[7] the

alpha dispersion of drawn blend films is a single peak, indicating that the HDPE and LLDPE polymers are cocrystallized.[8]

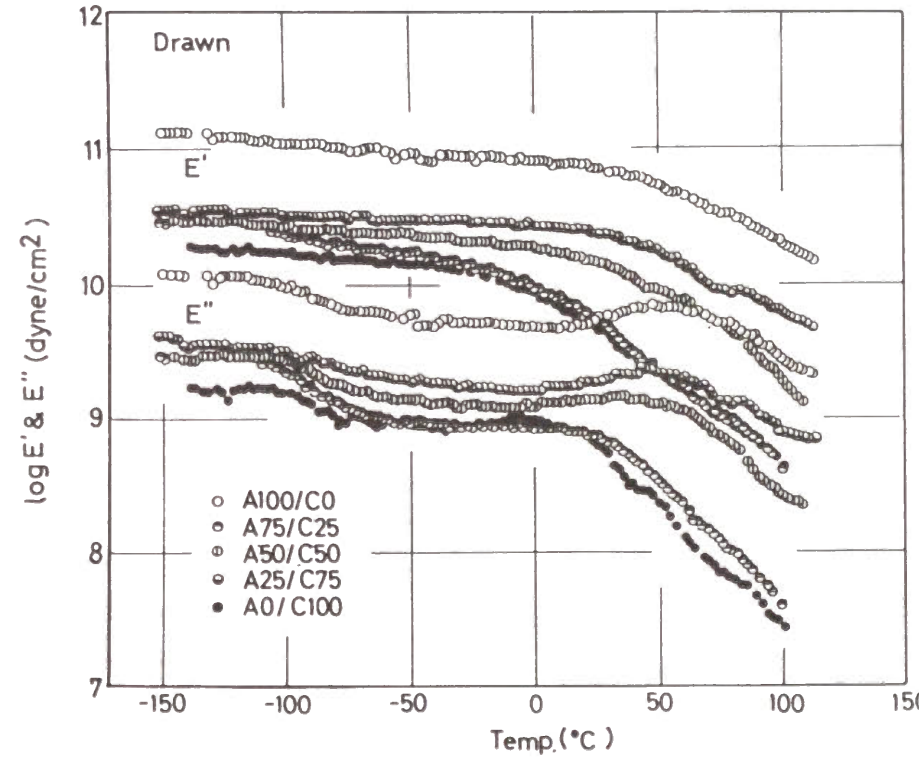

Fig.5-1 *Variation of the mechanical storage modulus E' and loss modulus E" with temperature for drawn HDPE(A), LLDPE(C), and their blend films. The frequency used was 110 Hz.*

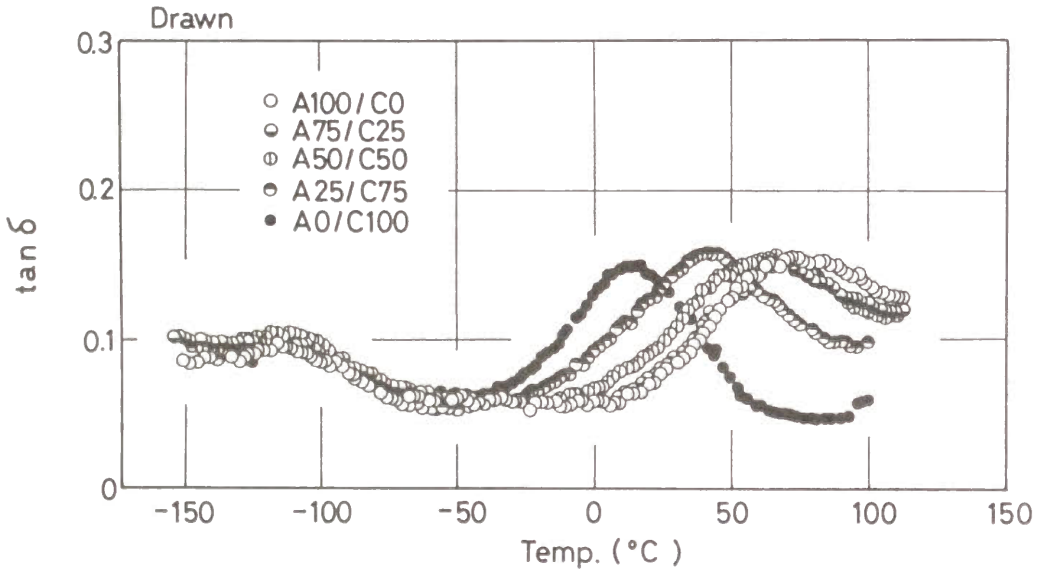

Fig.5-2 *Variation of loss tangent with temperature for drawn HDPE(A), LLDPE(C), and their blend films. The frequency used was 110 Hz.*

Fig.5-3 shows the temperature dependence of the attenuation coefficient for all the drawn films. As is seen in the figure, the attenuation coefficient increases with increasing temperature for all the drawn films. The increase becomes greater as the content of LLDPE increased. Moreover, the films having higher contents of LLDPE exhibits higher attenuation over the entire temperature range.

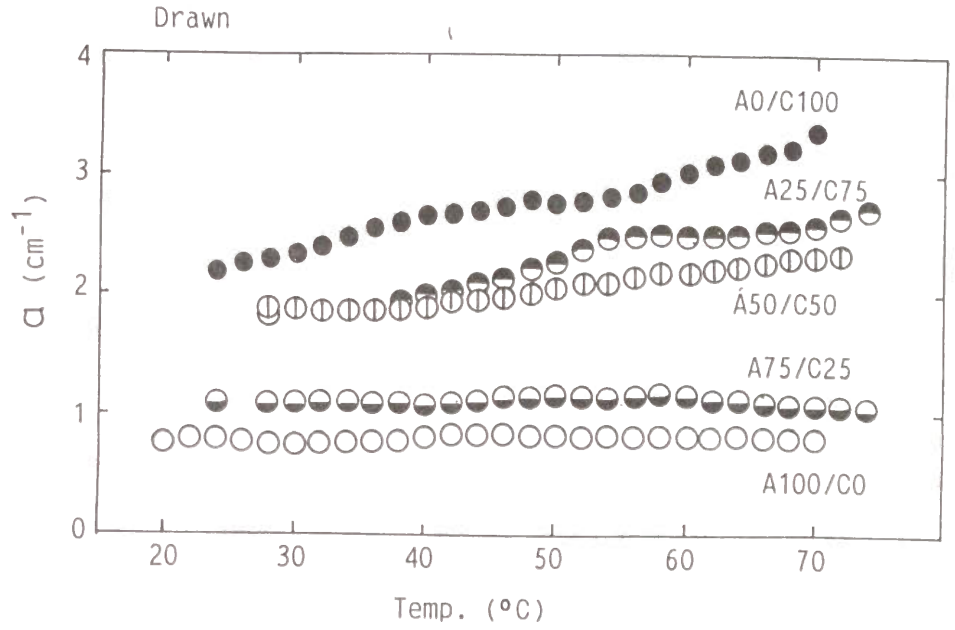

Fig.5-3 *Temperature dependence of ultrasonic attenuation coefficient α with temperature for drawn HDPE(A), LLDPE(C), and their blend films.*

Fig.5-4 shows the temperature dependence of the ultrasonic velocity. The velocity decreases with increasing temperature for all the films, and the decrease in velocity becomes greater as the content of LLDPE increased. Moreover, the velocity is lower for films having higher LLDPE content.

Temperature and content dependencies of the ultrasonic velocity and the attenuation coefficient for drawn films were very similar to those for undrawn films. The changes in ultrasonic properties with temperature, however, was smaller for drawn films than for undrawn films.

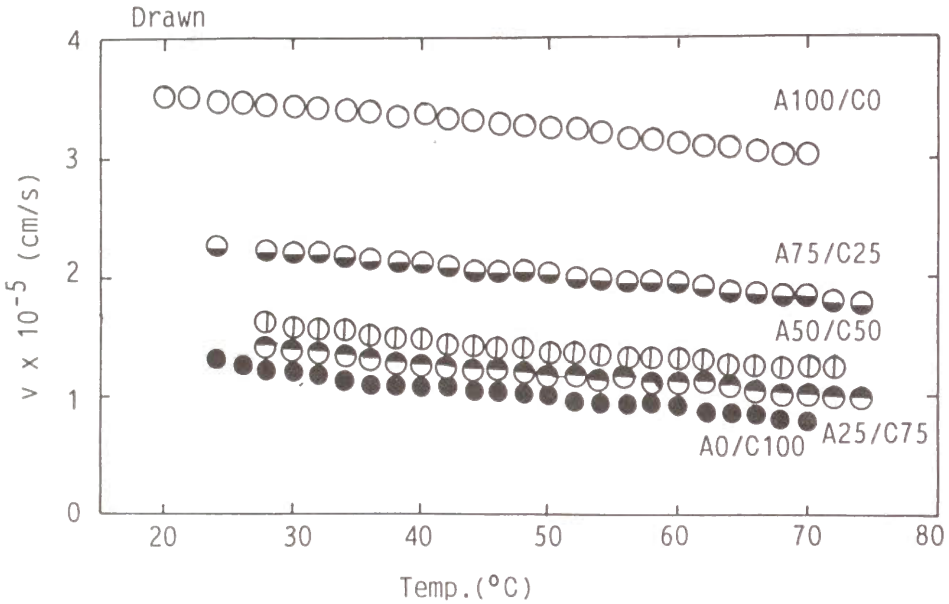

Fig.5-4 *Temperature dependence of ultrasonic velocity v for drawn HDPE(A), LLDPE(C), and their blend films.*

Fig.5-5 shows the comparison of the velocity between drawn and undrawn films at 40° C. In the figure, the horizontal axis is the content of HDPE. As is obvious from the figure, the velocities of drawn films are higher than those of undrawn films. The high velocity in oriented materials is presumed to result from the participation of oriented molecular chain (or stiff intramolecular bond) in the processes of sound transmission.[9-12]

Moseley[12] showed that the Herman's orientation parameter[13,14] f can be

evaluated by velocity data as follows:

$$f = 1-(v_u/v_d)^2 \qquad (5\text{-}1)$$

where v_u and v_d denote the sonic velocity in the undrawn (unoriented) states and in the drawn (oriented) states, respectively. The orientation parameters calculated using the Eq.(5-1) were as follows: 0.90 for A100/C0, 0.71 for A75/C25, 0.50 for A50/C50, and 0.33 for A25/C75 and A0/C100.

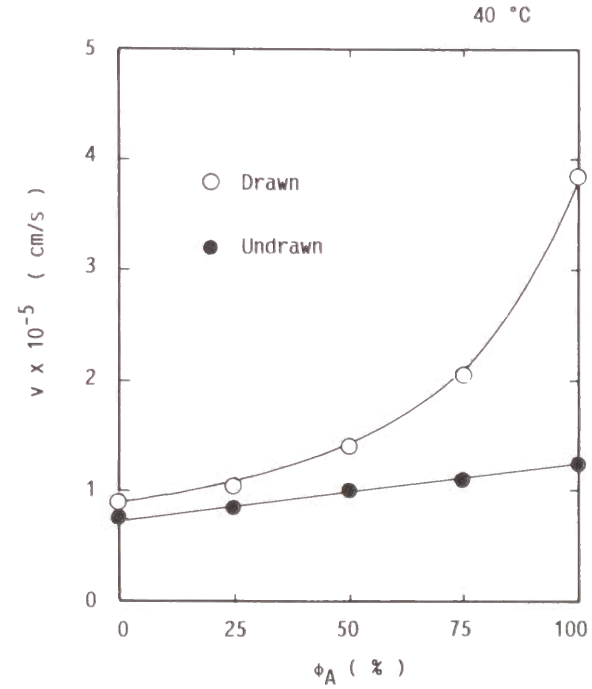

Fig.5-5 *Comparison of ultrasonic velocity at 40° C between drawn films (open circles) and undrawn films (closed circles) plotted against HDPE content.*

5-2-3 Measurements

Ultrasonic velocity and attenuation coefficient were measured under oscillatory deformation simultaneously with mechanical and optical (birefringence) properties. Measurements were carried out at 30°, 40°, and 50° C. Several levels of dynamic strain from 0.1 to 3.0% was superposed on a static strain of 5%. The drawn A100/C0 (HDPE) films could not be measured at 30° C because the films were broken during dynamic experiments.

5-3 Results and Discussion

5-3-1 Dynamic Mechanical and Optical Properties.

In Fig.5-6, the dynamic mechanical coefficients; that is, the absolute value of the complex modulus $|E_1^*|$, the loss tangent $\tan\delta_1$, and the mechanical nonlinear parameter P_σ are plotted against the dynamic strain amplitude γ_d. As shown in the figure, the modulus $|E_1^*|$ and the loss tangent $\tan\delta_1$ gradually decreases as the LLDPE content increases. Also, $|E_1^*|$ decreases with increasing temperature for all the films. The nonlinear parameter P_σ is extremely small and close to zero, indicating that the time-dependent nonlinearity is extremely small. These results were similar to those of undrawn films.

Fig.5-7 shows the dynamic optical coefficients plotted against the dynamic strain amplitude γ_d. As shown in the figure, the absolute value of the complex strain-optical coefficient $|K_1^*|$ increases with increasing the LLDPE content. This was also seen for undrawn films, but the increase was smaller for drawn films than for undrawn films. This indicates that the changes in molecular orientation during oscillatory deformation for the films having fibrous structure are less than those for the films having spherulitic structure. Tan δ_{B1} is positive and close to zero for all the drawn films; on the contrary, that for undrawn films was negative (see Fig.4-8). This is likely because the c-axis for fibrous structure lies

in parallel direction to the dynamic deformation, whereas that for the spherulitic structure lies in perpendicular. The nonlinear parameter P_Δ was higher for drawn films than for undrawn films.

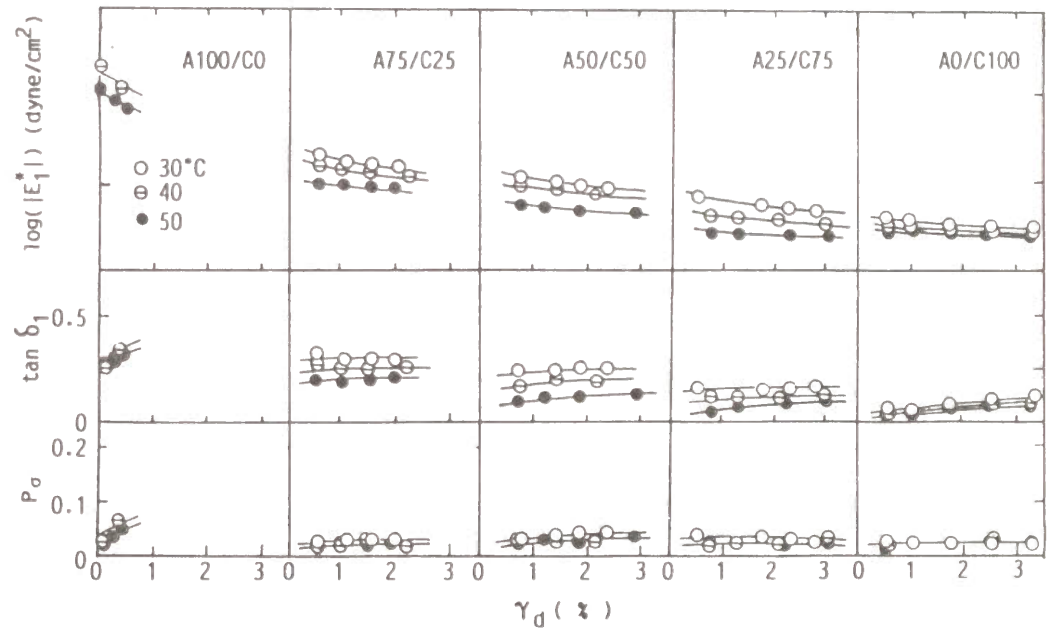

Fig.5-6 *Variation of* $|E^*_1|$, $\tan\delta_1$, *and* P_σ *with dynamic strain* γ_d *at different temperatures for drawn HDPE(A), LLDPE(C), and their blend films.*

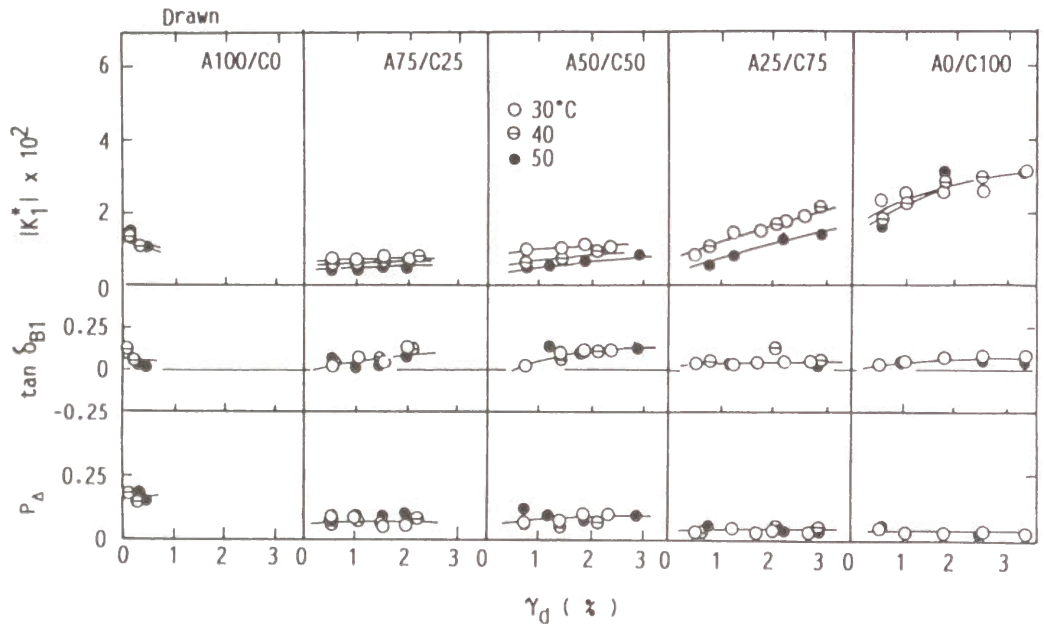

Fig.5-7 *Variation of* $|K^*_1|$, $\tan\delta_{B1}$, *and* P_Δ *with dynamic strain* γ_d *at different temperatures for drawn HDPE(A), LLDPE(C), and their blend films.*

5-3-2 Dynamic Attenuation Coefficient

Fig.5-8 shows the amplitude of the dynamic attenuation coefficient plotted against dynamic strain amplitude for the drawn films of A75/C25 (a) and A0/C100 (b). As is obvious from Fig.5-8a, the amplitude of the dynamic attenuation coefficients $|\alpha_1^*|$ for A75/C25 film decreases with increasing temperature.

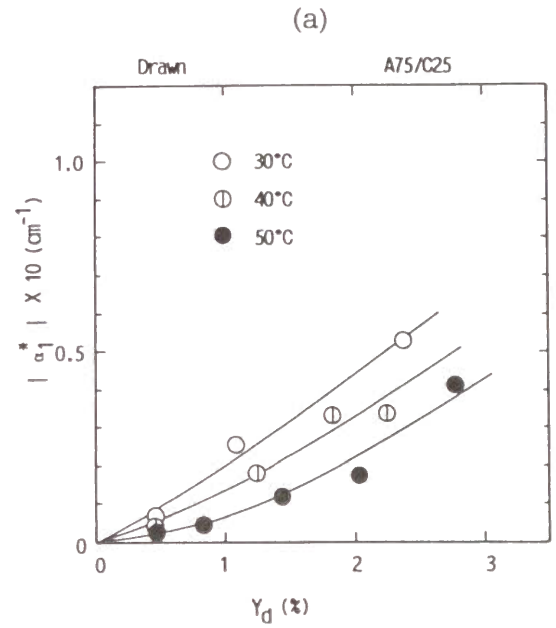

Fig.5-8 *Variation of* $|\alpha_1^*|$ *with dynamic strain amplitude* γ_d *for drawn A75/C25 and A0/C100 films.*

The similar temperature dependence was also seen for the A100/C0 film. For A0/C100 film, however, $|\alpha_1^*|$ increases with increasing temperature, as shown in Fig.5-8b. The temperature dependence was also seen for the A50/C50 and A25/C75 films.

Fig.5-9 shows the phase difference of the dynamic attenuation coefficient with respect to the dynamic strain plotted against the dynamic strain amplitude. As is obvious from the figure, δ_{A1}'s of the A100/C0 and A75/C25 films are around zero degrees at all temperatures, indicating that the attenuation coefficient increases elastically on the stretching process. This positive contribution will be caused by the formation of voids and defects. For the A0/C100 (*i.e.* LLDPE) film, on the other hand, δ_{A1} is around 180 degrees at all temperatures, indicating that the attenuation coefficient decreases elastically on the stretching process. This negative contribution will be caused by the molecular orientation.

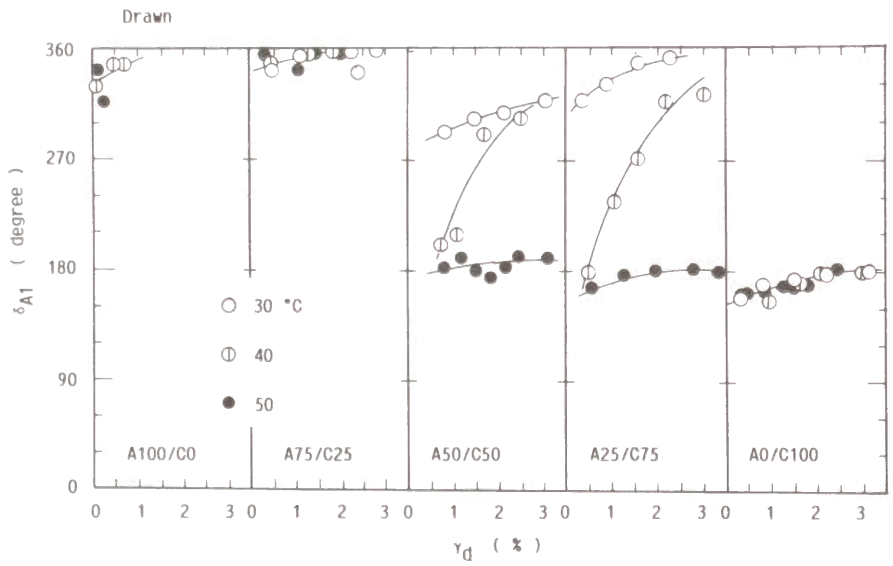

Fig.5-9 *Variation of δ_{A1} with dynamic strain amplitude for drawn HDPE(A), LLDPE(C), and their blend films at different temperatures.*

For A50/C50 and A25/C75 films, δ_{A1} lies around zero at lower temperature (30° C), around 180 degrees at higher temperature (50° C), and from zero to 180 degrees at intermediate temperature (40° C). This indicates that the negative and positive mechanism coexists and the negative contribution increases with increasing dynamic strain amplitude and/or temperature.

Above results were almost similar to those obtained for the undrawn films. However, the following point was different: $|\alpha_1^*|$ increased with increasing HDPE-content for undrawn films, whereas it increased with increasing LLDPE-content for drawn films (see Fig.5-10 and 5-11). This suggests that the major mechanism contributing to the attenuation coefficient is the molecular orientation for drawn films, whereas that is the void- and defect-formations for undrawn films.

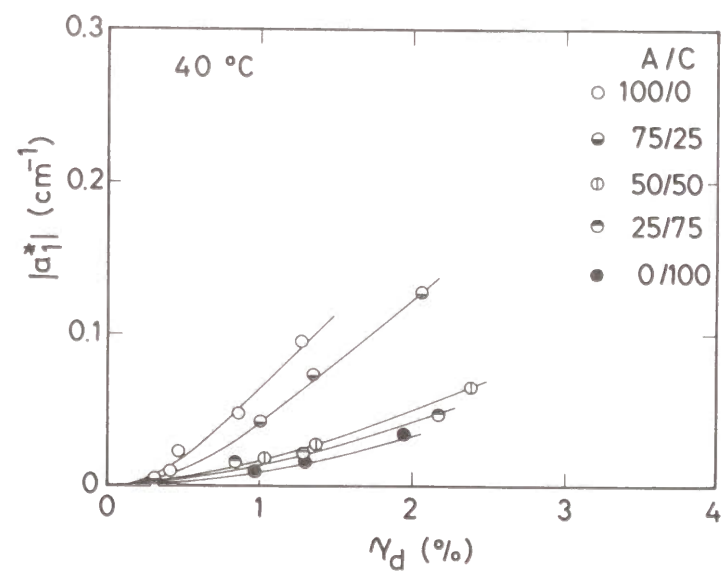

Fig.5-10 *Variation of $|\alpha^*_1|$ with dynamic strain amplitude at 40° C for undrawn HDPE(A), LLDPE(C), and their blend films. .*

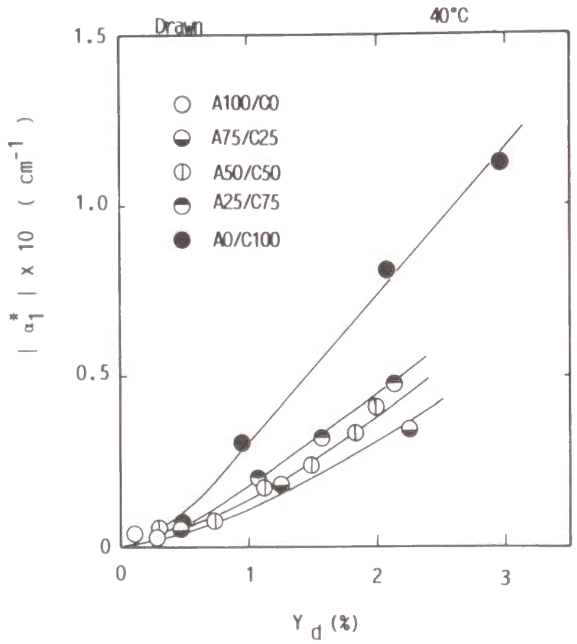

Fig.5-11 *Variation of | α^*_1 | with dynamic strain amplitude at 40° C for drawn HDPE(A), LLDPE(C), and their blend films.*

5-3-3 Dynamic Ultrasonic Wave Velocity

Fig.5-12 shows the variation of the amplitude of dynamic ultrasonic velocity plotted against dynamic strain amplitude. As is shown in the figure, | v^*_1 | increases linearly with γ_d for all the drawn films. The slope of the plots increases with increasing the HDPE content. The similar results were obtained for undrawn films. The slope for the drawn films, however, was about three times greater than that for the corresponding undrawn films.

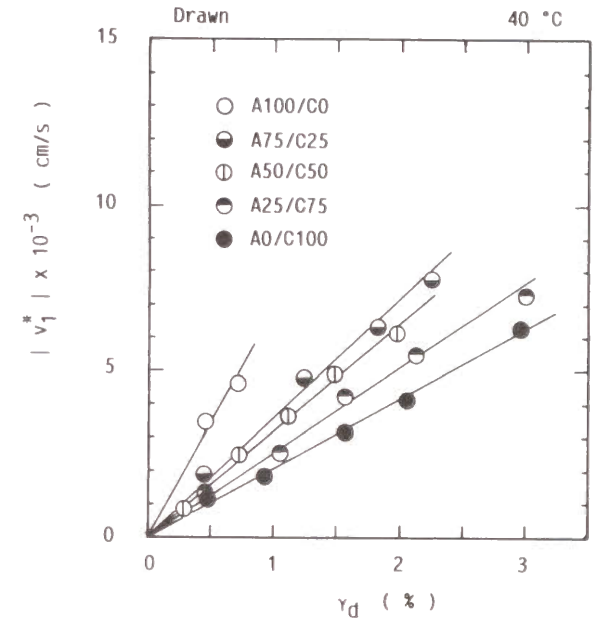

Fig.5-12 *Variation of | v^*_1 | with dynamic strain amplitude at 40° C for drawn HDPE(A), LLDPE(C), and their blend films.*

Fig.5-13 shows the phase difference of dynamic velocity with respect to dynamic strain plotted against dynamic strain amplitude at 40° C for various drawn films. As is obvious from the figure, δ_{v1} for all the drawn films lies in the range from 0 to -45 degrees, namely in the fourth quadrant. At other temperatures, δ_{v1} also lay in the same quadrant. This result was in marked contrast with that of undrawn films in which δ_{v1} lay in the first quadrant (see Fig.4-14). The phase difference in the fourth quadrant indicates that the dynamic velocity leads in phase, whereas that in the first quadrant indicates that the dynamic velocity lags in phase behind dynamic strain.

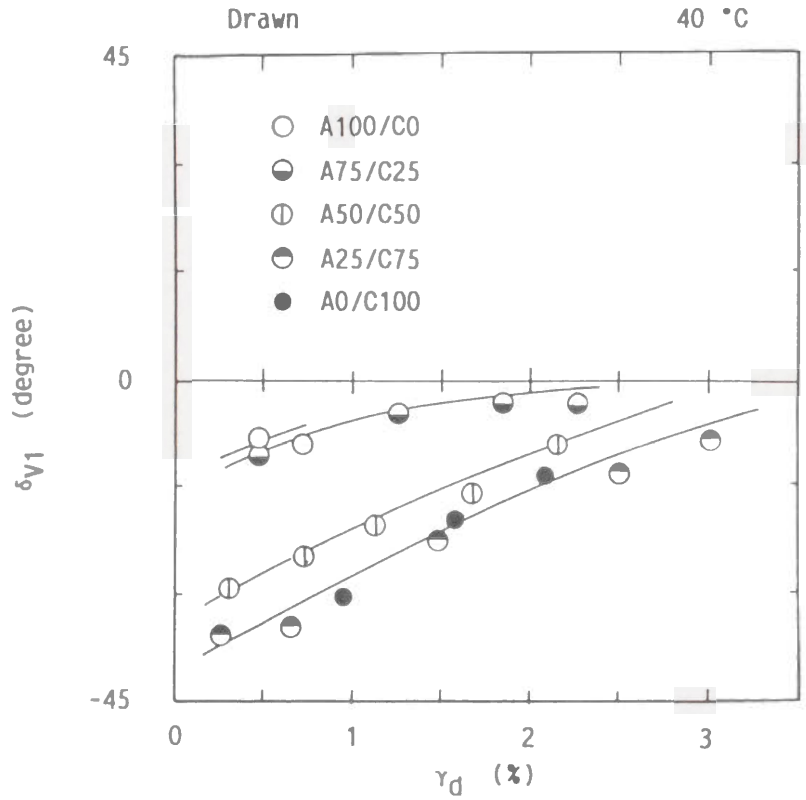

Fig.5-13 *Variation of δ_{V1} with dynamic strain amplitude for drawn HDPE(A), LLDPE(C), and their blend films.*

The phase difference in the fourth quadrant will be caused by the superimposition of negative and positive deformation mechanism, although positive mechanism dominantly contributes (see Fig.3-5a). In such a case of where δ_{V1} lies near zero in the fourth quadrant, the contribution of the negative deformation mechanism is small but not negligible. The positive mechanism by which the ultra-

sonic velocity is enhanced may be due to the orientation of fibrous chains.[9-12] The negative one by which the ultrasonic velocity is lowered may arise from plastic deformation such as molecular chain scission, interchain slippage, and dislocation,[15] which accompanies crystallites and/or molecular chain orientation. As is also seen in Fig.5-13, δ_{V1} approaches -45 degrees with increasing LLDPE content; this shift to -45 degrees was more pronounced as the temperature increased. The shift to -45 degrees indicates that the negative mechanism has a phase lag. It is likely that the higher the LLDPE content or the higher the temperature, the orientation of crystallites and/or molecular chain becomes more viscous. Accordingly, plastic deformation accompanied by orientation of crystallites and/or molecular chains has more phase lag for the films with higher LLDPE content.

5-3-4 Dynamic Density

Dynamic density can be determined from the dynamic modulus and dynamic velocity, as already shown in Chapter 3. Fig.5-14 shows the dynamic density amplitude per unit of dynamic strain amplitude plotted against dynamic strain amplitude for various drawn films. As is shown in the figure, the values are around 10^{-1} g/cm^3 in the entire range of the dynamic strain amplitude for all the films. (The order of the dynamic density amplitude is about 10^{-3}g/cm^3.)

Fig.5-15 shows the phase difference of the dynamic density with respect to the dynamic strain plotted against the dynamic strain amplitude. As is obvious from the figure, the phase difference δ_{D1} lies in the range from 0 to 30 degrees (*i.e.* in the first quadrant) for all the drawn films.

In the case of undrawn films, δ_{D1} lay around 180 degrees for HDPE-rich films, whereas it lay in the first quadrant for LLDPE-rich films. The value of 180 degrees indicates that negative deformation mechanism by which the density is lowered is dominant.

Positive deformation mechanism may be molecular orientation of crystallites or amorphous chains: orientation causes an increase in mass in the stretching direction. Negative deformation mechanism may be crystal defects, microvoids, or dislocation: such mechanism cause volume expansion in the stretching direction.

Therefore, the orientation of crystallites and/or amorphous chains can dominantly contribute to the dynamic density for drawn films.

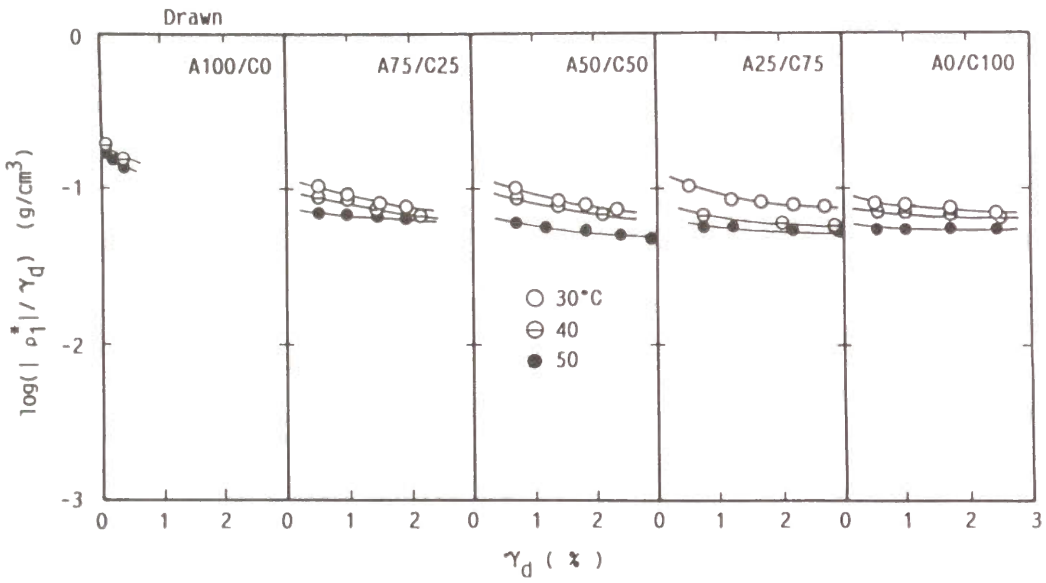

Fig.5-14 *Variation of dynamic density amplitude per unit dynamic strain amplitude* $|\rho_1^*|/\gamma_d$ *and their phase angles* δ_{D1} *with dynamic strain* γ_d *for drawn HDPE(A), LLDPE(C), and their blend films.*

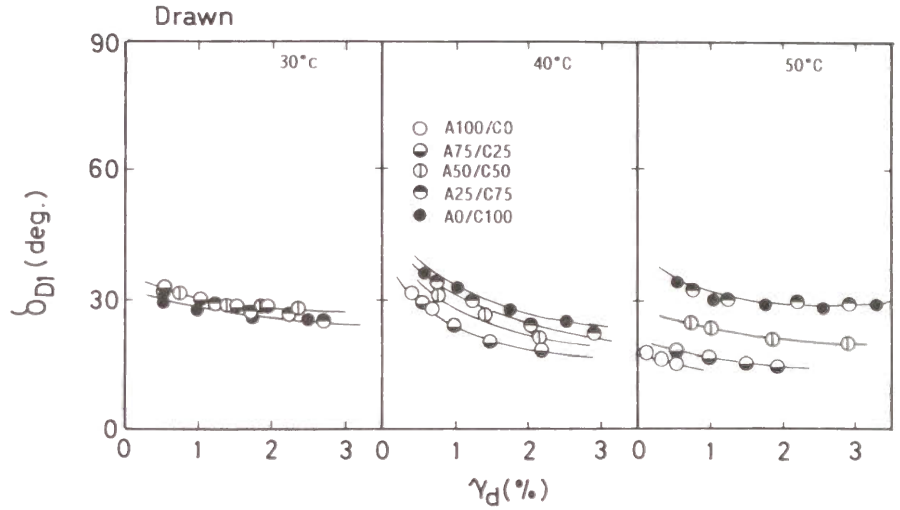

Fig.5-15 *Variation of the phase difference of dynamic density* δ_{D1} *with dynamic strain* γ_d *for drawn HDPE (A)/LLDPE (C) blend films at 30°, 40°, and 50° C.*

5-4 Summary

All kinds of dynamic ultrasonic data led a consistent conclusion: in the case of HDPE-rich films, nonlinearity can be ascribed to plastic deformation such as dislocation and microvoids occurring in the fibrous structure. In the case of

LLDPE-rich films, on the other hand, nonlinearity can be ascribed to nonlinearity in orientation. This conclusion was strongly supported by dynamic birefringence data simultaneously obtained: the higher the LLDPE content, the change in the dynamic strain-optical coefficient become higher. Furthermore, the nonlinearity for drawn films was simpler than for undrawn films. This may arise from rather uniform deformation mechanism in which the mechanism is mainly due to chain and/or crystallite.

REFERENCES

1. R. J. Samuels, *J. Polym. Sci. Polym. Phys. Ed.*, **6**, 1101 (1968).
2. A. Perterlin, *J. Macromol. Sci. (B)*, **8**, 83 (1974).
3. A. Keller, *Polymer*, **3**, 393 (1962).
4. A. Peterlin, *J. Polym. Sci. Polym. Phys. Ed.*, **7**, 1152 (1969).
5. H. P. Nandella, J. E. Spruiell, and J. L. White, *J. Appl. Polym. Sci.*, **22**, 3121 (1972).
6. H. W. Wychoff, *J. Polym. Sci.*, **62**, 83 (1962).
7. R. H. Boyd, *Polymer*, **26**, 323 (1985).
8. S. Hu, T. Kyu, R. Stein, *J. Polym. Sci., Polym. Phys. Ed.*, **25**, 71 (1987).
9. J. G. Rider and K. M. Watkinson, *Polymer*, **18**, 845 (1978).
10. O. K. Chan, F. C. Chen, C. L. Choy, and I. M. Ward, *J. Phys. D, Appl. Phys.*, **11**, 617 (1978).
11. R. A. Phethrick, *Prog. Polym. Sci.*, **9**, 197 (1983).
12. W. W. Moseley, *J. Appl. Polym. Sci.*, **3**, 266 (1960).
13. R. S. Stein, *J. Polym. Sci.*, **24**, 709 (1959).
14. R. J. Samuels, *J. Polym. Sci. A2*, **3**, 1741 (1965).
15. K. Adachi, G. Harison, J. Lamp, A. M. North, R. A. Pethrick, *Polymer*, **22**, 1026 (1981).

CHAPTER 6

ULTRASONIC PROPERTIES UNDER ELONGATION

6-1 Introduction

Mechanical properties of polymeric solids have been often examined using stress-strain tests,[1-6] in which the film specimen is elongated at a constant rate, particularly because of the availability of commercial testing machines. However, the precise nature of the stress-strain behavior remains still unclear; in particular for crystalline polymers, the stress-strain relation exhibits a significant nonlinearity which is hardly understood.

The previous rheo-optical studies[7-9] suggested that the nonlinear stress-strain behavior is caused by complicated deformation mechanism occurring in the transformation from the spherulitic structure to the fibrous one. The complicated deformation mechanism may be ascribed to complicated molecular aggregation or to various kinds of interactions such as inter-molecular and inter-aggregation interactions.

The purpose of this study is to investigate the origin of the nonlinear stress-strain relation of crystalline polymers. For the purpose, the ultrasonic properties were measured under a constant rate of elongation. Furthermore, a molecular theory based on the molecular interaction was applied to the experimental stress-strain curves. The crystalline polymers used are also identical to those used in the previous chapters: the quenched films of HDPE, LLDPE, and their blends.

6-2 Experimental

Tensile tests were performed at a fixed rate of strain (1.0 %/sec) with Rheovibron Model DDV-IIIc (Toyo Baldwin Co., Ltd.). The temperature was 30°, 40°, and 50° C. The tensile strain was calculated from the ratio of the increment of the length to the initial length between clamps. The tensile stress was determined using appropriate correction in the cross section. The birefringence and the ultrasonic properties (velocity and attenuation coefficient) were measured using optical and acoustic equipments mounted on the Rheovibron, which has already described in Chapter 3 (see Fig.3-1). It should be noticed here again that the ultrasonic velocity and the attenuation coefficient were measured in the direction of elongation.

6-3 Results

6-3-1 Stress-Strain Relation

Stress-strain curves were obtained at 30°, 40°, and 50° C for HDPE, LLDPE, and their blend films (see Fig.6-6). (The dotted line in Fig.6-6 denotes the experimental curves.) Young's modulus can be evaluated from the tangent slope of the initial portions. Young's modulus (E_0) at 30° , 40° , and 50° C are summarized in Table 6-I.

Both stress and Young's modulus increased with increasing the content of HDPE. For LLDPE-rich films, the stress increased monotonously with strain, and it leveled off at higher strains. For stress-strain curves of HDPE-rich films (A100/C0 and A75/C25 films), on the other hand, a clear yield point was seen around 20 % of strain. The yielding was always accompanied with necking. The yielding, however, disappeared at higher temperatures, *i.e.* at 50°C for A100/C0 and at 40° C for A75/C25.

Table 6-I *Young's modulus and Grüneisen parameter*

	Young's Modulus ($\times 10^{-8}$ dyne/cm^2)			Grüneisen Parameter		
	30°C	40°C	50°C	30°C	40°C	50°C
A100/C0	21.0	9.80	5.80	4.26	4.43	4.88
A75/C25	17.0	5.50	4.52	5.20	5.02	5.10
A50/C50	6.90	4.72	1.50	5.48	5.60	5.10
A25/C75	5.02	3.50	1.38	5.33	5.45	4.27
A0/C100	2.40	1.50	0.99	4.05	4.05	2.80

6-3-2 Birefringence-Strain Relation

Fig.6-1 shows the birefringence-strain curves at 30° C. For the films showing no yielding, the birefringence varied linearly with elongation, indicating that the material was uniformly deformed. For the films showing a clear yield point, however, the birefringence did not immediately increase, but it began to increase after a finite strain. This strain-lag in birefringence can be ascribed to the affine deformation of spherulites: the deformation from sphere to ellipsoid causes a negative birefringence, because the *b*-axis orients to the stretching direction so that the *c*-axis orients perpendicular to the stretching direction. After the finite strain, the orientation of crystallites within lamellae leads to increase in birefringence; however, the increase in birefringence is nonlinear in the initial strain range. The nonlinearity in birefringence may be related to the irreversible disruption of the spherulites.[8)]

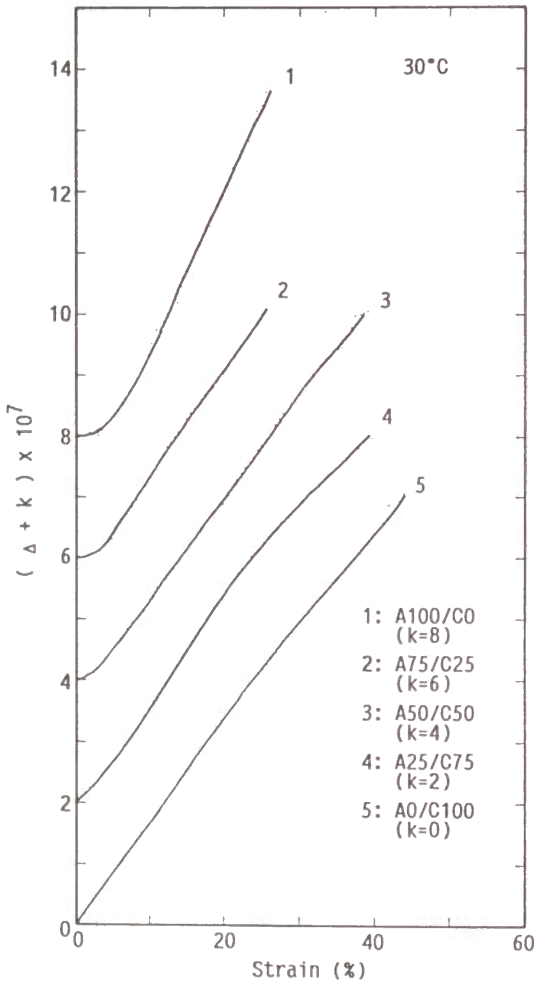

Fig.6-1 *Birefringence-strain curves at 30° C for HDPE, LLDPE, and their blends.*

6-3-3 Ultrasonic Attenuation Coefficient-Strain Relation

Fig.6-2 shows the plot of the attenuation coefficient against strain at

30° C. For LLDPE-rich films, the attenuation coefficient decreases monotonously with increasing strain, whereas for the HDPE-rich films the attenuation coefficient increases initially and then decreases with elongation. The maximum appeared in the strain region between 10 and 20 %. It is noteworthy that the increase in the attenuation was observed uniquely for the films showing yielding.

The increase in the attenuation coefficient can be due to the formation of defects and/or voids, which is caused by the disruption of the spherulites; whereas the decrease in the attenuation coefficient can be ascribed to the molecular orientation, as described in Chapter 4.

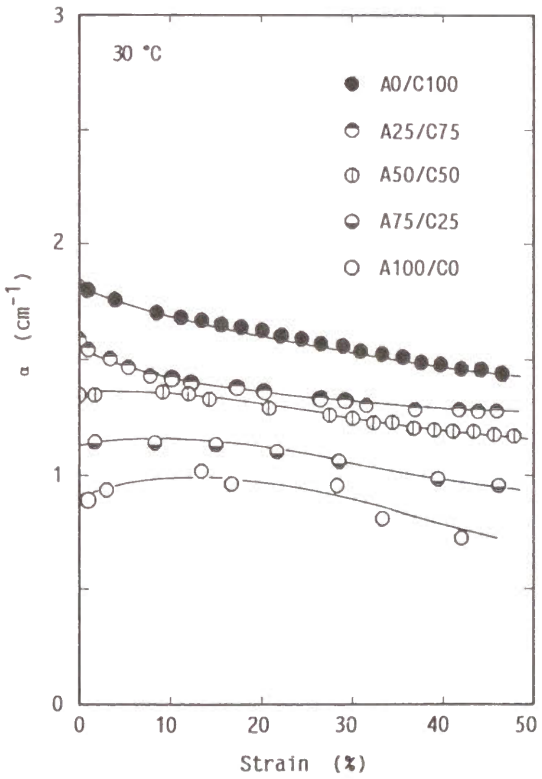

Fig.6-2 *Attenuation coefficient-strain curves at 30° C for HDPE, LLDPE, and their blends.*

6-3-4 Ultrasonic Velocity-Strain Relation

Fig.6-3 shows the plot of ultrasonic velocity against strain relations at 30°C. As shown in the figure, the velocity decreases with increasing the content of LLDPE in the entire range of strain. The velocity also decreased with increasing temperature, although the figure was not presented here. The decrease in the velocity will be ascribed to the softening of the materials.

The velocity increased linearly with increasing strain for all the films, suggesting the increase in the ultrasonic modulus[11,12] due to the molecular orientation in the direction parallel to the stretching direction.[13] For the films showing yielding or necking, however, velocity-strain line has a bending point around yield point. The slope of the line became greater beyond the bending point. The greater slope (or bending) may be due to the underestimation of the strain in the necking region.

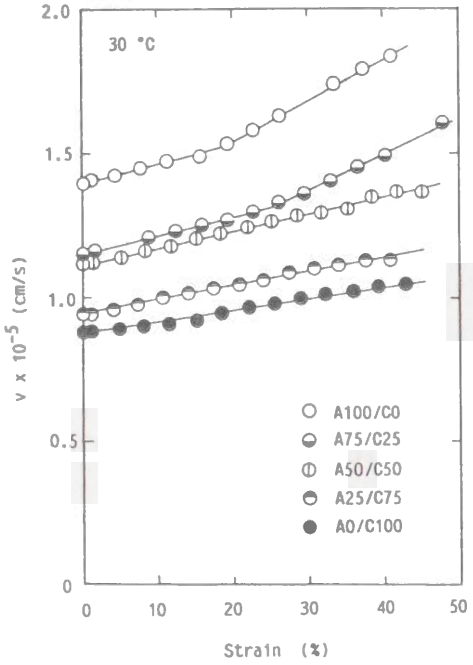

Fig.6-3 *Ultrasonic velocity-strain curves at 30° C for HDPE, LLDPE, and their blends.*

6-3-5 Summary

HDPE-rich films showed a clear yield point in the stress-strain curve at lower temperatures. For the films showing a yield point, a strain-lag appeared on the birefringence-strain curve, a initial increase on the attenuation-strain one, and a bending point on the velocity-strain one. These features indicate that the defects and voids occur at initial strain region. For the films showing no yielding, on the other hand, the birefringence, attenuation, and velocity monotonously changed with strain.

6-4 Analysis of Stress-Strain Curve by Toda-Potential

6-4-1 Background

Theoretical analysis of the stress-strain curves for polymeric solids have been extensively carried out for several decades.[14] Roughly speaking, they are classified into two types of theoretical approaches. One is the approach based on the extension of the linear viscoelastic theory to nonlinear behavior.[8,15,16] Another is based on the expansion of the elastic coefficient in the strain potential function to higher order terms.[17-19] Most of the approaches belong to the former one, which has been phenomenologically applied to the stress-strain behavior of various amorphous polymers such as glassy and rubbery polymers. As well known, however, the nonlinearity in crystalline polymers cannot be described adequately only using the extension of the viscoelastic theory. As mentioned earlier in this chapter, the nonlinearity will be due to the complicated intermolecular interaction. Thus, the latter approach will be adequate to the investigation of the mechanical nonlinearity of crystalline polymers.

In this section, the experimental stress-strain curves are analyzed using a model of molecular interacting with anharmonic potential.

6-4-2 Toda Lattice Model

Toda[20,21] introduced a lattice model with an anharmonic interaction, in

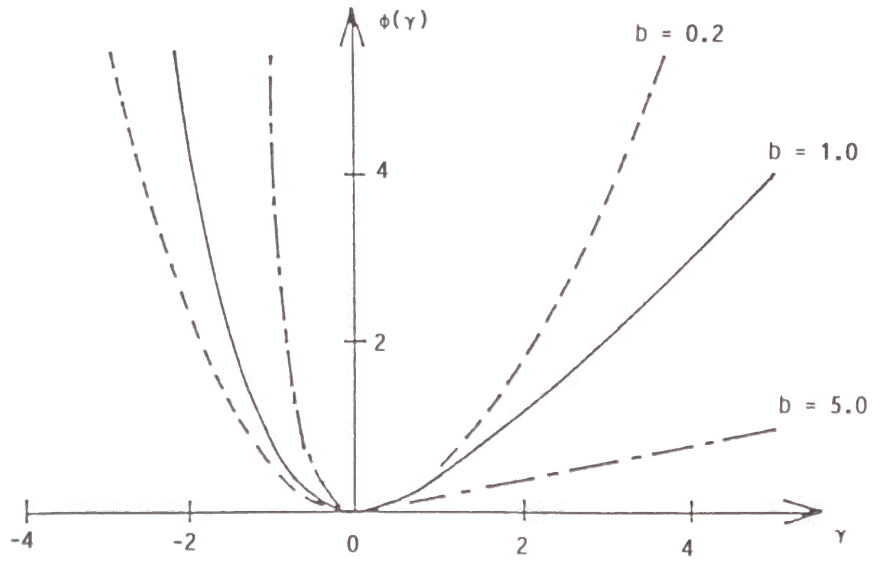

Fig.6-4 *Toda-potential curve in the case of ab=1.*

order to study nonlinear waves, namely "*Soliton*"[22]. The anharmonic potential function is of the form:

$$\Phi(\gamma)=a\gamma-\frac{a}{b}\left[1-\exp(-b\gamma)\right] \qquad (6\text{-}1)$$

where a and b are positive constants, γ the strain, and $\phi(\gamma)$ the interaction energy expressed as a function of strain. The two terms in the equation imply repulsive and attractive forces, respectively. The parameters are chosen so as the potential to be minimum at $\gamma=0$:

$$\left(\frac{d\Phi(\gamma)}{d\gamma}\right)_{\gamma=0}=0 \qquad (6\text{-}2)$$

If one expands $\phi(\gamma)$ in power series of γ, one gets

$$\Phi(\gamma)=\frac{1}{2}ab\gamma^2-\frac{1}{3!}ab^2\gamma^3+\frac{1}{4!}ab^3\gamma^4-\cdots\cdots \qquad (6\text{-}3)$$

When one keeps ab=finite and takes the limit $b\longrightarrow 0$, one obtains the harmonic case: the equation becomes quadratic function of γ. When one take $b\longrightarrow\infty$, the equation becomes one for the interaction between hard spheres. Thus, Toda-potential function has wide applicability. In Fig.6-4 the examples of the potential curves in the case of ab=1 are presented.

Differentiating Eq.(6-1) by strain, one gets the equation for the stress-strain curve;

$$\sigma(\gamma)=a\left[1-\exp(-b\gamma)\right] \qquad (6\text{-}4)$$

As is obvious from Eq.(6-4), the stress increases exponentially (or nonlinearly) as a function of strain.

If one expands the stress function in power series of γ, then

$$\sigma(\gamma)=ab\gamma-\frac{1}{2}ab^2\gamma^2+\frac{1}{3!}ab^3\gamma^3-\frac{1}{4!}ab^4\gamma^4+\cdots\cdots \qquad (6\text{-}5)$$

$$=ab\left[\gamma-\frac{1}{2}b\gamma^2+\frac{1}{3!}b^2\gamma^3-\frac{1}{4!}b^3\gamma^4+\cdots\cdots\right] \qquad (6\text{-}6)$$

It should be noted that all the elastic coefficients are expressed by the two parameters, a and b, and also that the ratio of the high-order coefficients to the first-order coefficient depend only on the parameter b (see Eq.(6-6)). This means that the anharmonicity or shape of potential curve depends on the value of b.

Again, differentiating Eq.(6-4) by strain, one gets the modulus

$$E(\gamma)=ab\exp(-b\gamma) \qquad (6\text{-}7)$$

Young's modulus E_0, initial tangent modulus, can be obtained by putting $\gamma=0$ in Eq.(6-7):

$$E_0=E(0)=ab \qquad (6\text{-}8)$$

Thus, Young's modulus can be also expressed by the product of a and b. This

indicates that the greater the value of E_0 is, the value of b becomes greater if a is constant. In other wards, Toda-potential predicts that a system having high Young's modulus tends to exhibit high degree of nonlinearity.

Grüneisen parameter γ_G[23,24], which determines the degree of anharmonicity in the molecular interaction,[25-28] is given by the following equation.

$$\gamma_G = -\frac{1}{2}\frac{d\,lnE(\gamma)}{d\,\gamma} \tag{6-9}$$

Substituting Eq.(6-7) into Eq.(6-9), Grüneisen parameter of the Toda-potential is given by

$$\gamma_G = \frac{b}{2} \tag{6-10}$$

Thus, Grüneisen parameter is proportional to b. Consequently, the stress-strain relationship resulting from the Toda-potential can be rewritten as follows:

$$\sigma(\gamma) = \frac{2E_0}{\gamma_G}\,[1-\exp(-2\gamma_G\gamma)] \tag{6-11}$$

$$= E_0\gamma - E_0\gamma_G\gamma^2 + \frac{2}{3}E_0\gamma_G{}^2\gamma^3 - \cdots\cdots \tag{6-12}$$

The anharmonicity of potential function will be proposed from the fact that materials usually exhibit the thermal expansion.[25-29] Assuming a harmonic potential, thermal oscillators vibrate symmetrically at the potential minimum. Therefore, their mean position is always at the minimum. This means that no thermal expansion occurs. In contrast, assuming anharmonic potential such as Toda-potential, the mean position of thermal oscillators becomes longer than the equilibrium position. (The mean position shifts to right direction on the abscissa in Fig.6-4.) That is, thermal expansion can occur. In fact, Toda demonstrated[20] that the thermal expansion estimated from Toda-potential is in accordance with the result which is given by the conventional method of statistical mechanics.

6-4-3 Comparison of Experimental and Theoretical Stress-Strain curves

The theoretical stress-strain curves can be obtained using Eq.(6-11). Young's modulus was determined by the initial tangent slope of the experimental

stress-strain curves. Grüneisen parameter can be estimated from the ultrasonic velocity-strain relation as follows.

The change in ultrasonic velocity with strain corresponds to the change in the intrinsic frequency with strain; then Grüneisen parameter can be written as in the following equation.[30]

$$\gamma_G = \frac{d\,ln\,v}{d\,\varepsilon} \tag{6-13}$$

where ε is the strain due to molecular chain orientation. The strain γ defined in elongation tests is not always identical to the strain ε since γ includes the strains due to molecular rotation and chain separation. Therefore, Eq.(6-13) can be rewritten as in the following equation.

$$\gamma_G = \frac{d\gamma}{d\varepsilon}\frac{d\,ln\,v}{d\gamma} \tag{6-14}$$

$d\,ln\,v/d\gamma$ is can be experimentally obtained. Considering an anisotropic lattice model by Wada *et al.*,[31,32] the following relation between γ and ε becomes:

$$\gamma = \sqrt{\frac{f}{g}}\,\varepsilon \tag{6-15}$$

where f is the intrachain force constant and g the interchain force constant. The ultrasonic velocity $v_{//}$ in the parallel to the chain direction is proportional to $\sqrt{f}$ and the velocity $v_\perp$ in the perpendicular to the chain direction is proportional to $\sqrt{g}$.[33,34] Thus, the following equation can be obtained.

$$\gamma_G = \frac{v_{//}}{v_\perp}\frac{d\,ln\,v}{d\gamma} \tag{6-16}$$

In the case of linear polyethylene, the value of $v_{//}/v_\perp$ becomes approximately 10.[34]

The values of Grüneisen parameter obtained using Eq.(6-16) are plotted against the HDPE content in Fig.6-5 and were summarized in Table 6-I. The values were from 3 to 6; which are comparable to the previous data for various polymeric materials.[31,32,35-37] It should be noted that Grüneisen parameters of the blend polymers were greater than those of the pure polymers. This indicates that the anharmonicity of intermolecular potential becomes greater by blending.

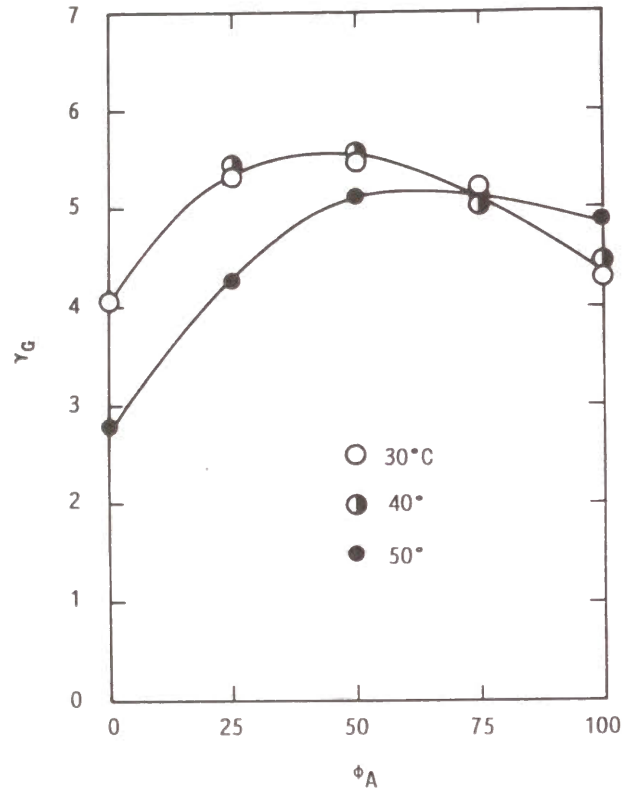

Fig.6-5 *Variation of Grüneisen constant with the content of HDPE.*

The theoretical stress-strain curves were obtained by putting the values of Table 6-I in Eq.(6-11). The theoretical stress-strain curves are shown in Fig.6-6. The solid line in Fig.6-6 denotes the theoretical one. As is evident from Fig.6-6, the agreement between the experimental and theoretical curves is surprisingly excellent, although the experimental curves of the films showing a clear yield point are in disagreement with the theoretical ones at higher strains.

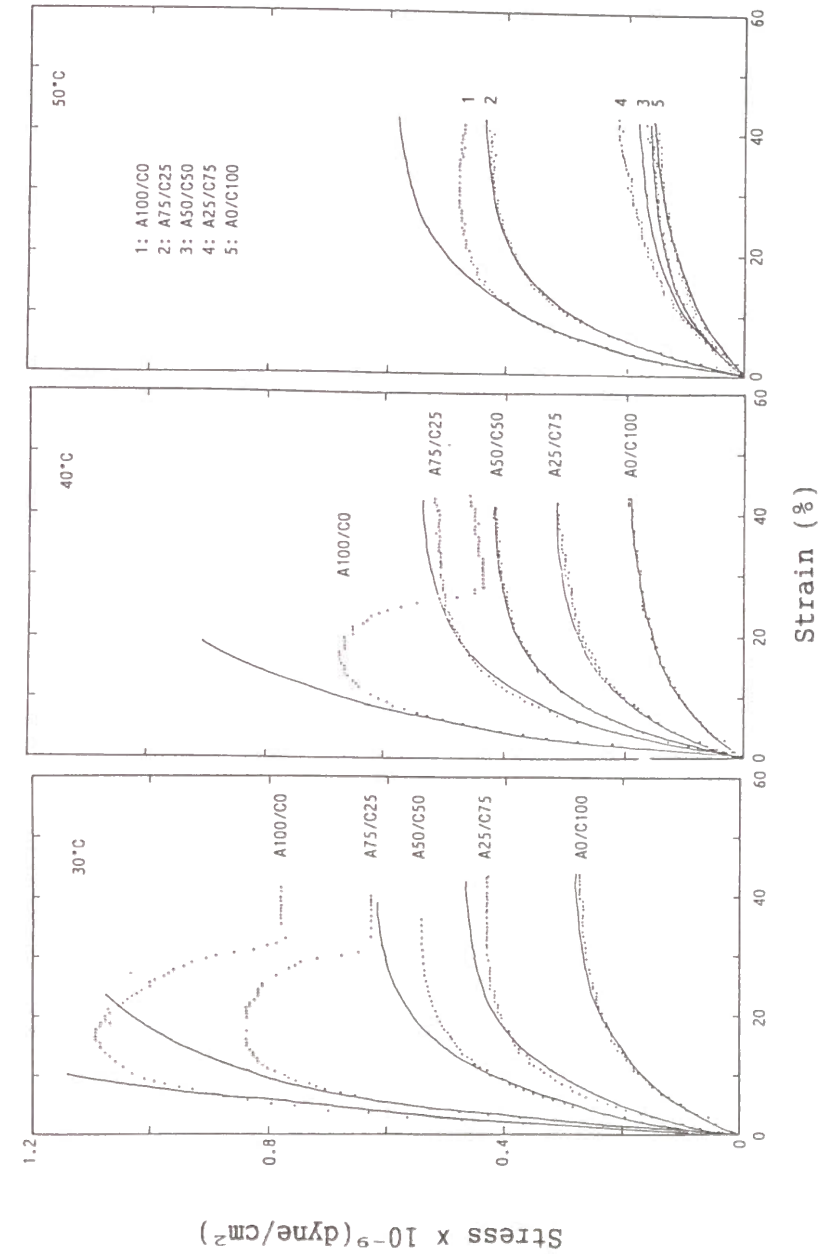

Fig.6-6 *Comparison of theoretical and experimental stress-strain curves for HDPE, LLDPE, and their blend films at different temperatures. The solid line denotes the theoretical curve, and the dotted line the experimental one.*

The excellent agreement suggests that Toda-potential satisfactorily describes the deformation mechanism on the elongation process. The disagreement in the yield regions can be ascribed to the following: (1) the strain was underestimated in the necking regions, and (2) different types of the deformation mechanism such as plastic deformation (yielding) and fibrous deformation appeared. For describing the stress-strain curves even in the yield regions, it is necessary to estimate the parameters a and b (or potential function) appropriate to each deformation mechanism as a function of the real strain.

As is well known, the temperature and the strain-rate change the shape of stress-strain curve for polymeric solids.[14] This fact indicates that the polymeric solids deform viscoelastically. Some investigators attempted to analyze the stress-strain curves by viscoelastic models.[8,15,38]

In the case of linear viscoelastic system with a single relaxation time τ, the relaxation modulus is given by

$$E(t)=E_0\exp(-t/\tau) \qquad (6\text{-}17)$$

If one consider a special case where the strain increases at a constant rate $R(=d\gamma/dt)$, then Boltzmann's superposition principle[39,40] gives the following stress-strain relation:

$$\sigma(\gamma)=E_0R\tau\ [1-\exp(-\gamma/R\tau)] \qquad (6\text{-}18)$$

The above equation is also derived from Maxwell model when subjected to a constant rate of strain.

It should be noted here that the form of Eq.(6-18) is identical to that of Eq.(6-4). This indicates that the experimental stress-strain curves in the present study can be also characterized by the viscoelastic model.

The author attempted to determine the relaxation time τ in such a way that Eq.(6-18) fits well to experimental curves. The resultant τ's are summarized in Table 6-II. In general, the relaxation time τ increases with increasing temperature and with decreasing the degree of crystallinity (or the content of HDPE). As

However, the relaxation times in Table 6-II were inconsistent with the general tendency; furthermore, the values were considerably small as compared with ones obtained from usual stress relaxation tests.[41] This suggests that the nonlinear stress-strain relation of the polyethylene films cannot be ascribed to the viscoelastic effect.

Table 6-II *Relaxation time obtained by curve fitting.*

	30°C	40°C	50°C
A100/C0	13.0	14.0	15.0
A75/C25	15.0	16.0	16.5
A50/C50	13.5	15.0	14.0
A25/C75	15.5	15.0	23.5
A0/C100	20.0	23.0	28.0

(sec)

6-5 Summary

Stress-strain curves of polyethylene films were analyzed by Toda-lattice model, in which intermolecular potential is assumed to be asymmetric. The film specimens of HDPE, LLDPE, and their blends were used.

Parameters in Toda-potential were experimentally determined from Young'

modulus and Grüneisen parameter. Young's modulus was evaluated from the initial slope of stress-strain curves, and Grüneisen parameter from the initial slope of ultrasonic velocity-strain ones. Theoretical stress-strain curves were obtained at different temperatures using the parameters. The theoretical curves fitted well to the experimental ones except in the yielding region. It was concluded that the nonlinear nature of polyethylene films is ascribed to the anharmonicity in the Toda-potential.

REFERENCES

1. J. D. Ferry, "*Viscoelastic Properties of Polymers*", John Wiley & Son (1961).
2. R. J. Samuels, *J. Polym. Sci. Polym. Phys. Ed.*, **6**, 1101 (1968).
3. A. Peterlin, *ibid.*, **7**, 1152 (1969).
4. A. Peterlin, *J. Macromol. Sci.(B)*, **8**, 83 (1974).
5. A. Keller, *Polymer*, **3**, 393 (1962).
6. H. P. Nandella, J. E. Spruiell, and J. L. White, *J. Appl. Polym. Sci.*, **22**, 3121 (1978).
7. S. Onogi, D. A. Keedy, and R. S. Stein, *J. Polym. Sci.*, **50**, S15 (1961).
8. R. S. Stein, S. Onogi, K. Sasaguri, and D. A. Keedy, *J. Appl. Phys.*, **34**, 80 (1963).
9. A. Tanaka and S. Onogi, *Polym. Eng. Rev.*, **3**, 235 (1983).
10. P. K. Datta and R. A. Pethrick, *Polymer*, **19**, 145 (1978).
11. M. Baccaredda and E. Butta, *J. Polym. Sci.*, **22**, 217 (1956).
12. P. D. Davidse, H. I. Waterman, and J. B. Westerdijik, *ibid.*, **59**, 389 (1962).
13. K. Adachi, G. Harrison, J. Lamb, A. M. North, and R. A. Pethrick, *Polymer*, **22**, 1026 (1981).
14. I. M. Ward, "*Mechanical Properties of Solid Polymers*," John Wiley & Sons (1971).
15. T. L. Smith, *Trans. Soc. Rheol.*, **6**, 61 (1962).
16. O. Nakada, *J. Phys. Soc. Japan*, **15**, 2280 (1960).
17. G. Halsey, H. L. White, and H. Eyling, *Text. Res. J.*, **15**, 296 (1945).
18. T. Bateman, W. P. Mason, and H. L. McSkimin, *J. Appl.Phys.*, **32**, 928 (1961).
19. N. G. Einspruch and R. J. Manning, *ibid.*, **35**, 560 (1964).
20. M. Toda, *J. Phys. Soc. Japan*, **22**, 431 (1967).
21. M. Toda, *ibid.*, **23**, 501 (1967).
22. N. J. Zabusky and M. D. Kruskal, *Phys. Rev. Letters*, **15**, 240 (1965).
23. J. C. Slater, "*Introduction to Chemical Physics*," McGrow HIll, New York (1966).
24. C. Kittel, "*Introduction to Solid State Physics*," John Willey & Sons,

New York (1966).
25. O. Yamamoto, *Polym. J.*, **2**, 509 (1971).
26. T. Kijima, K. Koga, K. Imada, and M. Takayanagi, *ibid.*, **7**, 14 (1975).
27. E. L. Rodriguez and F. E. Filisko, *J. Mater. Sci.*, **22**, (1987).
28. R. M. Barron, T. H. K. Barron, P. M. Mummery, and M. Sharkey, *Can. J. Chem.*, **66**, 718 (1988).
29. L Engeln, M Meissner, and H. E. Pape, *Polymer*, **26**, 364 (1985).
30. R. S. Bretzlaff and R. P. Wool, *J. Appl. Phys.*, **52**, 5964 (1981).
31. Y. Wada, A. Itani, T. Nishi, and S. Nagai, *J. Polym. Sci. A-2*, **7**, 201 (1969).
32. Y. Wada, "*Kobunshibussei to Bunshikouzo*" (in Japanese), edited by M. Nagasawa etal., Kagakudoujin, pp.113 (1973).
33. R. E. Baker, *J. Appl. Phys.*, **38**, 4234 (1967).
34. W. W. Moseley, *J. Appl. Polym. Sci.*, **9**, 266 (1960).
35. M. G. Broadhurst and F. I. Mopsik, *J. Chem. Phys.*, **52**, 3634 (1970).
36. T. G. Gibon, *ibid.*, **60**, 1094 (1974).
37. D. S. Hughes, E. B. Blackenship, and R. L. Mims, *J. Appl. Phys.*, **21**, 294 (1950).
38. S. Matsuoka, *Polym. J.*, **17**, 321 (1985).
39. H. Leadermen, "*Elastic and Creep Properties of Filamentous Materials and Other High Polymers*", The Textile Foundation, Washington, D.C. (1943).
40. J. R. MacDonald and M. K. Brachmann, *Rev. Mod. Phys.*, **28**, 393 (1956).
41. S. Onogi, A. Tanaka, Y. Ishikawa, and T. Igarashi, *Polymer J.*, **7**, 467 (1975).

PART III

CHAPTER 7

ULTRASONIC STUDIES ON MOLECULAR ORDERING

7-1 Introduction

Whether or not molecular ordering occurs in glassy polymers has been a long standing issue. Some experimental work[1-8] suggested that the molecular ordering exists in usually amorphous polymers. Some theories predicted that repulsive and/or attractive forces can cause the supermolecularly ordered structure not only in polymer glasses but also in polymer melts. Onsager theory[9], in which only repulsive force is taken into account, has successfully predicted lyotropic nematic-isotropic transition for rigid-chain polymers. On the other hand, Meier-Saupe theory[10], in which attractive force is taken into account, has predicts thermotropic nematic-isotropic transition for semi-rigid polymers having regions of rigid and flexible fragments. Thus, any kinds of forces can induce molecular ordering in glassy polymers.

In the nonequilibrium state in which potential energy of polymer molecules distributes heterogeneously, potential gradient exists within a molecule and/or between molecules. The potential gradient possibly results in molecular ordering even in flexible-chain polymers. In the present study, such molecular ordering is called MONE (molecularly ordering which is formed under a non-equilibrium state). The nonequilibrium state possibly appears in the process of the phase transitions such as precipitation and crystallization, and in the process of phase separation in multi-component systems. Thus, MONE will expectedly be formed in

block copolymer systems where phase separation often occurs.

The purpose in this chapter is to show that MONE appears in styrene-butadiene-styrene triblock copolymer (designated as SBS) films, and to examine the effects of thermal history and casting solvent on the formation and/or development of MONE.

For the sake of utilities of SBS polymer as thermoplastic elastomers, extensive work has been carried out on this polymer in past two decades. The morphology of SBS films is represented by domain shapes such as particles, rods, and lamellae. The morphology depends not only on the composition of styrene and butadiene blocks but also on the casting solvent.[11-16] The effects of the morphology on nonlinear viscoelastic properties have been previously examined using the SBS films having different kinds of morphology.[16] As expected, the linear viscoelastic properties were largely dependent on the morphology; however, the nonlinear viscoelasticity was independent of the morphology. For example, the nonlinearity changed significantly with physical aging, although the domain structure did not changed with the physical aging. This supposes that a smaller scale of structural change has affected the nonlinearity. The structural change may be associated with the formation of MONE. This supposition is one of the motives for the present study.

7-2 Experimental

SBS used in this study was a commercial polymer, Kraton 1101 Shell Chem. Co). This sample contains 28 weight percent polystyrene. The number average molecular weight of the block polymer has been reported[11] to be 76,000 and two polystyrene blocks of equal length exist primarily at the two ends of the A-B-A type molecule. Consequently, the block lengths in molecular weights become approximately 11,000-54,000-11,000. The polybutadiene portion consists of 51% trans-1,4, 41% cis-1,4, and 8% vinyl structure.[11]

The film specimens were prepared by casting from dilute solutions. Two

different types of solvents were used as casting solvent: one was tetrahydrofuran containing 10% methyl ethyl ketone by volume (designated as T/M) and the other cyclohexane (designated as Cy). T/M solvent is a nonpreferential one for polybutadiene, whereas Cy solvent is preferential for polybutadiene.

Arai *et al.*[12] observed the electron microscope on the SBS films prepared using the same polymers and the same solvents. According to their observations, the sphere-shaped polystyrene domains are dispersed within polybutadiene matrix for Cy-films and the lamella domains of polystyrene and polybutadiene are alternately formed for T/M films.

7-3 Results and Discussion

7-3-1 Dynamic Mechanical Properties

Dynamic mechanical properties were measured at a frequency of 110Hz and at temperatures between -170° and 110°C for both T/M- and Cy-films using Rheovibron Model DDVIIB (Toyo Baldwin Co. Ltd.). Two distinct dispersions were observed at -80° and 100°C for both films. The temperature of -80°C is very close to the glass transition temperature (T_g) of pure polybutadiene, and that of 100° C to T_g of pure polystyrene. This indicates that both polybutadiene and polystyrene molecules are well phase-separated. The dynamic modulus E' decreased drastically at the glass transition temperatures for both films. The decrease of E' around -80° C (T_g of polybutadiene) was greater for Cy-films (from 10^{10}dynes/cm^2 to 10^8dynes/cm^2) than for T/M-films (from 10^{10}dynes/cm^2 to 10^9dynes/cm^2). This is consistent with the previous morphological observation:[11-14] polybutadiene domains receive a large part of the stresses for Cy-films, whereas both polybutadiene and polystyrene domains share the stresses for T/M-films.

As shown in Figs.7-1 and 7-2, a novel dispersion is observed as a shoulder around 65° C on tan δ -T plot besides glass transitions of polybutadiene and polystyrene. Fig.7-1 shows the variation of tan δ with temperature for T/M films having different thermal histories. As is shown in the figure, the shoulder de-

veloped with aging at room temperature (see plot of the film aged for 88 days). The shoulder, on the other hand, disappeared by heat-treating at 60° C (see the plot of the film heat-treated for 22 hrs).

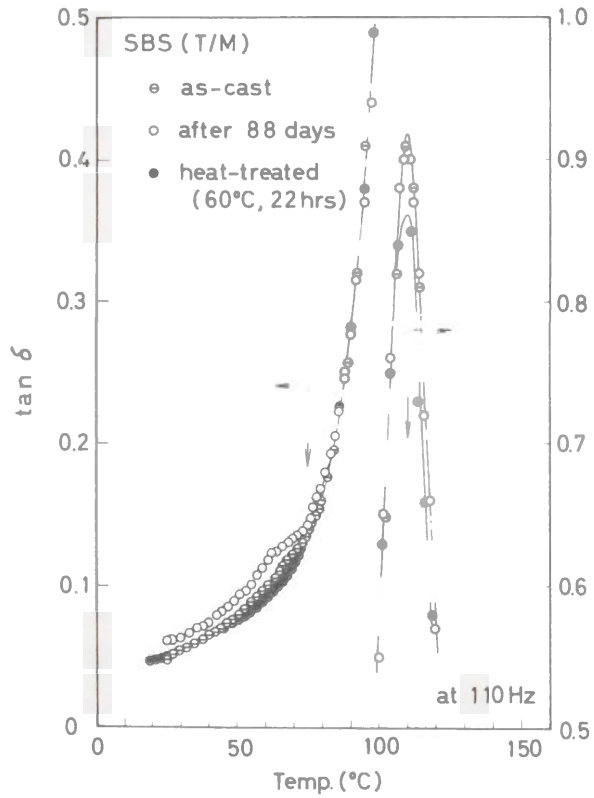

Fig.7-1 *Variation of tan δ with temperature for T/M films as-cast, aged at room temperature for 88 days, and heat-treated at 60° C for 22 hrs.*

For as-cast Cy-films, the similar (but more distinct) dispersion is observed, as shown in Fig.7-2. In this case, the dispersion do not change with aging for 76 days. Similarly, the dispersion disappeared by heat-treating at 60° C for 22 hrs.

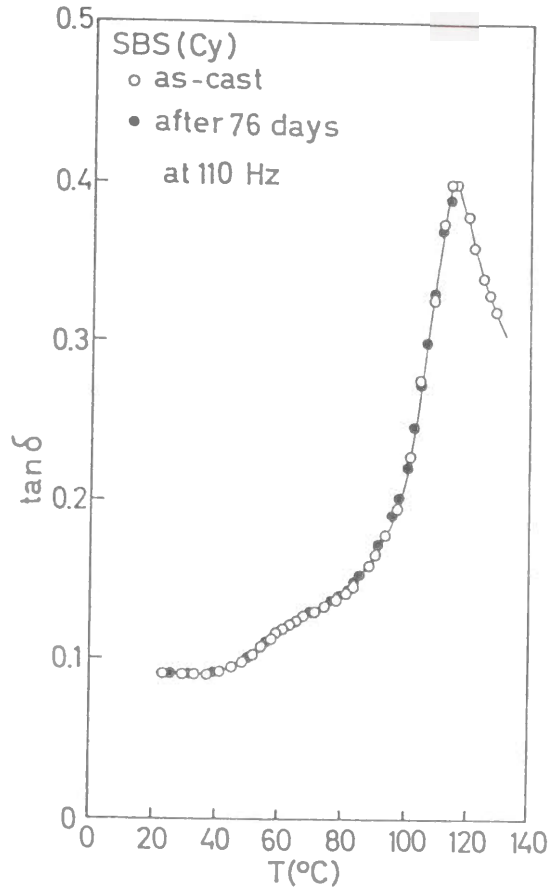

Fig.7-2 *Variation of tan δ with temperature for Cy-films as-cast and aged at room temperature for 76 days.*

Also, at different frequencies (35, 11, and 3.5 Hz), the dynamic mechanical properties were measured as a function of temperature. For all kinds of films, the temperature of the novel dispersion was independent of the frequency. This suggests that the dispersion can be ascribed not to a viscoelastic relaxation but to a phase transition, such as the melting of an ordered structure.

7-3-2 Density

Density was measured at 30° C using flotation method. Ethyl alcohol and water mixture was used for the measurement. The results were summarized in Table 7-I. As is shown in the table, the density of aged films is significantly higher than that of the heat-treated films for T/M- and Cy-films. That is, heat-treating lowers the density.

Table 7-I *Density of aged and heat-treated SBS films cast from T/M and Cy solutions.*

	Aged	Heat-treated
T/M-cast Films	0.9415 ± 0.0003	0.9407 ± 0.0003
Cy-cast Films	0.9419 ± 0.0003	0.9405 ± 0.0003

(g/cm^3)

7-3-3 Ultrasonic Properties

Figs.7-3 and 7-4 shows the variations of ultrasonic velocity and attenuation coefficient with temperature for aged and heat-treated T/M-films and those for Cy-films. As shown in the figures, the velocity decreases with increasing temperature, whereas the attenuation coefficient increases with temperature. This is plausible since molecular mobility increases with increasing temperature. However, the following are noteworthy.

First, the ultrasonic velocity for Cy-films was lower than that of T/M-films, whereas the attenuation coefficient was higher. In general, rubbery materials showed lower ultrasonic velocities and higher attenuation coefficients than

glassy materials did. Accordingly, the above difference between Cy- and T/M-films can be ascribed to the difference in their morphology: in the case of Cy-films in which continuous phase is composed of rubbery polybutadiene phase, the ultrasonic wave will travel mostly through polybutadiene phase; whereas, in the case of T/M-films the ultrasonic wave can travel through the both glassy polystyrene and rubbery polybutadiene phases.

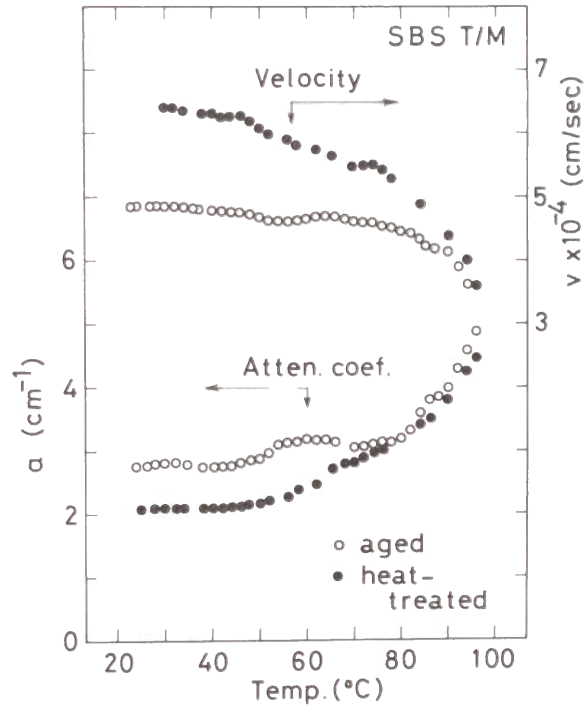

Fig.7-3 *Variation of the ultrasonic velocity and attenuation coefficient with temperature for T/M-films aged at room temperature and heat-treated at 60° C for 22 hrs.*

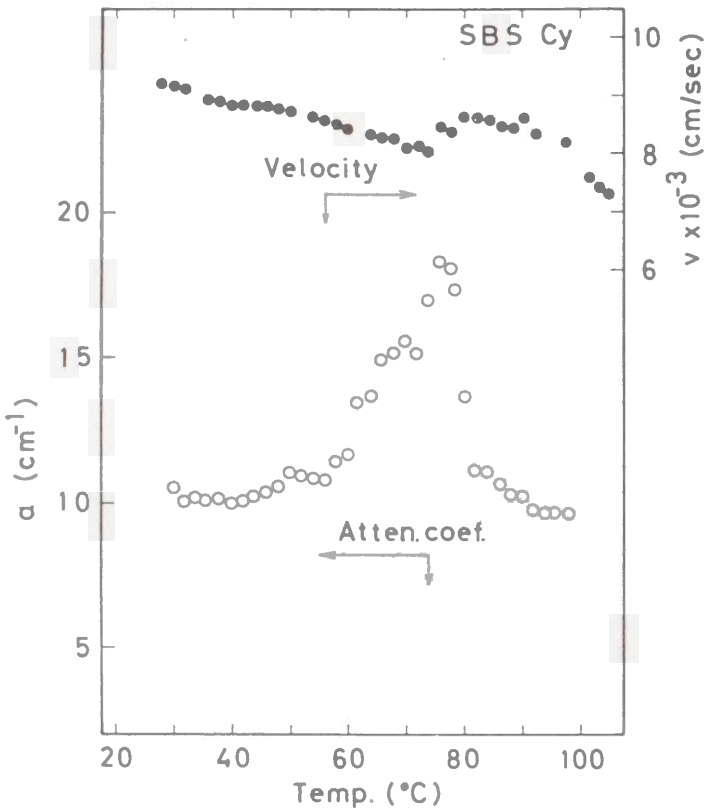

Fig.7-4 *Variation of the ultrasonic velocity and attenuation coefficient with temperature for Cy-films.*

Second, the velocity for aged T/M-films was lower than that for heat-treated films, and the attenuation coefficient was higher. Above 80° C, however, both velocity and attenuation coefficient of aged films became closer to those of heat-treated films.

As is well known, the increase in density raises the ultrasonic velocity and lowers the attenuation coefficient. The fluctuation of the density, on the other hand, lowers the velocity and raises the attenuation (see Chapter 1).

Considering this together with density data, the lower velocity and higher attenuation coefficient on the aged T/M-films can be ascribed to the fluctuation of the density. In other words, the heterogeneous (fluctuated) state has a higher density than homogeneous ones. Thus, the heterogeneous (fluctuated) state can be due to a local molecular ordering. Other types of heterogeneous states are possibly considered: they are the states in which residual (thermal or mechanical) stress exists. However, this is unlikely because the heterogeneous state caused by the residual stress has lower density than homogeneous state.

Third, in the case of aged T/M-films, a downward peak was observed between 50°and 75°C on the plot of the velocity vs. temperature, and an upward peak was observed between 50°and 80°C on the plot of the attenuation vs. temperature. In the case of heat-treated T/M-films, however, any distinct peak was not observed on their plots. In the case of Cy-films, a relatively broad downward peak was observed between 50° and 75° C on the plot of the velocity vs. temperature, and a great upward peak was observed between 50°and 80°C on the plot of the attenuation vs. temperature.

Usually, such ultrasonic peaks can be ascribed to a phase transition. Here again, the appearance of the ultrasonic peaks would strongly suggest the existence of ordered state.

Previously, differential scanning calorimetry (DSC) measurements were carried out for SBS-T/M and SBS-Cy films.[17] For aged films (249 days), an endothermic peak appeared around 350°K on the first heating run. For heat-treated films (60°C/29 hrs), however, the peak did not appear around 350°K, but a small peak appeared around 370° K. Both endothermic peaks disappeared on the second heating run.

Kovacs *et al.*[18] and Hodge *et al.*[19-22] have observed the endothermic heat

capacity peaks below T_g in several polymers: the peaks (sub-T_g) increased in magnitude and shifted to higher temperatures with increasing annealing time (or aging time) and annealing temperature. Furthermore, they demonstrated that the development of the sub-T_g heat capacity peaks with aging is a consequence of the glass transition kinetics.

The endothermic peak appearing at 370°K for heat-treated films will be due to the glass transition kinetics (enthalpy relaxation). However, it is unlikely that the endothermic peak appearing at 350° K on the aged films is due to the glass transition kinetics, when one takes into account the following observation: all the endothermic peaks for three kinds (T/M, Cy, and comp-molded) of aged films appeared at the same temperature (350°K), in spite of the fact that the aging condition such as aging time differed between these samples. This observation rather indicates that the endothermic peak at 350°K is due to an ordered structure.

Thus, the DSC data will also support the conclusion that the novel dispersion of tan δ is ascribed to the melting of an ordered structure, and that the development of the novel dispersion by aging is ascribed to the formation and/or development of the ordered structure.

The dynamic mechanical test was also previously carried out for pure polystyrene films.[17] The films were prepared by melt-pressing, and by casting from the T/M- and Cy-solutions. One did not observed any novel dispersion on melt-pressed and T/M-cast films. However, when melt-pressed polystyrene film was elongated by ca. 10% around T_g (100° C) and then air-cooled, the novel dispersion was observed but it disappeared by heat-treating. ALso, the novel dispersion was also observed on Cy-cast polystyrene films. These suggest that the molecular ordering occurs in the polystyrene domain but neither in polybutadiene domain nor their interface region.

The molecular ordering can be derived and stabilized by some forces. In the case of T/M-films, the driving force is supposed to be entropic force of rubbery polybutadiene chains. In the case of Cy-films, on the other hand, the force will be exclusion force: when the films are cast from cyclohexane which is a preferential

solvent for polybutadiene, polystyrene molecules should be preferentially excluded from cyclohexane molecules. The exclusion force will cause molecular ordering in polystyrene molecules. The molecular ordering thus formed may be stabilized by entropic force of rubbery polybutadiene chains.

In conclusion, the novel dispersion of ordered structure formed in the polystyrene domain. The ordered structure may be derived by some forces in nonequilibrium circumstances.

7-3-4 Change in Molecular Aggregation during Solvent Evaporation

Phase separation occurs in SBS solutions when the solvent was allowed to evaporate. the concentration increases. In this section, the changes in molecular aggregation during solvent evaporation are investigated for T/M and Cy solutions of SBS. For the purpose, the ultrasonic velocity and propagation intensity (corresponding to the inverse of the ultrasonic attenuation) were measured under the solvent evaporation. Details of the experimental methods are described in Chapter 2.

In Fig.7-5 are shown the variations of velocity and propagation intensity of ultrasonic waves with polymer concentration for T/M solutions. The propagation intensity, *i.e.* the amplitude of ultrasonic wave at a given distance was almost constant in the concentration range less than 40 wt% and then it decreased with increasing the concentration. After it reached a minimum at ca. 90 wt%, it increased again. The velocity also had a minimum at the similar concentration. These changes in ultrasonic properties with concentration are very similar to the changes near the Curie point of a second-order phase transition[23] and near nematic-smectic phase transition.[24] Thus, it is supposed that these changes are caused by the morphological transition from a single-phase-state (mixing state of two components) to a two-phase-state (separated state into polystyrene and polybutadiene domains).

In the case of SBS-Cy solutions, the ultrasonic velocity abruptly decreases around 57 wt% and then it gradually decreases, as shown in Fig.7-6. On the other hand, the ultrasonic intensity drops down near 50 wt% and then it

increases. This indicates that the phase transition from homogeneous single-phase to separated two-phases occurs around 50-60 wt%. Thus, the critical concentration of the phase separation can be obtained by ultrasonic measurements. It was also found that the critical concentration of Cy solutions was lower than that of T/M solutions. This is presumably due to the fact that cyclohexane is nonpreferential solvent for polystyrene.

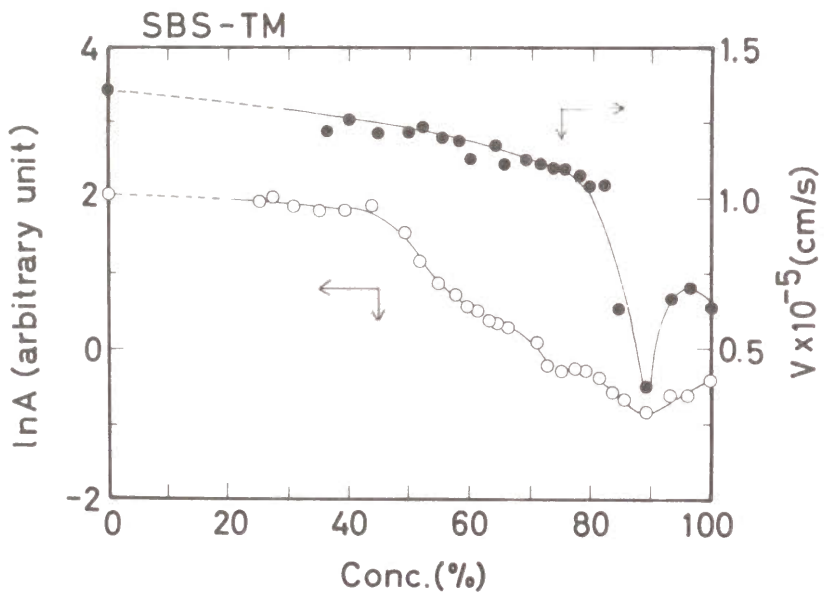

Fig.7-5 *Variation of the ultrasonic velocity and propagation intensity with concentration of T/M solutions.*

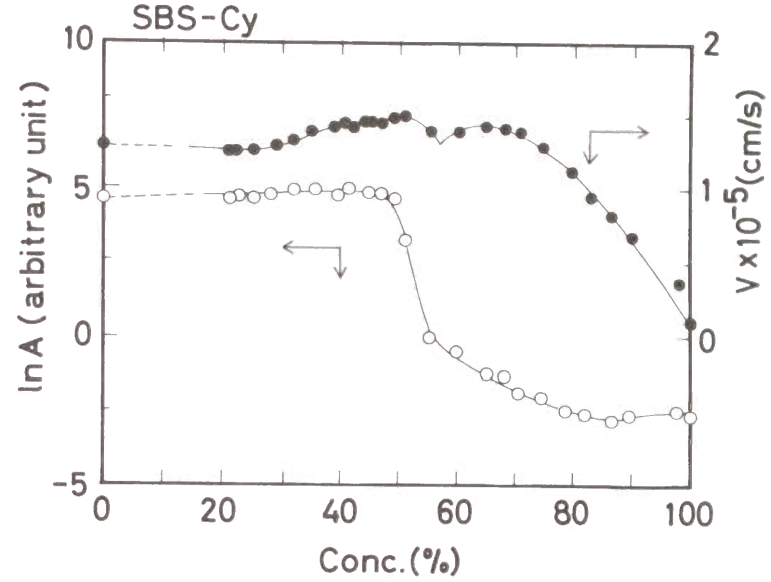

Fig.7-6 *Variation of the ultrasonic velocity and propagation intensity with concentration of Cy-solutions.*

7-4 Summary

The dynamic mechanical properties were measured for styrene-butadiene-styrene triblock copolymer films. A novel dispersion was found as a shoulder around 65° C on tan δ -T or log E''-T curve for films cast from solutions of

tetrahydrofuran containing 10% methyl ethyl ketone by volume. The novel dispersion became distinct with physical aging, but it disappeared with heat-treatment at 60° C. The similar dispersion was also found for films cast from cyclohexane solutions. The novel dispersion was examined by ultrasonic properties. The following have been concluded from these investigation: molecular ordering is formed in the polystyrene domain, and the novel dispersion is originated from melting of the molecularly ordered structure; the ordered structure would be caused by a repulsive force of surroundings. Furthermore, it was found that the critical concentration of phase separation in Cy solutions is about 50-60 wt% and that in T/M solutions is around 90 wt%.

REFERENCES

1. G. D. Wignal and G. W. Longman, *Polym. Preprints*, **15**, 18 (1974).
2. P. H. Geil, *J. Macromol. Sci.-Phys.*, **B12**, 173 (1976).
3. P. J. Harget and J. M. Aharoni, *ibid.*, **B12**, 209 (1976).
4. W. Knappe and H. J. Otto, *ibid.*, **B12**, 225 (1976).
5. R. F. Boyer, *ibid.*, **B12**, 253 (1976).
6. A. Colebrooke and A. H. Windle, *ibid.*, **B12**, 373 (1976).
7. K. P. Grosskurtz, *Colloid Polym. Sci.*, **225**, 120 (1977).
8. A. V. Sidrovich and Y. S. Nadezhin, *J. Macromol. Sci.-Phys.*, **B16**, 35 (1979).
9. L. Onsager, *Ann. N. Y. Acad. Sci.*, **51**, 627 (1949).
10. W. Maier and A. Saupe, *Z. Naturforsch.*, **13a**, 564 (1958).
11. J. F. Beecher, L. Marker, R. D. Bradford, and S. L. Aggarwal, *J. Polym. Sci.-Part C*, **26**, 117 (1969).
12. K. Arai, T. Miki, and T. Kotaka, *Polymer Preprints, Japan*, **27**, 406 (1978).
13. T. Miyamoto, K. Kodama, and K. Shibayama, *J. Polym. Sci. Part A-2*, **8**, 2095 (1970).
14. G. Kraus, K. W. Rollmann, and J. O. Gardner, *J. Polym. Sci. Polym. Phys. Ed.*, **10**, 2061 (1972).
15. A. Tanaka, Y. Jono, and S. Onogi, *Repts. Progr. Polym. Phys. Japan*, **24**, 295 (1981).
16. A. Tanaka, M. Shinohara, N. Wakabayashi, and S. Onogi, *ibid.*, **26**, 305 (1981).
17. A. Tanaka, N. Wakabayashi, and S. Onogi, *ibid.*, **27**, 311 (1984).
18. A. J. Kovacs, J. J. Aklonis, J. M. Hutchingson, and A. R. Ramos, *J. Polym. Sci. Polym. Phys. Ed.*, **17**, 1097 (1979).
19. I. M. Hodge and A. R. Berens, *Macromolecules*, **14**, 1598 (1981).
20. I. M. Hodge and A. R. Berens, *ibid.*, **15**, 762 (1982).
21. I. M. Hodge and G. S. Huvard, *ibid.*, **16**, 371 (1983).
22. I. M. Hodge, *ibid.*, **16**, 898 (1983).

23. K. R. Atkins, "*Liquid Helium*," Cambridge Univ. Press, (1959).Japan
24. S. Bhattacharya, *Phys. Rev. Part-B*, **23**, 2397 (1981).

CHAPTER 8

ULTRASONIC AND DYNAMIC MECHANICAL STUDIES OF MOLECULAR AGGREGATION

8-1 Introduction

Poly [1-(trimethylsilyl)-1-propyne] (designated as PTMSP) is one of new substituted polyacetylenes synthesized by Masuda *et al.*[1,2] and it has received much attention as a polymer showing significantly high gas-permeability. In general, most polymers showing high gas-permeability are rubbery around room temperature as exemplified in poly(dimethyl siloxane) and cis-polyisoprene, and their high gas-permeability can be attributed mainly to their flexible backbones and resultant high free volumes. Masuda *et al.*[2,3] found that PTMSP shows gas-permeability higher than that of the poly(dimethyl siloxane) irrespective of being glassy polymers. Takada *et al.*[3] and Odani *et al.*[4] also found that the high gas-permeability of PTMSP is significantly reduced by physical aging or heat-treating.

Polymer molecules in glassy states are often frozen in a nonequilibrium state, and relax toward equilibrium state. This phenomena is commonly referred to as physical aging. Aging affects a large number of properties such as density, modulus, and the rate of enthalpy relaxation.[5-10]

The purpose in the present chapter is to elucidate the origin of the gas-permeability of PTMSP and the effect of aging or heat-treating on the gas-permeability from a standpoint of the molecular aggregation, using ultrasonic and dynamic mechanical measurements.

8-2 Experimental

PTMSP polymers were polymerized with group 5 transition metal chlorides ($TaCl_5$ and $NbCl_5$) as catalysts.[1] Polymers synthesized with $TaCl_5$ catalyst, designated as PTMSP-Ta, have molecular weight $Mw=8.5X10^5$, while polymers synthesized with $NbCl_5$, designated as PTMSP-Nb, have molecular weight $Mw=3.2X10^5$. In Fig.8-1 is presented the structural formula. The geometrical structures are unknown.

Films specimens were prepared by casting toluene and/or hexane solutions of both polymers. For PTMSP-Ta polymers, the cast-films were prepared from toluene and hexane solutions (designated as Ta-tol and Ta-hex, respectively), whereas for PTMSP-Nb polymers the cast-films were prepared only from toluene (designated as Nb-Tol) because PTMSP-Nb polymers could not be dissolved in hexane. All films were thoroughly dried under vacuum for three days. X-ray diffraction,[2] dynamic mechanical properties,[11] and the small angle X-ray scattering (SAXS) studies indicated that all PTMSP (Ta-tol, Ta-hex, and Nb-Tol) films showed an amorphous nature.

Dynamic mechanical properties were determined with Rheovibron Model DDV-IIc (Toyo Badlwin Co., Ltd.). Measurements were carried out at 110Hz between room temperature and 200° C. Ultrasonic attenuation and velocity were measured from room temperature to ca. 100° C.

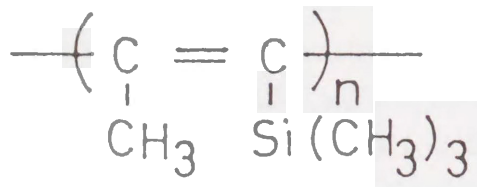

Fig.8-1 *Structural formula of Poly [1-trimethylsilyl-1-propyne]*

The permeability coefficients P were measured using a *K-315-N* gas-permeability apparatus (Rikaseiki Co., Japan) equipped with a *MKS* Baratron detector. P was determined as follows: The reservoir is separated by a film, or membrane (circle film with 4 cm diameter). The downstream side of the film is evacuated to a constant pressure (0.1 mm Hg), and the upstream side is provided with a gas-permeate at about 1 atm. The pressure in the downstream side , p, is recorded as a function of time, and the rate of increase in pressure, dp/dt, in the steady-state (where Fick's law holds) gives a permeation coefficient P. The permeation coefficient P is defined as cm^3 at s.t.p. which passes per second through 1 cm^2 of polymer 1cm thick when there is a pressure difference of 1cm Hg across the sample.

8-3 Results

8-3-1 Gas-Permeability

Table 8-I lists the permeability coefficients of three PTMSP films to oxygen and nitrogen at room temperature. The gas-permeability coefficients of Ta-tol and Nb-tol films were reduced with aging, on the contrary, that of Ta-hex film was almost independent of aging. This is associated with the result that Ta-hex showed a low permeability coefficient even for as-cast films.

Table 8-I *Gas-Permeability Coefficient and Density.*

		Ta-tol		Ta-hex		Nb-tol	
		as-cast	heat-treated	as-cast	heat-treated	as-cast	heat-treated
Gas-Permeability Coefficient*)	O_2	5.81	1.61	1.86	1.60	5.50	2.08
	N_2	3.89	0.78	1.01	0.85	3.73	0.69
Density (g/cm^3)		0.9350	0.9386	0.9478	0.9491	0.9260	0.9279

*) In units of $\frac{cm^3(S.T.P.)cm}{cm^2 sec\ cm\ Hg} \times 10^7$

8-3-2 Density

The density was measured using a flotation method. The results are also listed in Table 8-I. For all kinds of films, the density of aged films was higher than that of as-cast ones.

8-3-3 Viscoelastic and Ultrasonic Properties

1) PTMSP-Ta films cast from toluene. Fig.8-2 shows temperature dependence of the dynamic viscoelastic coefficients for as-cast and aged Ta-tol films. The storage modulus E' for both films is almost independent of temperature, and the loss modulus E'' and the loss tangent $\tan\delta$ ($= E''/E'$) monotonously decreases with increasing temperature. This indicates that there are no dispersions over the entire temperature range. Incidentally, the glass transition temperature of the polymers is above 200° C, as indicated by Masuda *et al.*[11]

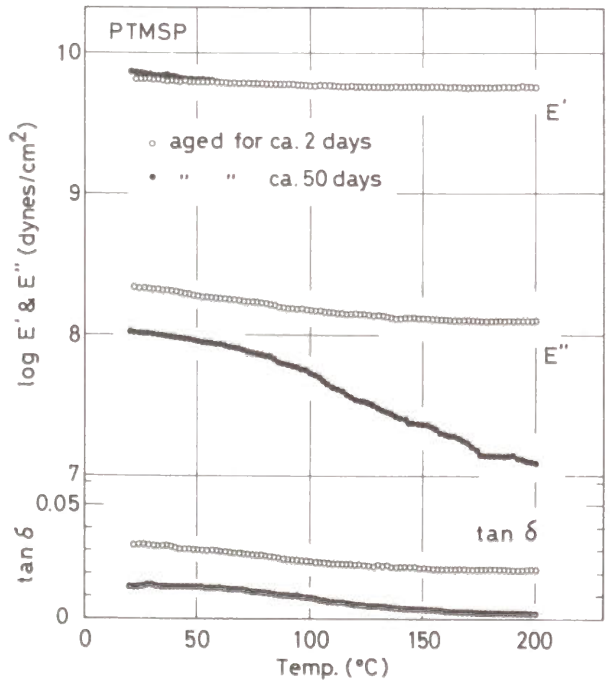

Fig.8-2 *Effect of aging on dynamic mechanical properties for PTMSP-Ta films cast from toluene solutions.*

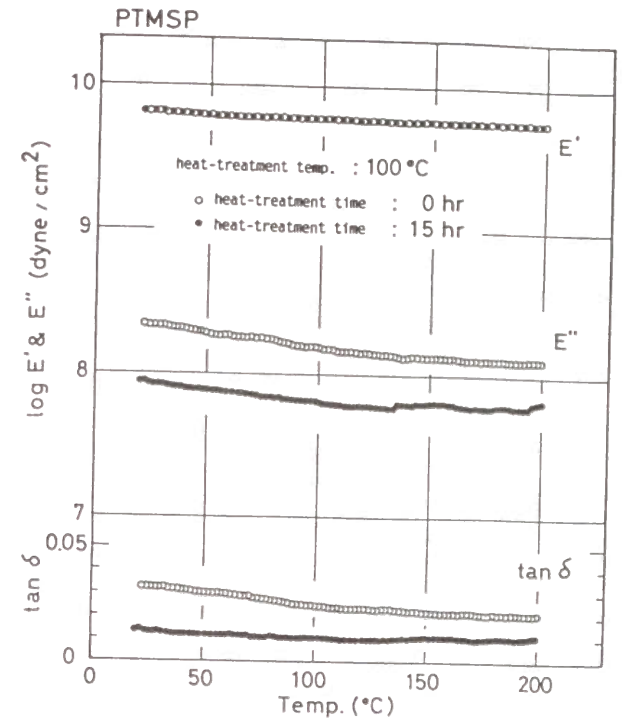

Fig.8-3 *Effect of heat-treatment on dynamic mechanical properties for PTMSP-Ta films cast from toluene solutions.*

It should noted here that there are little difference in E' of the as-cast and that of the aged films; on the other hand, E'' or $\tan\delta$ of the aged films was significantly lower than that of as-cast ones over the temperature range.

In Fig.8-3 are shown the effect of the heat-treatment (at 100° C for 15 hrs) on dynamic mechanical properties. E' was almost independent of the heat-treatment; however, the heat-treatment lowered the E'' or $\tan\delta$ decreased over the entire temperature range. The effect of heat-treatment was quite similar to that of physical aging.

The values of E', E'', and $\tan\delta$ at 50°, 100°, and 150° C plotted against the heat-treatment time are shown in Fig.8-4. As is obvious from the figures, E'' and $\tan\delta$ decreases with increasing heat-treatment period but E' is constant. From

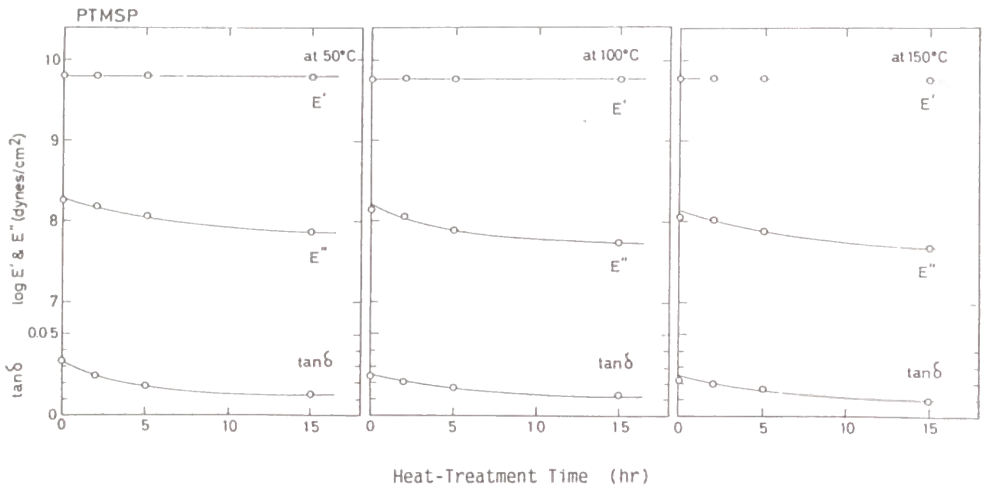

Fig.8-4 *Dependence of heat-treatment on dynamic mechanical properties for PTMSP-Ta films cast from toluene.*

the reduction rate of E'' which is determined from the initial slope, the apparent activation enthalpy ΔH can be estimated using following equation.

$$k = A\exp(\Delta H/RT) \qquad (8\text{-}1)$$

where k is the reduction rate, T the heat-treatment temperature in ° K, R the gas constant, and A the positive constant. Similarly, the reduction rate in aging process can be obtained. Aging experiments were conducted at room temperature, which varied from 10° to 30° C. In Fig.8-5, the natural logarithm of k is plotted against $1/T$. Consider the fluctuation of temperature, three lines were drawn: the two doted lines denote the upper and lower limit lines and the solid line denotes an averaged line of two doted lines. The slope gave the enthalpy ΔH = 9.0 kcal/mole. The error in ΔH estimated from scatter in the points was at most ±2 kcal/mole. This suggests that a small size of structural changes occur during aging or heat-treating.

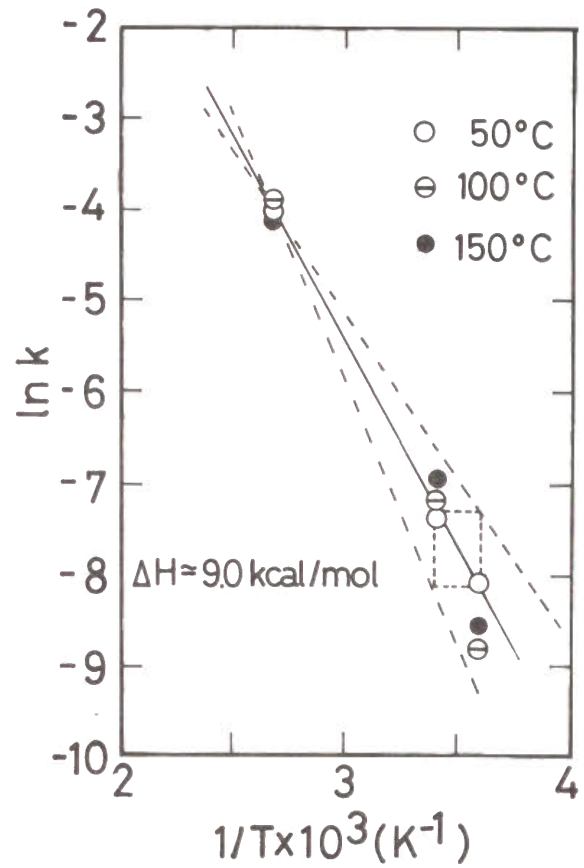

Fig.8-5 *Arrhenius plot of PTMSP-Ta films cast from toluene solution.*

Fig.8-6 shows the temperature dependence of the attenuation coefficient and velocity for Ta-tol films having different aging times. The attenuation of as-cast (3 days aged) Ta-tol films was low and almost independent of temperature, whereas the attenuation of aged films was high and rapidly increased above 50° C. In contrast, the velocity was almost independent of aging.

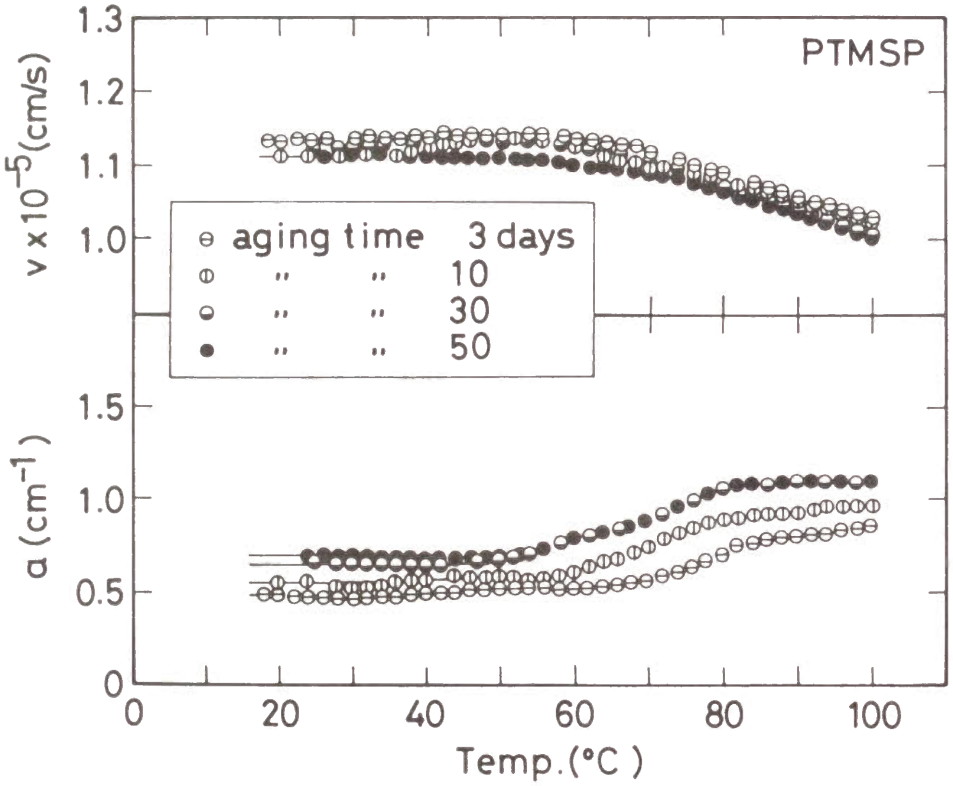

Fig.8-6 *Temperature dependence of the ultrasonic velocity and attenuation coefficient for PTMSP films cast from toluene with various aging times.*

The effect of heat-treatment on attenuation and velocity were also investigated (see Figs.8-7). As is obvious from the figures, the effects of heat-treatment on the attenuation and velocity are quite similar to those of aging.

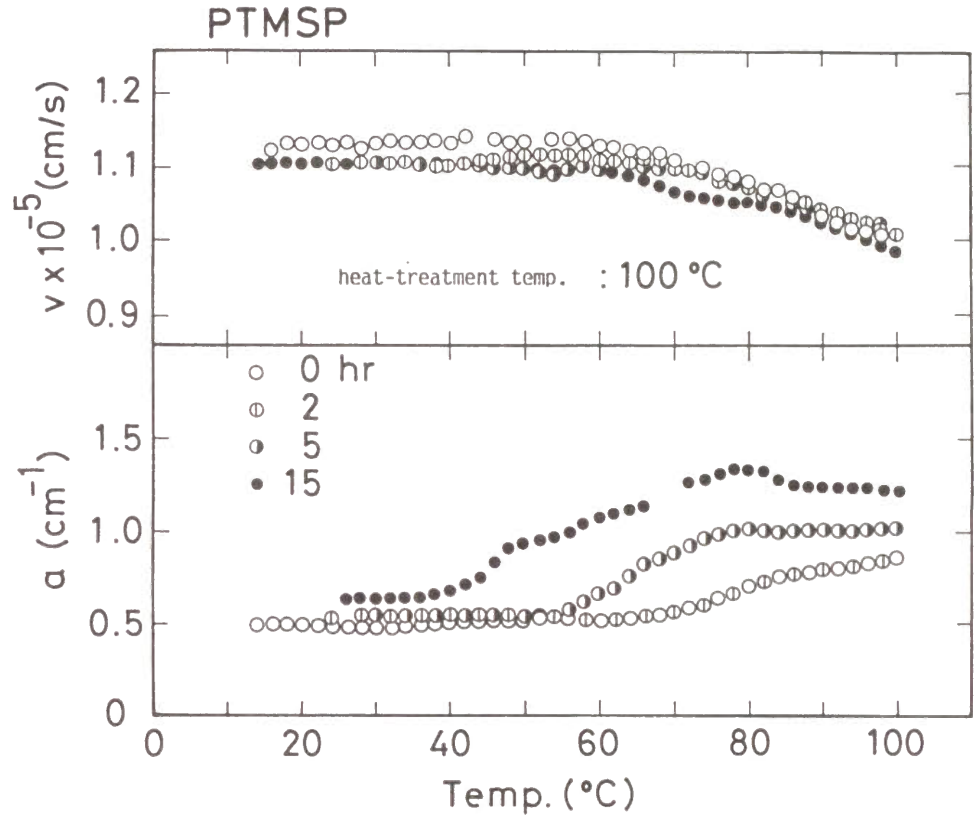

Fig.8-7 *Temperature dependence of the ultrasonic velocity and attenuation coefficient for PTMSP films cast from toluene with various heat-treatment times.*

2) PTMSP-Nb films cast from toluene. Fig.8-8 shows the temperature dependence of the tan δ for toluene cast films of PTMSP polymerized by Nb-based catalysts. For comparison, Fig.8-8 includes data of Ta-tol films. As is seen in the figure, the decrease in tan δ with heat-treatment is also observed for Nb-tol films, although the decrease is smaller than that for Ta-tol films. Furthermore, tan δ of the heat-treated Nb-tol films is comparable to that of heat-treated Ta-

tol films. In the case of Nb-tol films, rising of tan δ is observed above 170° C for both as-cast and heat-treated films. This may be associated with the onset of glass transition. The storage modulus E' of Nb-tol films was lower than that of Ta-tol but it was also independent of the heat-treatment, although the figures are not presented here.

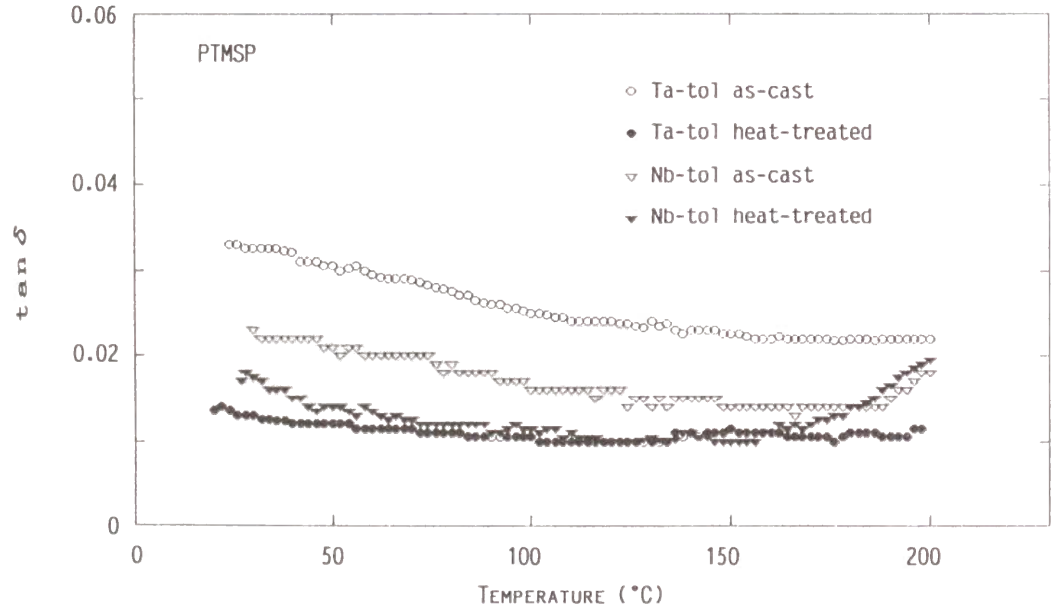

Fig.8-8 *Temperature dependence of tan δ for PTMSP-Ta and PTMSP-Nb films cast from toluene.*

In Fig.8-9, the temperature dependence of the attenuation coefficient for Ta-tol and Nb-tol films are shown. As is obvious from the figure, the temperature dependence of the attenuation is quite similar between both the heat-treated films. The velocity of the Nb-tol was also independent of the heat-treatment (although the velocity was lower than that of Ta-tol ones).

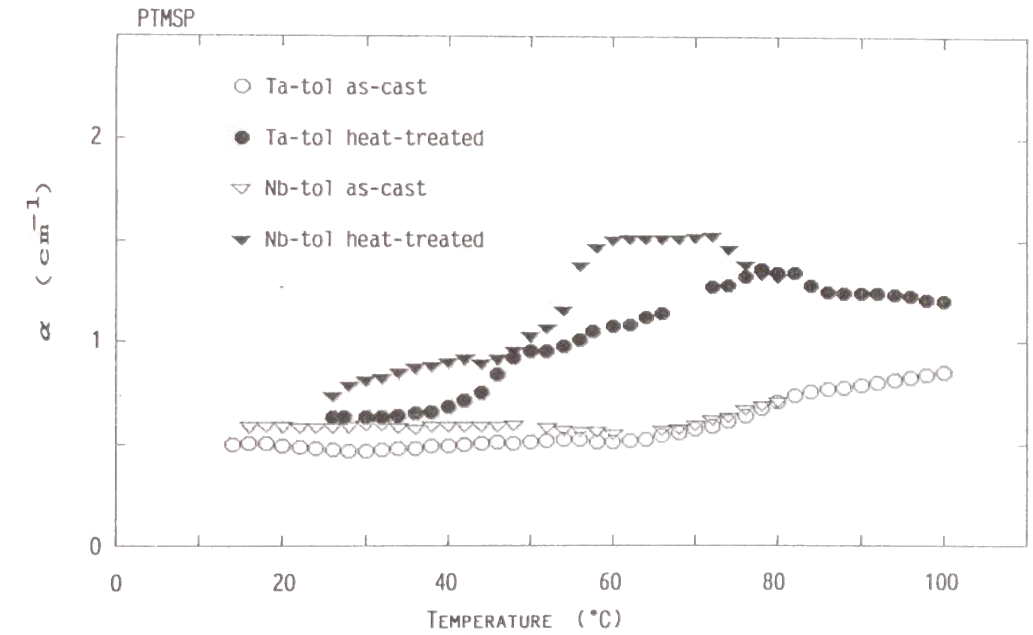

Fig.8-9 *Temperature dependence of the attenuation coefficient for PTMSP-Ta and PTMSP-Nb films cast from toluene.*

3) PTMSP-Ta films cast from hexane. Figs.8-10 and 8-11 show the temperature dependence of tan δ and the attenuation coefficient for PTMSP-Ta films cast from hexane, namely Ta-hex films. For comparison, the figures include data of Ta-tol films. As is obvious from the figures, in the case of Ta-hex films, the effects of heat-treatment on tan δ and α are quite small: tan δ is low and α is high even for as-cast films, which values are comparable to those of heat-treatment films of Ta-tol and Ta-hex. Also for Ta-hex films, E' and the ultrasonic velocity of the Ta-hex films were also independent of the heat-treatment; however, those of Ta-hex films were slightly higher than those of Ta-tol ones.

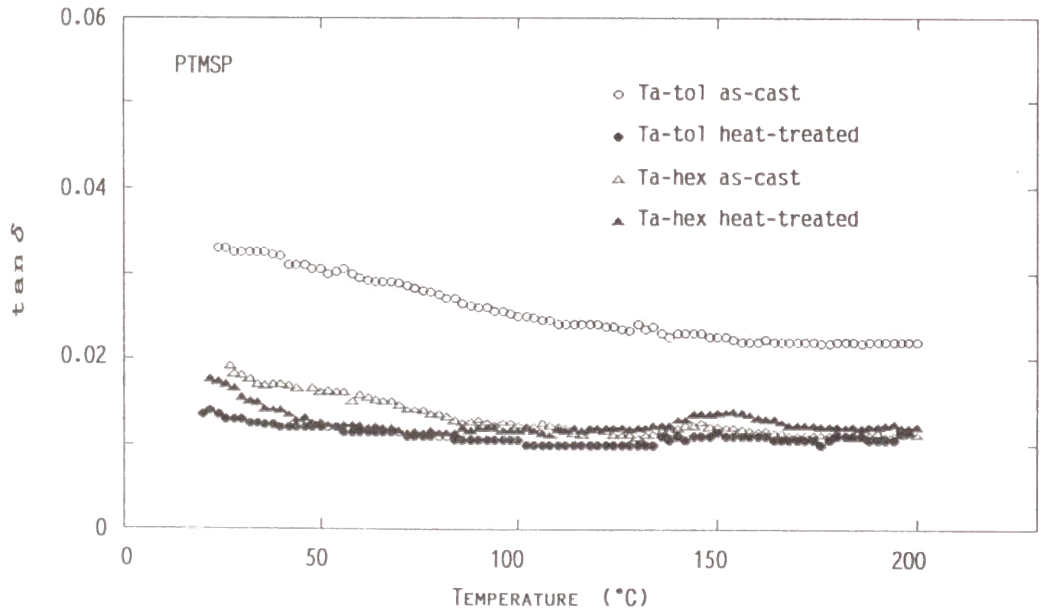

Fig.8-10 *Temperature dependence of tan δ for PTMSP-Ta films cast from toluene and hexane.*

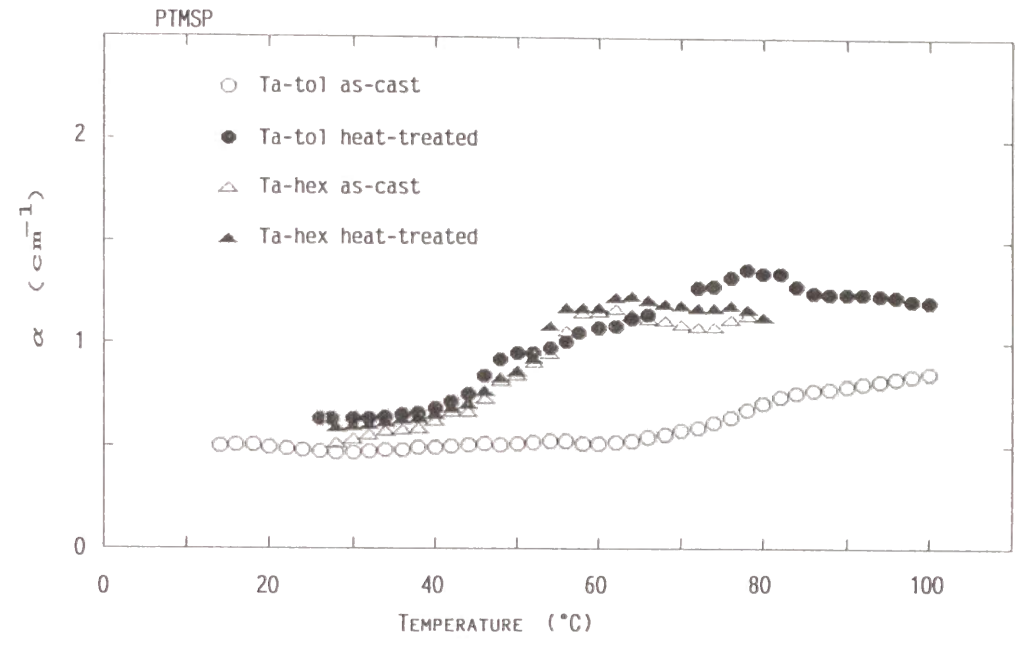

Fig.8-11 *Temperature dependence of the attenuation coefficient α* for PTMSP-Ta films cast from toluene and hexane.

The gas-permeability of PTMSP-Ta and -Nb films cast from toluene was reduced by physical aging or heat-treatment. Correspondingly, the mechanical loss decreased and the ultrasonic attenuation increased with aging or heat-treatment. On the other hand, those of PTMSP-Ta films cast from hexane did not significantly changed with aging or heat-treatment. In any case, it was found that PTMSP films showing higher (or lower) gas-permeability exhibit lower (or higher) the loss modulus (or tan δ) and higher (or lower) the ultrasonic attenuation. Moreover, the storage modulus and the ultrasonic velocity were independent of physical aging or heat-treatment.

8-4 Discussion

The independency of E' and velocity with aging or heat-treatment in the Ta-tol and Nb-tol films suggests that the backbone structure of polymers does not change with aging or heat-treatment; in other words, the backbone structure is not responsible for the change in gas-permeability with aging or heat-treating. Thus, the changes in tan δ and attenuation can be ascribed to structural changes associated with substituents; that is, the gas-permeability may be directly associated with a molecular aggregation of substituents.

There are many processes responsible for sound attenuation in solid materials as described in Chapter 1. These include viscothermal absorption, heat-conduction, sound scattering due to dislocation and boundaries, and coupling with thermal vibration. PTMSP films did not show a clear yield point on the stress-strain curves, as shown in the previous study;[11] furthermore, it showed no SAXS peaks. These results suggest that PTMSP films were not semicrystalline solids but glassy ones. Accordingly, the sound scattering due to dislocation and boundaries can be ruled out. The viscothermal and heat-conduction processes (viscous effects) must raise tan δ. Consequently, the excess attenuation of aged or heat-treated films would be caused by the interaction of sound waves with thermal motion[12]; namely, vibrational motion of substituents.

The following were considered from above discussion. The substituents (*i.e.* trimethylsilyl group) aggregate heterogeneously during casting process and the heterogeneous structure is frozen. When the heterogeneous aggregation is released by thermal motion, the substituents will be mobile enough. As a result, the attenuation becomes high. Also, the heterogeneous molecular aggregation would raise the free energy (or lower the entropy) of the polymers; thus, it operates as a loss component (or energy absorber) with respect to the mechanical excitation. Consequently, tan δ is reduced by the release of energy for the molecular aggregation

(or relaxation of the heterogeneous structure). The energy around 9.0 kcal/mole is likely to the above structural relaxation.

8-5 Summary

It can be concluded that the high permeability of PTMSP films is attained by which gas molecules permeate through sparsely sites caused by the heterogeneous aggregation of substituents. The relaxation of heterogeneous structure toward the homogeneous one occurs during physical aging or heat-treating; therefore, the disappearance of the sparse parts leads to the reduction in the gas-permeability. Also, the reduction in density with aging or heat-treating support such structural relaxation.

Ta-hex films showed a low gas-permeability, low tan δ, and high ultrasonic attenuation even for as-cast films. Hexane may cause PTMSP polymers to form a different geometric micro-structure which allows the molecular aggregation of substituents not to develop.

REFERENCES

1. T. Masuda, E. Isobe, and T. Higashimura, *Macromolecules*, **18**, 841 (1985).
2. T. Masuda, E. Isobe, T. Higashimura, and K. Takada, *J. Am. Chem. Res.*, **17**, 51 (1984).
3. K. Takada, H. Matsuya, T. Masuda, and T. Higashimura, *J. Appl. Polym. Sci.*, **30**, 1605 (1985).
4. H. Odani, H. Shimomura, K. Nakanishi, T. Masuda, and T. Higashimura, *Japan-US Polymer Symposium Prepts.*, Kyoto Japan, pp 251 (1985).
5. A. Kovacs, J. Atkins, J. Hutchingson, and A. Ramos, *J. Polym Sci., Polym. Phys. Ed.*, **17**, 1097 (1979).
6. I. Hodge and A. Berens, *Macromolecules*, **15**, 762 (1982).
7. I. Hodge and G. Huvard, *ibid.*, **16**, 371 (1983).
8. I. Hodge and A. Berens, *ibid.*, **14**, 1598 (1981).
9. R. Roe and G. Millman, *Polym. Eng. Sci.*, **23**, 318 (1983).
10. F. Maurer, J. Parmen, and H. Booji, *Rheolog. Act.*, **24**, 243 (1985).
11. T. Masuda, B.-Z. Tang, A. Tanaka, and T. Higashimura, *Macromolecules*, **19**, 1459 (1986).
12. T. Woodruff and H. Ehrenreich, *Phys. Rev.*, **123**, 1553 (1961).

CHAPTER 9

ULTRASONIC STUDIES OF MOLECULAR AGGREGATION IN LIQUID CRYSTALLINE POLYMERS

9-1 Introduction

The molecular aggregation in liquid-crystalline polymers is particularly unique: liquid crystalline states differs from isotropic liquid states showing no long range order and from crystal states sowing cubic long range order. Liquid-crystalline polymers have optical anisotropy due to long range orientational order. Thus, the molecular aggregation in the liquid-crystalline polymers is of very interest particularly for better understanding of the aggregation states in polymers.

In the past decade, numerous studies[1-5] have shown that most cellulose derivatives form cholesteric liquid crystalline phases in solution or in the bulk. In particular, hydroxypropyl-cellulose (designated as HPC) has been widely studied because mesophases can be easily formed in both water and common organic solvents.[1,2]

The cholesteric structure consists of rotating layers of the rod-like molecules[4,6] and is characterized by the presence of a helical twist of uniform pitch. If the cholesteric materials have a cholesteric pitch comparable to the wavelength of visible light, it is expected from de Vries theory[10] that the materials will show the cholesteric color which is due to the selective reflection of the visible light caused by the uniform cholesteric twisted structure.

The purpose of this study is to examine the molecular aggregation state in

the process of development and/or collapse of cholesteric structures. For the purpose, the ultrasonic properties of the HPC solutions were investigated as a function of concentration during the solvent evaporation process. Furthermore, the molecular aggregation in the cast films showing various cholesteric colors were also investigated using the ultrasonic measurements.

9-2 Experimental

Hydroxypropyl-cellulose used in this study is a commercial polymer, HPC-SL produced by Toyo Soda Co. Ltd. The structural formula is shown in Fig.9-1. According to Horio *et al.*[11], the weight average molecular weight *Mw* is 164300, the number average molecular weight *Mn* 41600, the degree of molar substituent *MS* is 3.5, and the degree of substituent *DS* 2.3. HPC solutions of 20 wt% were first prepared using various solvents (distilled water, ethyl alcohol, acetic acid, and dioxane). Ultrasonic velocity and intensity (corresponding to inverse of attenuation) were measured during solvent evaporation; that is, as a function of the concentration from 20 to 100 wt%. Ultrasonic measurements were also carried out on the HPC films prepared by casting from water and these organic solvents. Details of the experimental conditions for preparing the cast films showing various cholesteric colors will be described later.

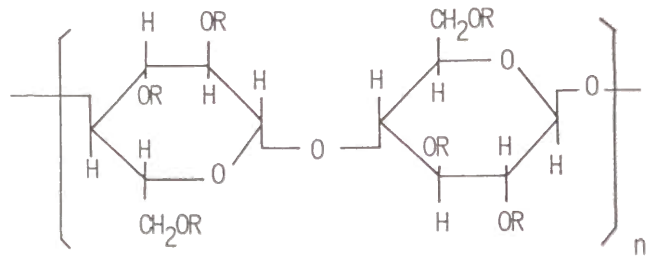

Fig.9-1 *Structural formula of Hydroxypropyl-cellulose (HPC).*

9-3 Results and Discussion

9-3-1 Change in Molecular Aggregation with Solvent Evaporation

Fig.9-2 shows the variations of the ultrasonic velocity and intensity with concentrations for HPC-ethanol solutions. The propagation intensity of the ultrasonic wave dramatically drops at ca. 50 wt% and reaches a minimum at ca. 75 wt%. The ultrasonic velocity, on the other hand, starts falling at ca. 65 wt% and then reaches a minimum at ca. 85 wt%. Correspondingly, iridescent colors based on the cholesteric pitches were observed in the concentration range between 70 and 85 wt%. Thus, such anomalous decreases in velocity and intensity will be ascribed to the phase transition from isotropic to liquid crystalline phases.

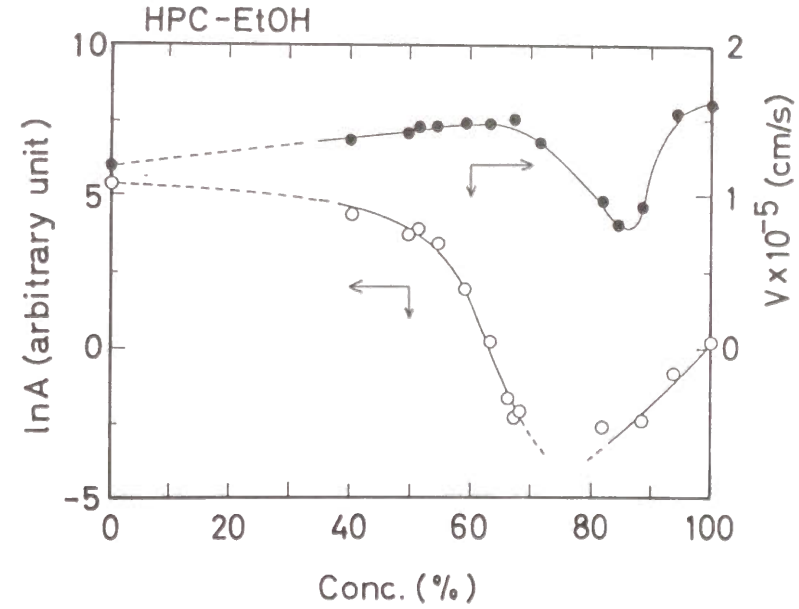

Fig.9-2 *Variation of the ultrasonic velocity and propagation intensity with concentration for HPC-ethanol solutions.*

It has been already well known that for thermotropic liquid crystalline materials, such an anomalous change in both velocity and attenuation was observed near phase transition temperature (nematic-isotropic transition). The anomalous change is referred as Landau-Khalatnikov relaxation.[12, 13] It is of very interest that the Landau-Khalatnikov relaxation were also observed for the lyotropic system.

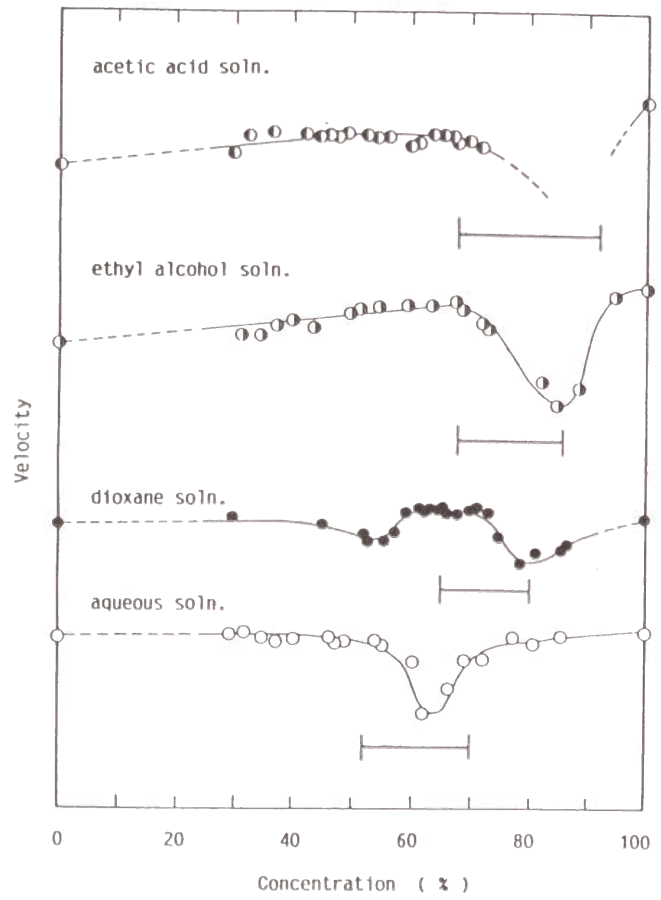

Fig.9-3 *Variation of the ultrasonic velocity with concentration for various solutions.*

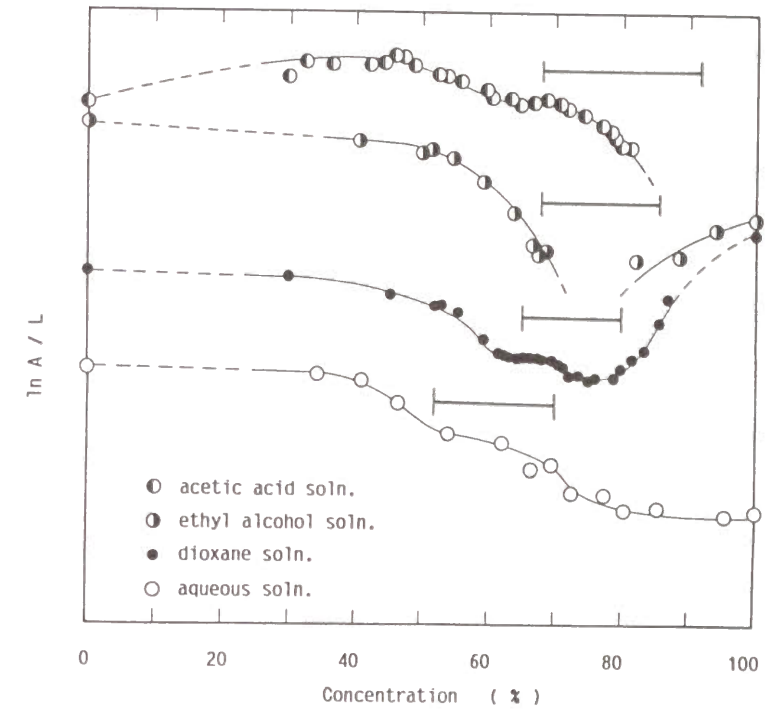

Fig.9-4 *Variation of the propagation intensity with concentration for various solutions.*

The concentration dependence of ultrasonic properties for HPC solutions of other solvents were also investigated and the results are shown in Figs.9-3 and 9-4. The solid bars in these figures indicate the concentration range in which iridescent colors appeared in HPC solution. As is evident from the figures, the anomalous decreases in the velocity and intensity occurs in the concentration range where iridescent colors appeared in all the solutions; in other words, the decreases can be ascribed to the phase transformation from isotropic to liquid-crystalline phases. The critical concentration for the phase transition was in order of acetic acid, ethanol, dioxane, and water. In the case of HPC-dioxane, two

drops in the ultrasonic velocity and intensity are observed. This suggests that different types of phase transition occur in the dioxane solutions.

9-3-2 Ultrasonic and Mechanical Properties of HPC Films

Preparations of Cholesteric Colored Films.

HPC films were prepared by casting from water, ethanol, acetic acid, and dioxane solution. The colored films could be obtained in the following procedures.

Step 1: polymers were allowed to dissolve (ca.30 wt%) for at least two weeks. Step 2: the solutions was poured on a pan with flat Teflon surface, and solvent was allowed to evaporate in the normal laboratory environment. Step 3: when iridescent colors appeared in the solution, the pan was wrapt up in a saline film in order to remain in the anisotropic concentration range long enough to achieve a high degree of order. Step 4: when an iridescent color appeared in the whole of the solution, one took off the saline film and allowed the solution to evaporate up to ca. 80 to 85 wt% at a fixed temperature between the glass transition temperature of HPC (ca. 25°C)[16] and the freezing point of the solvent. Step 5: the colored films can be obtained by heating the concentrated solution. The films thus prepared had various cholesteric colors depending on the heat-treating conditions. Step 6: the cast-films were dried thoroughly under vacuum for at least few weeks and then kept in a dry atmosphere.

In the case of HPC-acetic acid solutions, a cholesteric color appeared at higher concentrations (60-80%); thus, steps 3 and 4 were unnecessary. A colored film could be obtained only by heating the corresponding colored solution at 120° C for 2 min (step 5).

HPC-ethanol solutions was given by allowing to evaporate slowly up to ca. 85% in a refrigerator (at ca. 7° C) (step 4). The various colored films could be prepared by heating the concentrated solution at 120°C for various times (step 5). For example, violet films could be obtained by heating for 10 min, green ones for 12 min, and red ones for 15 min. This marked variation is indicative of thermotropic liquid-crystalline characteristics.[17-21] Also for HPC-dioxane, red, yellow, green, and violet films can be obtained in the same manner. Here, evaporation temperature was slightly higher than the freezing temperature of dioxane (11.8°C) (step 4).

HPC-water solutions showed iridescent colors at lower critical concentrations (50-70%). In this case, it was very difficult to evaporate without collapsing of cholesteric structures for the sake of high molecular mobility at low concentration. Accordingly, colored films showing relatively longer wavelength (namely, red, yellow, and green) could be hardly obtained, but blue and violet films could be obtained by repetition of heating at 120°C for 10 min (step 5).

UV-visible spectrophotometric measurements for HPC cast films were performed at room temperature using a Jasco UVIDEC-1 Double-Beam Spectrophotometer. The wavelength range used in this study was from 310 to 760 nm.

The transmittance of HPC films cast from ethanol, acetic acid, and dioxane is plotted against the wavelength in Figs.9-5, 9-6, and 9-7, respectively. The caption in the figures indicates the visible color observed at normal angle to the film surface. Open circle denotes the normalized transmittance and closed circle the net transmittance subtracted the background (solid lines). Here, it was assumed that the transmittance of the background was given by a Lorentz function. This is plausible because the transmittance curves of colorless films prepared by compression molding[21] can be described by a Lorentz function (see Fig.9-8).

As is shown in Figs.9-5, 9-6, and 9-7, the wavelength of UV absorption is in good agreement with the wavelength of visible color. This indicates that the colors of the films are due to the selective reflection of visible light caused by the cholesteric order.

Effect of Pitch on Ultrasonic Properties.

Ultrasonic velocity and attenuation coefficient were measured as a function of temperature (from room temperature to 80° C) for the HPC films having various cholesteric colors. The velocity and attenuation coefficient were measured in the directions of both parallel and perpendicular to the film surface. The attenuation in the perpendicular direction to the films was calculated by considering reflections of ultrasonic waves.

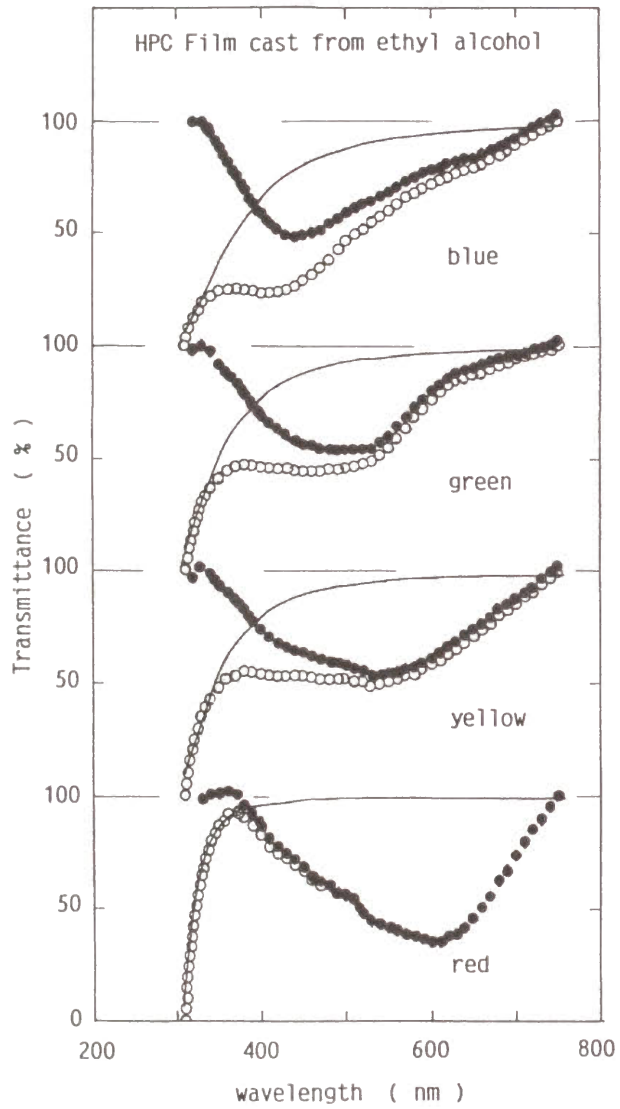

Fig.9-5 *UV-transmittance of HPC cast from ethyl alcohol. The captions indicate a visible colors at normal angle to the film surface. Open circle denotes the normalized transmittance, closed circle the net transmittance, and solid line the background intensity given by a Lorentz function.*

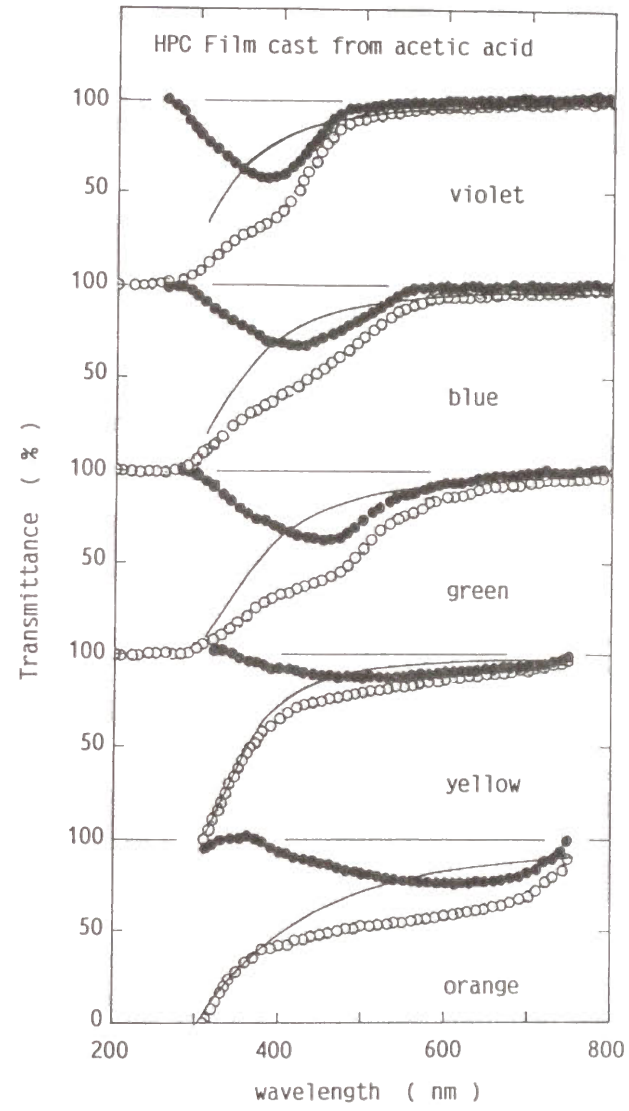

Fig.9-6 *UV-transmittance of HPC cast from acetic acid. The captions indicate a visible colors at normal angle to the film surface. Open circle denotes the normalized transmittance, closed circle the net transmittance, and solid line the background intensity given by a Lorentz function.*

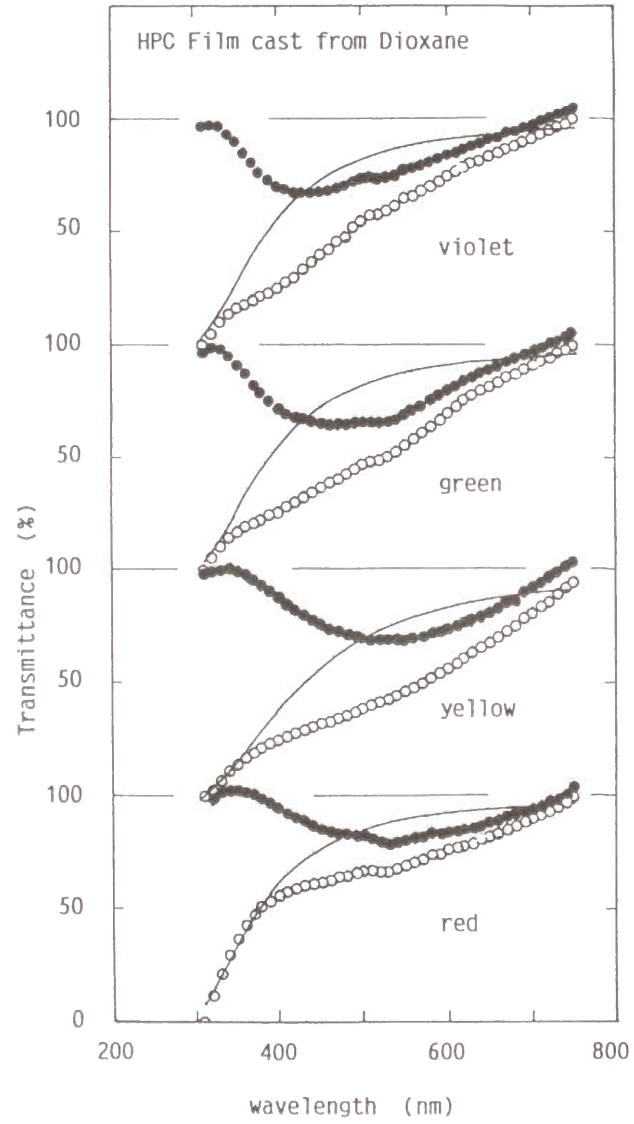

Fig.9-7 *UV-transmittance of HPC cast from dioxane. The captions indicate a visible colors at normal angle to the film surface. Open circle denotes the normalized transmittance, closed circle the net transmittance, and solid line the background intensity given by a Lorentz function.*

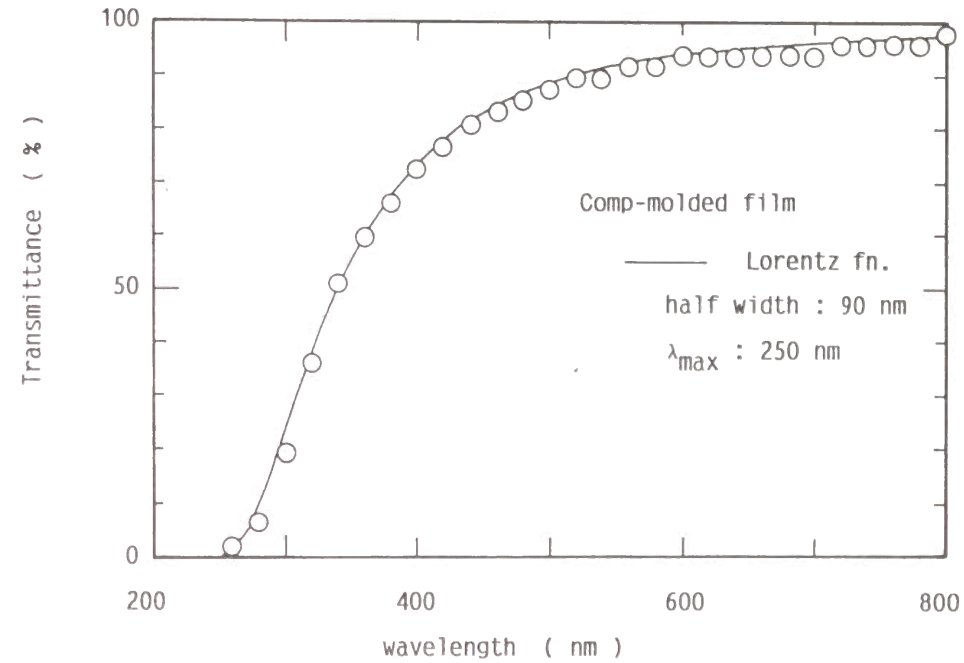

Fig.9-8 *UV transmittance of colorless films prepared by compression molding. Open circle denotes the normalized transmittance and the solid line the best fit to the Lorentz curve.*

For the colored (namely, yellow, green, and violet) films cast from acetic acid, the temperature dependence of ultrasonic velocities in the directions of perpendicular and parallel to the films surface are shown in Figs.9-9 and 9-10, respectively. Both velocities decreases monotonously with increasing temperature, reflecting "softening" of the materials. The ultrasonic velocities were in order of blue, green, and red films in the entire temperature range; that is, the velocity increased with decreasing the cholesteric pitch. This indicates that the decrease in pitch can lead to intensive molecular interaction.

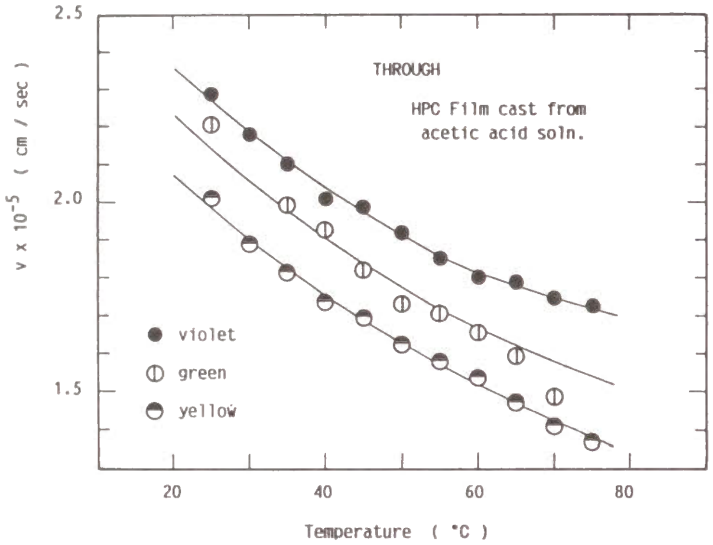

Fig.9-9 *Temperature dependence of the ultrasonic velocity in the direction of perpendicular to film surface for HPC films cast from acetic acid solutions.*

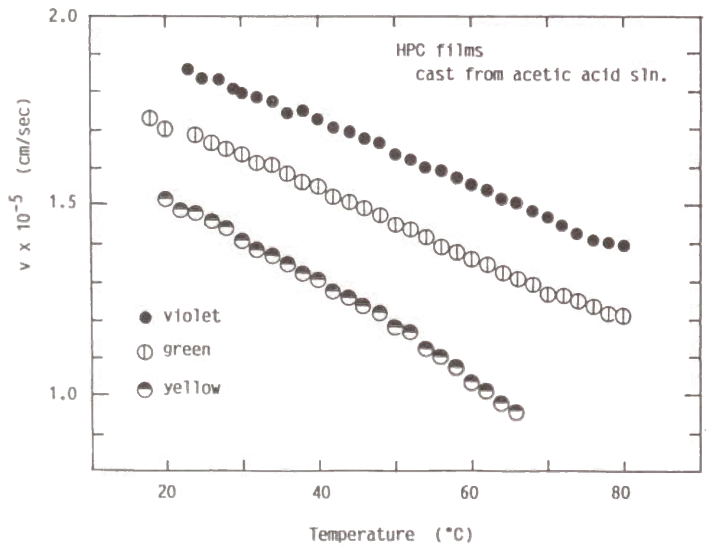

Fig.9-10 *Temperature dependence of the ultrasonic velocity in the direction of parallel to film surface for HPC films cast from acetic acid solutions.*

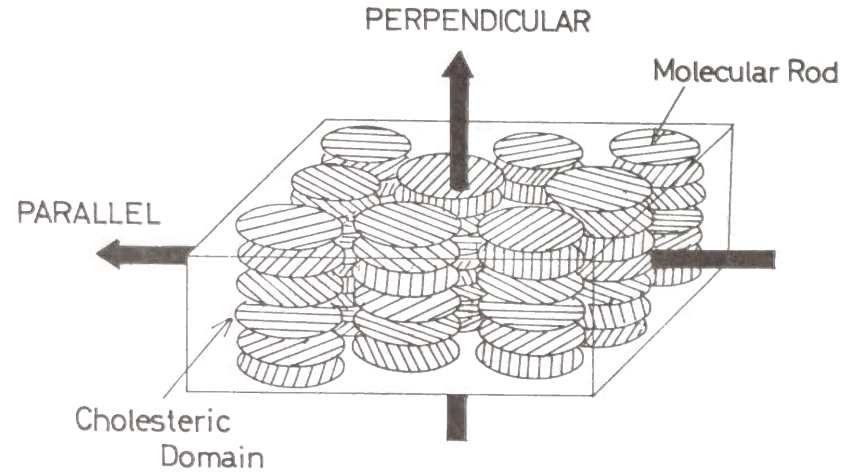

Fig.9-11 *Schematic representation of cholesteric structure. Arrows denote the directions of ultrasonic waves.*

The velocity in the perpendicular direction was higher than that in the parallel direction for all the colored films. As demonstrated by Samuels,[22] the polymer molecules of HPC films align preferentially in the plane of the film, and HPC shows a planner cholesteric arrangement in the solid state. Thus, the ultrasonic waves in the perpendicular direction to the film surface propagate by inter-layers interaction, whereas that in the parallel to the film surface propagate by both planner inter-molecular (inter-rods) and inter-domains interactions (see Fig.9-11). The interactions of inter-layers and inter-rods would be more intensive as compared with interaction between cholesteric domains; therefore, the ultrasonic velocity in the planer direction was lower than that in the perpendicular direction.

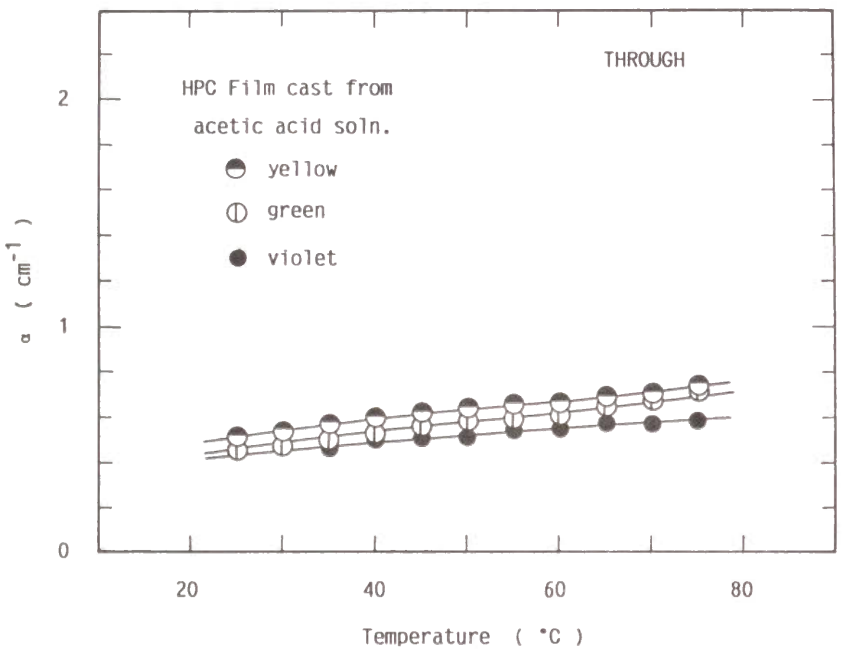

Fig.9-12 *Temperature dependence of the ultrasonic attenuation coefficient in the direction of perpendicular to the films cast from acetic solutions.*

In Fig.9-12, the attenuation coefficient in the perpendicular direction are plotted against temperature for the HPC films cast from acetic acid solution. The attenuation in the perpendicular direction was almost independent of cholesteric colors (or pitches) and temperature. On the other hand, the attenuation in the planner direction depends drastically on cholesteric pitches and on temperature (see Fig.9-13). Although the attenuation was almost constant at lower temperatures, it rose rapidly above a temperature. The temperature was lower as the

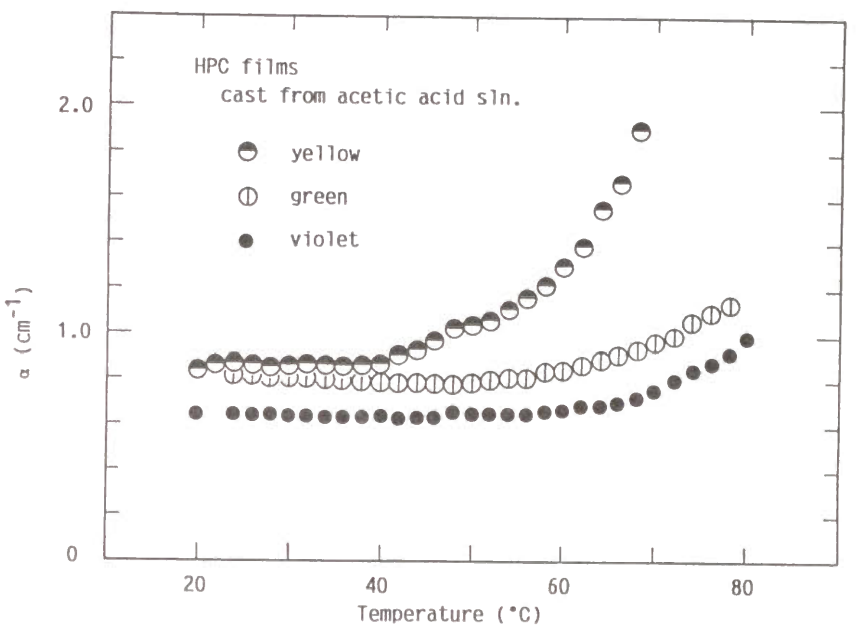

Fig.9-13 *Temperature dependence of the ultrasonic attenuation in the direction of parallel to the films cast from acetic acid solutions.*

cholesteric pitch became longer: for yellow films the temperature was ca. 40° , for green ones ca. 55°, and for violet ones ca. 65°C. Also, the attenuation in the planner direction is sufficiently higher than that in the perpendicular direction. The high attenuation in planner direction result from a contribution of the loose interaction between cholesteric domains to the process of sound transmission.

The dependence of cholesteric pitch on the ultrasonic properties for HPC-acetic acid films was similarly seen for colored films prepared by casting from ethanol and dioxane.

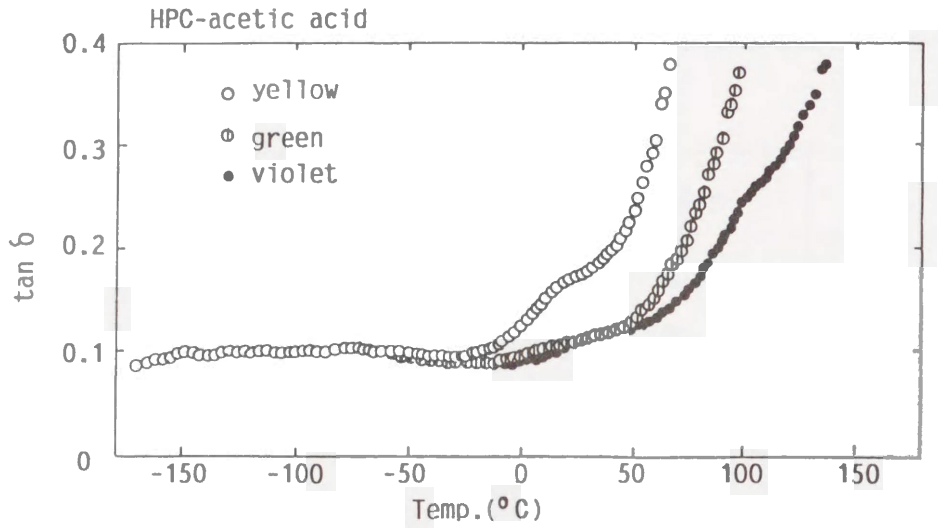

Fig.9-14 *Temperature dependence of loss tan δ* for HPC films cast from acetic acid solutions.

The dynamic mechanical properties were measured with a Rheo-vibron Model DDV-IIc. The loss tangent measured at 110 Hz for HPC films cast from acetic acid are plotted against temperature in Fig.9-14. The broad maximum of loss tangent at about 25° C is indicative of the glass transition.[16,21] The drastic increases at higher temperatures is related to the increase in molecular mobility.[21,22]

9-4 Summary

The molecular aggregation state of Hydroxypropyl-cellulose solution during evaporation was examined using ultrasonic measurements. The drops in ultrasonic velocity and the ultrasonic intensity were observed around a critical concentration at which the cholesteric colors appeared. The critical concentration varied with solvents and was in order of acetic acid, ethyl alcohol, dioxane, and water. It is of very interest that the Landau-Khalatnikov type of phase transition was found to be observed in lyotropic HPC materials.

For cholesteric colored HPC films, the velocity and attenuation in the both planner and normal direction to the film surface were measured. The ultrasonic velocity and attenuation depended largely on the cholesteric pitch. Moreover, the anisotropy was found in the ultrasonic properties: the ultrasonic velocity was higher in the normal direction to the film specimen than in the planner direction, and the attenuation was lower in the normal direction than in the planner direction.

REFERENCES

1. D. G. Gray, *J. Appl. Polym. Sci., Appl. Polym. Symp.*, **37**, 179 (1983).
2. R. D Gilbert and P. A. Patton, *Prog. Polym. Sci.*, **9**, 115 (1983).
3. D. G. Gray, *Faraday Discuss. Chem. Soc.*, **79**, 257 (1985).
4. R. S. Werbowyj and D. G. Gray, *Macromolecules*, **13**, 69 (1980).
5. J. Behda, J. F. Fellers, and J. L. White, *Colloid Polym. Sci.*, **258**, 1335 (1980).
6. T. Tsutsui and R. Tanaka, *Polym. J.*, **12**, 473 (1980).
7. R. S. Werbowyj and D. G. Gray, *Macromolecules*, **17**, 1512 (1984).
8. C. Robinson, *Trans. Faraday Soc.*, **52**, 571 (1956).
9. C. Robinson, *Mol. Cryst.*, **1**, 467 (1966).
10. Hl. de Vries, *Acta Cryst.*, **4**, 219 (1951).
11. M. Horio, E. Kamei, and Y. Uchimura, *Jpn J. Rheol.*, **13**, 25 (1985).
12. L. D. Landau and I. M. Khalatnikov, *Dok. Akad. Nauk USSR*, **96**, 469 (1954).
13. M. Fixman, *J. Chem. Phys.*, **36**, 1961 (1962).
14. H. Imura and K. Okano, *Chem. Phys. Lett.*, **19**, 387 (1973).
15. S. Bhattacharya, B. K. Sarma, and J. B. Ketterson, *Phys. Rev. B*, **23**, 2397 (1981).
16. J. S. Aspler and D. G. Gray, *Polymer*, **23**, 43 (1982).
17. K. Shimamura, J. L. White, and J. F. Fellers, *J. Appl. Polym. Sci.*, **26**, 2165 (1981).
18. S. Suto, J. L. White, and J. F. Fellers, *Rheol. Acta.*, **21**, 62 (1982).
19. I. Uematsu and Y. Uematsu, "*in Advances in Polymer Science*", Springer-Verlag Berlin, pp 37-73 (1984).
20. S. N. Bhadani and D. G. Gray, *Mol. Cryst. Liq. Cryst.*, **102**, 255 (1984).
21. G. Charlet and D. G. Gray, *Macromolecules*, **20**, 33 (1987).
22. R. J. Samuels, *J. Polym. Sci., A-2*, **7**, 1197 (1969).

List of Publications

Chapter 3

1. Ultrasonic Velocity and Attenuation of Polymeric Solids Under Oscillatory Deformation: Apparatus and Preliminary Results.

   Polym. Eng. Sci., **29**, 1124 (1989)

2. Evaluation of Dynamic Density by Simultaneous Measurement of Ultrasonic Velocity and Elastic Modulus Under Oscillatory Deformation.

   Polym. Eng. Sci., **29**, 1131 (1989)

Chapter 4

3. Ultrasonic Velocity and Attenuation of Polymeric Solids Under Oscillatory Deformation. 2. High Density- and Linear Low Density-Polyethylene and Their Blends.

   Polym. Eng. Sci., in press.

Chapter 5

4. Ultrasonic Velocity and Attenuation of Polymeric Solids Under Oscillatory Deformation. 3. Drawn Films of High Density- and Linear Low Density-Polyethylene and Their Blends.

   Polym. Eng. Sci., in press.

Chapter 6

5. Analysis of Stress-Strain Curve of Polyethylene Films by Toda-Lattice Model.

   Polymer J. submitted.

Chapter 7

6. A Novel Mechanical Dispersion and Molecular Ordering in Styrene-Butadiene-Styrene Triblock Copolymer Films.

   Polymer J. submitted.

Chapter 8

7. Ultrasonic Properties and Gas-Permeability of Poly [1-trimethylsilyl-1-propyne] Films.

   to be submitted.

Chapter 9

8. Ultrasonic Studies on Molecular Aggregation of Hydroxypropyl-cellulose in the Process of Solvent Evaporation.

   to be submitted.

9. Molecular Aggregation and Ultrasonic Properties of Hydroxypropyl-cellulose Films.

   to be submitted.

ACKNOWLEDGMENT

The author wishes to express his sincere gratitude to Emeritus Professor Shigeharu Onogi for his guidance on the present work.

The author is deeply indebted to Dr. Akira Tanaka for his continuous guidance, valuable discussions, and encouragement throughout the course of this work.

The author wishes to express his sincere gratitude to Professor Toshiro Masuda, Research Center for Medical Polymers and Biomaterials, Kyoto University, for his useful criticisms and encouragement throughout the course of this work.

The effort of Professor Sueo Kawabata is gratefully acknowledged. His careful reading of the original manuscript lead to many critical comments which were indeed valuable.

The author wishes to express sincere thanks to Professor Toshinobu Higashimura and Associate Professor Toshio Masuda for their valuable discussions and supplying samples.

The author is also grateful heartily to Messrs. Yorihisa Hamada, Hiroshi Onoda, and Yuichi Uchida for their kind help in supporting the research activities.

Finally, thanks are expressed to his parents, Satoshi Nitta and Reiko Nitta for their continuous encouragement during the course of this work.

March 1991

Koh-hei Nitta